HIDRAULICA

HYDRAULICS-PNEUMATICS-TRIBOLOGY-ECOLOGY-SENSORICS-MECHATRONICS

2022

September

No. 3

ISSN 1453 - 7303
ISSN-L 1453 - 7303

https://hidraulica.fluidas.ro

CONTENTS

Published by:
Hydraulics and Pneumatics Research Institute, Bucharest-Romania
Address: 14 Cuţitul de Argint, district 4, Bucharest, 040558, Romania
Phone: +40 21 336 39 91; Fax: +40 21 337 30 40; e-Mail: ihp@fluidas.ro; Web: www.ihp.ro
with support from:
National Professional Association of Hydraulics and Pneumatics in Romania - FLUIDAS
e-Mail: fluidas@fluidas.ro; Web: www.fluidas.ro

HIDRAULICA Magazine is indexed by international databases

ISSN 1453 – 7303; ISSN – L 1453 – 7303

EDITORIAL

Digitalizarea în domeniul hidraulicii

Dr. Ing. Petrin DRUMEA
DIRECTOR PUBLICAȚIE

Cu doi ani în urmă prezentam într-un editorial tendința digitalizării hidraulicii și scoteam în evidență marile avantaje ale trecerii la hidraulica inteligentă. Din păcate, pașii făcuți de specialiștii noștri sunt puțini, teoretici și de cele mai multe ori pe lângă subiect. Trebuie subliniat că dacă modelarea și simularea și-au găsit utilitatea în câțiva ani de la apariție, introducerea inteligenței artificiale prin hidraulica inteligentă încă nu a fost abordată serios în țara noastră, deși pe plan mondial acest subiect este tratat și teoretic, dar și aplicativ, de câțiva ani buni.

Este adevărat că fără un suport industrial important nu este posibil să trecem nici la hidraulica digitală, nici la pompele inteligente, nici la senzorii inteligenți, nici la actuatoarele inteligente și nici la sistemele inteligente. Cu eforturile nesemnificative ale câtorva persoane nu se poate spune că facem pașii necesari dezvoltării domeniului.

Probabil că încă nu se înțeleg nici la nivel teoretic importanța, dar mai ales modalitatea concretă de abordare a digitalizării în tehnologie, faptul că orice utilaj complex are în componență elemente în mișcare și că această mișcare este asigurată, de regulă, de sistemele și echipamentele electrice sau hidraulice. Ca urmare, trebuie să realizăm atât la nivelul echipamentelor, cât și la nivelul sistemelor digitalizarea.

Hidraulica inteligentă nu cuprinde doar componente hidraulice, ci și subansamble electronice, senzoristică, informatică și modalități de transmitere a datelor. Includerea tuturor acestor echipamente într-un sistem complex este realizabilă doar de către specialiști cu vaste cunoștințe în toate aceste domenii tehnice. Cine îi pregătește și mai ales unde? Este destul de dificil ca domeniul să evolueze atâta timp cât în școlile superioare sunt puțini profesori care să poată îndruma tineretul în această direcție.

Probabil că ar trebui niște cursuri de perfecționare pentru tinerii specialiști, care să depășească etapa jocurilor pe telefon sau calculator și să înțeleagă și să realizeze sistemele și echipamentele hidraulice inteligente. Pentru început, aplicațiile practice ar putea fi din zona standurilor și din zona instalațiilor tehnologice de complexitate medie.

Să reținem că lupta pentru dezvoltare are abordarea teoretică doar ca prim pas, baza fiind realizarea practică a digitalizării tehnologiilor.

EDITORIAL

Digitalization in the field of hydraulics

Ph.D.Eng. Petrin DRUMEA
MANAGING EDITOR

Two years ago, I wrote in an editorial about the trend of digitalizing hydraulics and I used to highlight the great advantages of moving on to intelligent hydraulics. Unfortunately, the steps taken by our specialists are few, theoretical and most of the time off topic. It should be pointed out that while modeling and simulation have found their usefulness within a few years of their emergence, introducing of artificial intelligence through intelligent hydraulics has not yet been seriously addressed in our country, although on a global level this topic has been dealt with theoretically as well as in an applied manner for several years.

It is true that with no significant industrial support it is not possible to move on to either digital hydraulics or smart pumps, smart sensors, smart actuators, and smart systems. With the insignificant efforts of a few people, it cannot be said that we are taking the necessary steps to develop the field.

They probably still do not understand the importance even at a theoretical level, but especially the concrete way of approaching digitalization in technology, the fact that any complex machine is made up of moving elements and that this movement is usually provided by electrical or hydraulic systems and equipment. As a result, we need to achieve digitalization both at the equipment level and at the system level.

Intelligent hydraulics includes not only hydraulic components, but also electronic subassemblies, sensors, informatics and data conveying methods. Including all these pieces of equipment in a complex system can only be achieved by specialists with extensive knowledge in all these technical fields. Who trains them and especially where? It is quite difficult for the field to progress as long as there are only few professors in the higher schools who can guide the young people in this direction.

Perhaps some training courses are needed for young specialists, in order for them to go beyond the stage of playing games on the phone or computer, and understand and develop intelligent hydraulic systems and equipment. To begin with, some practical applications could be in the area of the test benches and in the area of medium-complexity technological installations.

Let's remember that the struggle for development has the theoretical approach only as a first step, the most important being the practical implementation of the digitalization of technologies.

Simulation of the Working Cycle for a Hydraulic Press Equipped with a Flow Regulator Mounted in Graetz System

Prof. Dr. Eng. **Carmen DEBELEAC**[1,*]

[1]„Dunarea de Jos" University of Galati, Engineering and Agronomy Faculty of Braila,

Research Center for Mechanics of Machines and Technological Equipment

* carmen.debeleac@ugal.ro

Abstract: *The paper focuses on mathematic modelling of the working operation with the press unit, with hydraulic acting, where flow regulation in load is carried out with a flow regulator mounted in Graetz system. A non-linear simulation model has been developed in Matlab/SimHydraulics environment for highlighting the dynamic behaviour of the main parameters of working regime of hydraulic press unit.*

Keywords: *Hydraulic press, Graetz system, dynamic working regime, Matlab/SimHydraulics, simulation*

1. Introduction

Generally, the hydraulic system was gradually developed from the hydrostatic transmission theory (initiated by Pascal) until today when the control of these systems can respond to complex demands posed by actual technology. For example, a hydraulic press is a mechanical device using a hydraulic cylinder to generate a compressive force, to shape, deform, and configure various types of materials (e.g. metals, plastics, etc.). The basic working principle of the hydraulic press are simple. For better understanding of the working cycle of the press equipment, three phases are presented in schematization in figure 1.

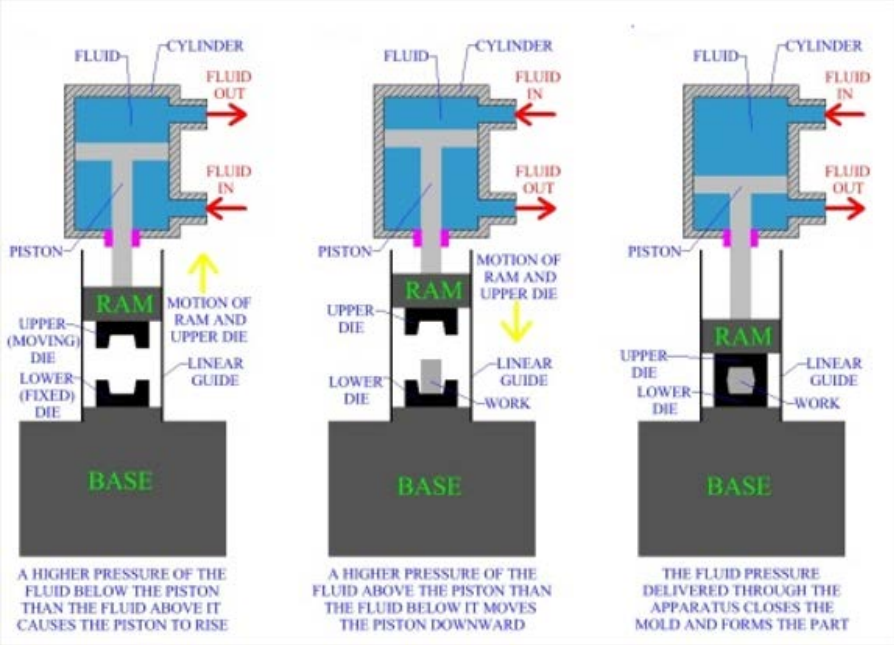

Fig. 1. Principle of operation of the hydraulic press [1]

The hydraulic press is a major part of a variety of manufacturing and production processes. Their main parts consist of a mainframe, power system, and control devices (fig. 2). The hydraulic presses in figure 2 use a single rod piston so the hydraulic pressure is applied over the entire diameter of the piston that drives the ram press.

Fig. 2. Examples of press equipment

The performances of hydraulic presses required for proper operation of the technological process consist on ability of force control or positioning control systems that follow-up varying reference signals [2-4].

2. Problem statement

The study carried out in this work proposes an analysis of the hydraulic cylinder from the component of a hydraulic press, where the flow control in the load is ensured with a Graetz system. This system consists of four directional valves placed so as to form a bridge (Fig.3). The scheme demonstrates how a bridge circuit works to ensure that fluid can only flow one way through a pressure-compensated flow-control.

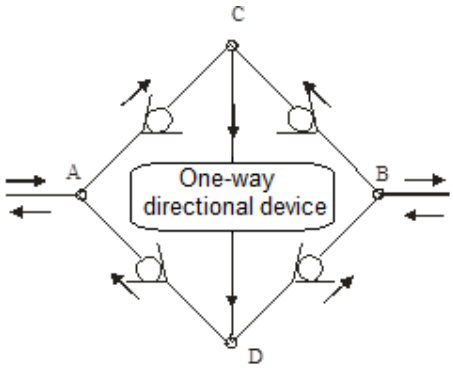

Fig. 3. Principle of operation of Graetz circuit diagram

Thus, the inlet and outlet of the system are placed in the corners of the bridge, and the regulating or measuring device is located on the other diagonal. However, the central component does not have to be a flow control (fig. 4). It could just as well be a filter or any other component that requires unidirectional flow (e.g. flow meter, pressure regulator, flow regulator, etc.).

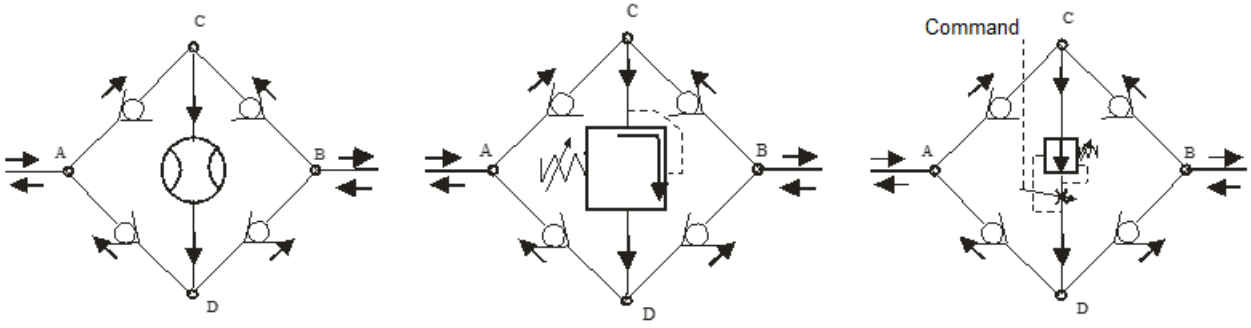

Fig. 4. Positioning of the bridge devices:
a) flow meter; b) pressure valve; c) flow regulator.

Into the hydraulic scheme for press acting with Graetz rectifier circuit, the four non-return valves are combined to assure a unitary functioning. The circuit diagram in figure 4c shows how this operates in conjunction with a flow control valve: flow passes through this valve from left to right during both the advance and return strokes of the cylinder (in the case of press equipment). The situation during the advance stroke is shown. It is observed that regardless of the direction of entry into bridge A or B, the circulation of the hydraulic agent on the diagonal CD is carried out only in the direction from C to D, a fact that leads to a unique adjustment of the parameters of the hydraulic system, whatever the direction of flow might be.
In the following, the diagram of the hydraulic circuit of a press unit will be equipped, for comparison, with the Graetz system and, respectively, with four directional valves, for adjusting the velocity of displacement of the working tool (press ram), regardless of the load on the piston active area.

3. Analysis and simulation of working regimes of hydraulic press equipment

The analysis of the behavior of the hydraulic system to the variation of the load on the press piston (corresponding to working operation) is based on a mathematical model for mechanical-hydraulic co-simulation of the driving unit of press [5-6], taking into account by flow rate and motion equations available for [7-8]:
- mathematical model of pump with constant flow;
- mathematical model of discrete hydraulic directional valve;
- mathematical model of flow regulator with pressure balance (Graetz bridge);
- mathematical model of linear hydraulic cylinder.

To simulate the behavior of the hydrostatic driven of press equipment, a scheme has been performed using the Matlab/SimHydraulics environment (Figure 5), usually used for a lot of virtual scenarios [9-11]. It was implemented a simplified model of an open circuit for ram piston acting from a simple acting cylinder. The global scheme contains the following blocks, namely: the driving unit of the circuit, the auxiliary equipment (directional valves, protection valves, pipelines), the regulated blocks of the flow rate into circuit (with throttles and Graetz bridge), and the sensor blocks for instantaneous monitoring of the hydraulic parameters (e.g. input and output pressures, fluid rate flow, piston force, kinematics parameters of the piston motion). Visual representation of the main blocks has been marked separately, in different colors, for better understanding of functional components of the hydraulic scheme.

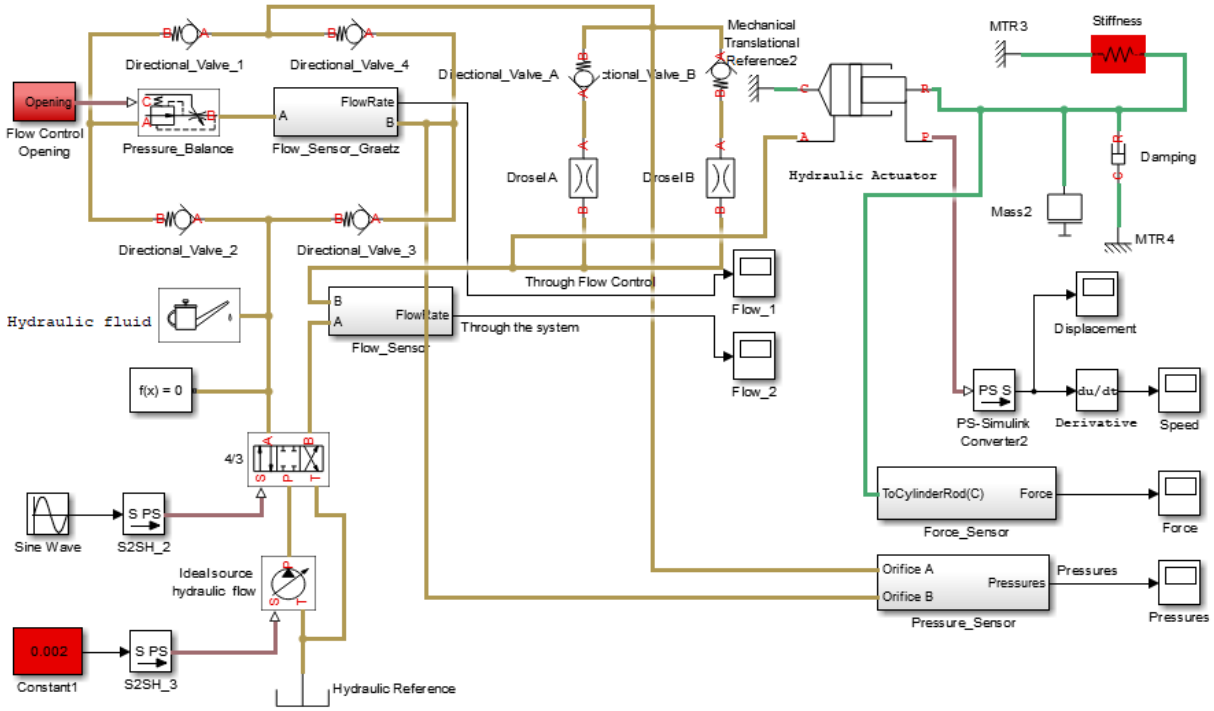

Fig. 5. Schematic of hydraulic circuit implemented in Matlab/SimHydraulics environment

The parameters that customize main blocks of the scheme in figure 5 are centralized in tables 1-4.

Table 1: Block parameters: Hydraulic fluid

Parameter	Value
Type	MIL-F-5606
Density	847.4 kg/m^3
Viscosity	12.15 cSt
Flow discharge coefficient	0.7

Table 2: Block Parameters: Pressure – Balance

Parameters	Value
Orifice maximum area	5x10^{-4} m^2
Orifice maximum opening	0.016 m
Pressure differential across the orifice	6x10^5 Pa
Pressure reducing valve regulation range	5x10^4 Pa
Flow discharge coefficient	0.7
Critical Reynolds number	12 m
Leakage area	10^{-12} m^2

Table 3: Block Parameters: 4/3-Way directional valve

Parameters	Value
Valve passage maximum area	5x10^{-4} m^2
Valve maximum opening	0.01 m
Flow discharge coefficient	0.7
Critical Reynolds number	12 m
Leakage area	10^{-6} m^2

Table 4: Block Parameters: Single-acting hydraulic cylinder

Parameters	Value
Piston area	0.035 m^2
Piston stroke	0.08 m
Piston initial position	0
Dead volume	10^{-4} m^3
Specific heat ratio	1.4
Contact stiffness	10^6 N/m
Contact damping	150 Ns/m

4. Results

The response of the actuation system, simulated for 5 seconds, starting from the moment of initialization of the movement, is presented in figure 6. The dynamic performance of the linear hydraulic actuator (in the case of Graetz system acting) is represented as piston displacement-time, piston speed-time and flow rate-time (controlling by Graetz bridge comparatively by resistive circuit).

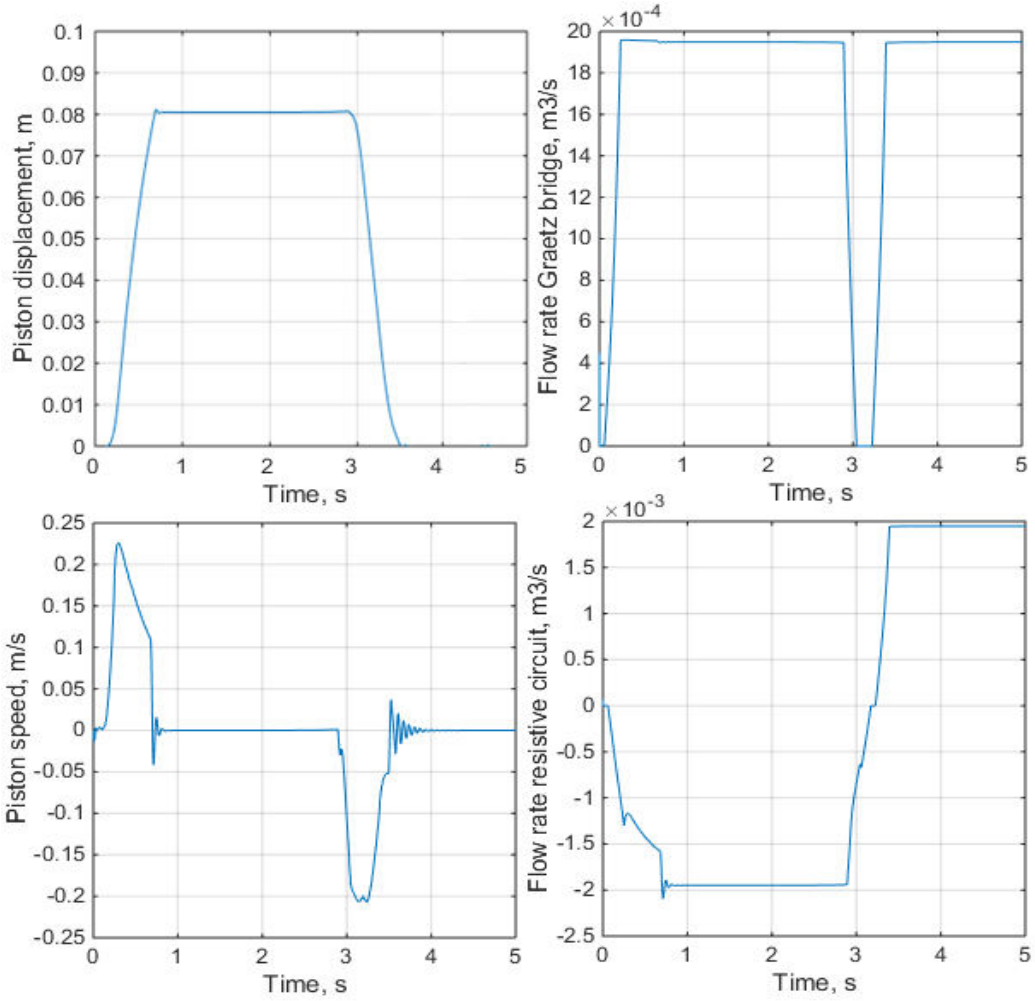

Fig. 6. Simulation results

Thus, these dynamic characteristic curves were simulated in one work cycle and one can see that they are characterized by intensive temporal variation of analysed parameters. In the flow control system (and implicitly in the piston force control), it is required that maximum overshoot must not be excessive. With Graetz bridge the control of flow rate is maintained around $2x10^{-3}$ m^3/s, curve different from the one through the resistive circuit. This aspect assures a maximum value of flow rate regardless of load at working tool. In addition, for simulating various loads acting at the piston rod, a subsystem that can vary working scenarios was implemented in the scheme. With help of the SimHydraulics module, it is easier to carry out sensitive analyses regarding the influence of some parameters on the performances of the press actuation system (e.g. pressures, impact force, acceleration piston, energy consumption, etc.).

5. Conclusions

This paper highlights the functioning of the Graetz bridge (known as a unit pressure balance), consisting of four direction valves and a flow regulator, embedded into a concrete engineering application (e.g. hydraulic press equipment).
Due to the constructive layout, this assembly determines the flow of hydraulic agent always in the same direction through the flow regulator. In this way, the flow of hydraulic agent with a constant and continuous value determines the stability and precision of the actuation system, which is simulated and shown on the response diagrams of the actuator.
The use of the Matlab/SimHydraulics analysis environment allows the direct modelling of the blocks that define the mathematical model of the hydraulic actuation system. The modelling results

highlight the interdependence of the process parameters, and the dimensional ones can be modified individually, for a qualitative refinement of the response of the press actuator.
Finally, the control of flow rate can be performed even with a Graetz system as alternative solution for resistive adjustment of the hydraulic agent speed by means of throttle devices.

References

[1] Kabra, Nilesh. "Forging & Press Working." *Slideshare*, October 23, 2015. Accessed July 20, 2022. https://www.slideshare.net/NileshKabra1/forging-press-working-54292765.
[2] Chen, Hong-Ming, Guo-Wei Yang, and Chong-Cyuan Liao. "Precision Force Control for an Electro-Hydraulic Press Machine." *Smart Science* 2, no. 3, (2014): 132-138.
[3] Rodriguez-Guerra, Jose, Carlos Calleja, A. Pujana, Iker Elorza, and Igor Azurmendi. "Real-time HiL for hydraulic press control validation." Paper presented at the 7th International Conference on Simulation and Modeling Methodologies, Technologies and Applications SIMULTECH 2017, Madrid, Spain, July 26-28, 2017.
[4] Šitum, Željko, Tihomir Žilić, and Vladimir Milić. "Improving performance of a hydraulic press with real-time nonlinear control". Paper presented at the 9th International Fluid Power Conference (9th IFK), Aachen, Germany, March 24-26, 2014.
[5] Curduman, Laurentiu, Silviu Nastac, Carmen Debeleac, and Mircea Modiga. "Computational dynamics of the rotational heavy loads mastered by hydrostatical driving systems." *Procedia Engineering* 181 (2017): 509–517.
[6] Curduman, Laurentiu, Carmen Debeleac, and Silviu Nastac. "On path oscillations analysis of mechanical multi-body and hydrostatical driving units coupled system." *Procedia Engineering* 181 (2017): 518–525.
[7] Axinti, Gavril, and Adrian-Sorin Axinti. *Fluid Power Systems – Components and systems, functions and characteristics. Vol. I / Acţionări hidraulice şi pneumatice – Componente şi sisteme, funcţii şi caracteristici. Vol. I*. Chişinău, Tehnica-Info Publishing House, 2008.
[8] Axinti, Gavril, and Adrian-Sorin Axinti. *Fluid Power Systems – Equipment and systems dynamics. Vol. II / Acţionări hidraulice şi pneumatice – Dinamica echipamentelor şi sistemelor. Vol. II*. Chişinău, Tehnica-Info Publishing House, 2008.
[9] Zheng, HongBo, MingJun Li, and ZhouLin Wang. "Simulation and optimization for pressing system of hydraulic brick press based on AMESim." *Journal of Physics: Conference Series* 2187 (2022): 012026.
[10] Debeleac, Carmen. "Dynamic Modeling and Simulation of Working Regime of the Hydraulic Driven of Auger Bucket for Loader Using Matlab/SimHydraulics ". *Hidraulica Magazine*, no. 4 (December 2021): 7-16.
[11] Eltantawie, Manar Abd Elhakim. "Design, manufacture and simulate a hydraulic bending press." *International Journal of Mechanical Engineering and Robotics Research* 2, no. 1 (January 2013): 1-9.

Algorithm in Python for Simulating Hydraulic Network for Educational Purposes

Prof. Dr. Eng. **Henrique PIZZO**[1, 2,*], Eng. Stud. Res. **Victor SANTOS**[3],
Prof. Spec. Eng. **Marina EVANGELISTA**[4]

[1] Estácio University of Juiz de Fora, Minas Gerais, Brazil

[2] Municipal Water and Sewage Company of Juiz de Fora, Brazil

[3] Federal University of Juiz de Fora, Brazil

[4] Gaia Engineering, Juiz de Fora, Brazil

* henriquepizzo.estacio@gmail.com

Abstract: *In order to make learning and fixing topics about water distribution networks simpler for students, by allowing quick tests, comparisons with results obtained by hand, and evaluation of the different head losses and nodal pressures generated by each specific situation of input values, an algorithm developed in Python language is presented. After a literature review on the subject of computational models in hydraulic systems and their application in the area of water distribution networks, the steps for the execution of the model are discussed and presented, with some illustrative screens. Finally, a test is carried out to assess the good functioning of the Python algorithm, by comparing its resolution of a random network with the solution by the SCALER software.*

Keywords: *Water distribution networks, Python programming, hydraulic models, education in engineering*

1. Introduction

Water supply system is defined by a set of works, equipment and services intended to supply drinking water to a community for the purposes of domestic consumption, public services and industrial consumption [1]. In general, it is composed of water source, intake, adduction, treatment, reservoir, distribution network, pumping or booster stations. A water distribution network is the unit of the supply system that brings water to the points of consumption (buildings, industries, etc.). It is formed by a set of pipes and special parts arranged conveniently in order to guarantee the good service of the consumption points.
The water supplied by the system must be in sufficient quantity and of the best quality, from a physical, chemical and bacteriological point of view. For the implementation of a water supply system, it is necessary to prepare studies and projects with a view to defining the works to be undertaken. These works must have their capacity determined not only for the current needs, but also for the future service of the community, with construction being planned in stages.

2. Overview of Computer Models in Hydraulic Systems

According to [2, 3], over the last few decades, a huge amount of effort has gone into building computer models for use in water resource planning and management. In all elements of water management, powerful generic software packages are becoming increasingly crucial. With recent improvements in computer technology, virtually everyone working in the water resources and environmental fields now has easy access to desktop computers with all of the hardware capabilities required to run the vast array of available models. New and different technologies are introduced every day in an overwhelming way. Access to globalized information through the internet, communication through emails, the production of increasingly faster processors, the increase in data storage capacity and the development of increasingly robust computer systems, are just a few good examples of this great evolution.
One of the most significant professional problems and possibilities confronting water and environmental practitioners and academics today is to utilize and leverage the fast rising sources of available data and computing capacity. Sensor expansion, large-scale and extensive data

acquisition, increasingly sophisticated modeling tools, digital infrastructure, the internet of things, and the rollout of 5G wireless networks will allow for the development of far more mutualistic relationships between rural residents, municipalities, urban citizens, and businesses [4]. A significant modeling application is the analysis of municipal water distribution networks.
In water distribution networks, hydraulic modeling is used to forecast hydraulic characteristics such as water velocity, flow rate, and pressure. Predictions can be made at various places throughout the network, as well as at the chosen seasons, dates, and periods. As a result, hydraulic characteristics may be predicted in space and time [5].
In the early days of water distribution computer modeling, simulations were primarily used by engineers to solve design problems, to plan fully functional water distribution systems [6]. The use of computer programs became standard practice, initially, because engineers may focus on design decisions because automated calculations save them from tiresome, iterative computations. Second, because models can account for considerably more of the complexity of real-world systems than manual calculations, they boost the engineer's confidence that the design will function after it is implemented. Finally, the simplicity and speed with which models may be employed allows engineers to investigate many more choices under a variety of scenarios, resulting in more cost-effective and resilient solutions.
There is no one strategy to utilize models that is completely right. Reference [7] describes how the application of a model for design goals varies depending on whether the model is used for master planning, preliminary design, subdivision development, or system rehabilitation. As detailed in the study, each model type has a distinct aim and set of attributes.
Models have become more sophisticated and easier to use as software technology has advanced and, because of that, operational workers have adopted computer simulations as a tool to assist them in keeping the distribution system functioning properly. As a result, models began to be utilized to address ongoing issues, examine suggested operational improvements, and plan for unexpected situations. Instead of relying on trial-and-error adjustments in the actual system, the operator may discover the reasons of system issues and propose alternatives that will work the first time by comparing model results with field operations [6].

3. Computer Applications in Education on Water Networks and Related Topics

According to [8], some of the most important characteristics of educational applications include ease of use, simplicity, information quality, and a lower cost for a functioning license. Because typical commercial software is both expensive and complex, free and/or open source code may be a better option for academic purposes.
Reference [9] provides free and helpful software for water distribution networks (WDNs). The software is free and open source, and it makes use of spreadsheet functions and options as well as MS Excel VBA programming. Because of the extensive mathematical processes required, the design of WDNs is one of the most difficult undertakings, particularly for engineering students. Several commercial software packages for the WDN project are prohibitively expensive for students, who frequently require open source software. According to the author, while some open source applications, such as EPANET, are accessible, students are frequently required to develop scripts in order to conduct a simulation with them. Furthermore, EPANET utilizes a different solution approach (global gradient algorithm), which frequently conflicts with the instructional objectives connected with the Hardy-Cross methodology. As a result, there is a scarcity of simple, open source programs ideal for training. The study's software is supposed to fill this need and provide a reliable source for engineers who cannot buy a commercial application.
An extensive set of computer tools for executing an active teaching-learning strategy on an undergraduate hydraulic engineering course in the subject units of pressure flow and free surface flow is presented in [10]. The tools include a variety of easy Excel based programs to help students learn basic principles, as well as a series of practical activities that employ the free professional simulators EPANET and IBER to familiarize students with the tools used in real life. The new technique resulted in more student satisfaction and engagement, as well as more contact with teachers and classmates. To ease their adaptation to different courses and/or degrees, the apps and practical sessions are easily transferable and freely accessible to the community.

References [11, 12] describe the creation of MS Excel applications for optimizing the process parameters in environmental engineering education. The software codes were written in Visual Basic for Applications version 7.0. A variety of test cases were also supplied to evaluate the tool's efficacy in the sectors of air pollution management, water treatment, anaerobic treatment, and water distribution networks for steady-state and extended period simulations. The computed coefficients of determination for each test instance were 0.98 and above. The results indicated that the MS Excel application gives satisfactory rapid and reliable results and may be utilized safely for optimization work in environmental investigations.
For both instructional and practical reasons, a computer program to solve water distribution networks (WDNs) is essential. To resolve WDN, [13] apply three approaches, including the h-based Newton-Raphson method, the finite element method, and the gradient algorithm. These are built with MATLAB and an Excel spreadsheet. The fundamentals of this computer program were discussed step by step using codes because the educational aspects of the system were the major emphasis of the paper. The codes and a software application are supplied with the hope that many instructors and candidates would evaluate them for both educational and practical uses in this engineering discipline.
The same authors of [13] describe in [14] a step-by-step application of Hardy-Cross, Linear Theory, and Q-based Newton-Raphson techniques for addressing water distribution networks employing MATLAB and Excel spreadsheet. These approaches are used to evaluate a basic pipe network in order to focus more on the educational elements of software programs.
Reference [15] presents an instructional software program designed to teach municipal engineering students real-time state modeling of water distribution networks. The state variable values were calculated using the weighted-least-square model and the Davidon-Fletcher-Powell method with real-time data. Network loading, state simulation, and data management were all elements of the software package. Delphi 7.0 was used to code the software and the appropriate graphical user interface. Two evaluation methodologies were used to demonstrate the software tool's effectiveness in teaching and learning. Furthermore, the favorable outcomes spurred software developers and professors to create or at least employ computer-aided instructional tools.
In [16], a new educational methodology called Implementation of Mathematical, Experimental, and Computer-based Education is proposed to investigate the synergistic impact of traditional mathematical solution procedure, visual implementation, and MATLAB-based modeling on engineering students' conceptions and quality of learning. The water discharge problem (a specific application of Bernoulli's principle and Toricelli's law) was selected as an illustration of application within the scope of the study. The paper provided in detail the empirical results of three distinct tank models (vertical cylindrical, conical, and spherical) and the solution methods created in MATLAB, as well as novel equations generated for each lab scale system experimental results. With the involvement of 84 learners, the efficiency of the suggested strategy was statistically tested. The performance of the applied approach was assessed as 97.73 percent, 67.36 percent, and 82.55 percent, accordingly, based on mean values collected from all participants.
In engineering education, online training systems are becoming increasingly popular. Education and management tasks can be merged into a single system by merging the pedagogical form of online learning with laboratory information management systems. A work described in [17] sought to create a collaborative education and administration system for a PHP-based water hydraulics laboratory. Throughout all experimental courses, the system provides a simple and multi-functional educational and administration platform for students and teachers. Attitudes of students were investigated and assessed. The findings demonstrated that the suggested approach might improve educational performance and learning efficacy.

4. Methodology

The network chosen for the simulations has a branched topology, as schematized in Figure 1. In view of the simple educational nature of the work, a very simple configuration network was purposely adopted. The purpose of this expedient was to focus the students' observations exclusively on the variations in the results (head losses and nodal pressures) caused by the different input parameters in the algorithm, without dispersion of their attention, and possible

demotivation, due to more in-depth questions. The network has 06 sections, of which 03 are branches with dead ends, and 01 section (A-B) with no distribution along its length. Such a profile allows several input values to be combined and tested. The pressure at the upstream point (A) must be set by the user.

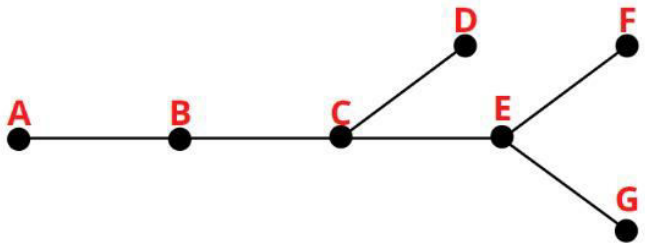

Fig. 1. Hydraulic network

The programming was developed in the Python language. Some libraries were used for data analysis, always aiming to adapt the best data processing model and computational routines. In this sphere, the first library used was Numpy, where it was possible to work with matrices and lists. Afterwards, the Pandas library was used, which includes more resources, through Data Frames. With the two mentioned libraries, it was possible to analyze a dataset without having to resort to huge "for" and "if" loops, facilitating the coding work and making the program better optimized. Figure 2 shows a partial screen of the respective listing.

```
#AB
TrechoDF['CP Jusante'] = [0,0,0,0,0,TrechoDF['CP Montante'][5]-TrechoDF['Perda de Carga Total [m]'][5]]
#BC
TrechoDF['CP Montante'] =[0,0,0,0,TrechoDF['CP Jusante'][5],x]
TrechoDF['CP Jusante'] = [0,0,0,0,TrechoDF['CP Montante'][4]-TrechoDF['Perda de Carga Total [m]'][4],TrechoDF['CP Montante'][5]-TrechoDF['Perda de Carga Total [m
#CD
TrechoDF['CP Montante'] =[0,0,0,TrechoDF['CP Jusante'][4],TrechoDF['CP Jusante'][5],x]
TrechoDF['CP Jusante'] = [0,0,0,TrechoDF['CP Montante'][3]-TrechoDF['Perda de Carga Total [m]'][3],TrechoDF['CP Montante'][4]-TrechoDF['Perda de Carga Total [m]'
#CE
TrechoDF['CP Montante'] =[0,0,TrechoDF['CP Jusante'][4],TrechoDF['CP Jusante'][4],TrechoDF['CP Jusante'][5],x]
TrechoDF['CP Jusante'] = [0,0,TrechoDF['CP Montante'][2]-TrechoDF['Perda de Carga Total [m]'][2],TrechoDF['CP Montante'][3]-TrechoDF['Perda de Carga Total [m]'][
#EF
TrechoDF['CP Montante'] =[0,TrechoDF['CP Jusante'][2],TrechoDF['CP Jusante'][4],TrechoDF['CP Jusante'][4],TrechoDF['CP Jusante'][5],x]
TrechoDF['CP Jusante'] = [0,TrechoDF['CP Montante'][1]-TrechoDF['Perda de Carga Total [m]'][1],TrechoDF['CP Montante'][2]-TrechoDF['Perda de Carga Total [m]'][2]
#EG
TrechoDF['CP Montante'] =[TrechoDF['CP Jusante'][2],TrechoDF['CP Jusante'][2],TrechoDF['CP Jusante'][4],TrechoDF['CP Jusante'][4],TrechoDF['CP Jusante'][5],x]
TrechoDF['CP Jusante'] = [TrechoDF['CP Montante'][0]-TrechoDF['Perda de Carga Total [m]'][0],TrechoDF['CP Montante'][1]-TrechoDF['Perda de Carga Total [m]'][1],T

TrechoDF
```

Fig. 2. Python algorithm partial listing screen

As per [18], Python is one of the most common languages among the community in the area, whether among teachers, data analysts and programming beginners. This fact can be explained through a significant number of libraries and frameworks to solve various real-world problems. Some reasons that made Python reach this level are ease, increased productivity, wide community and popularity, and versatile use.
The positive impact of programming that helps code review processes and understanding what each line is compiling is evident. In this field, the use of descriptive programming, as used, cooperates in the development of the entire algorithm, being able to locate each specific piece of programming [19].

5. Results and Discussion

Input and output data screens are shown in Figures 3 and 4, respectively. The input data to the simulator algorithm are the linear distributed flow rate, lengths of the stretches, diameters of each section (as this is a simulation problem, not a design one), terrain elevations of the notable points (nodes) and pressure at the network's initial node. The output data are the reference flow rates, the head losses, the piezometric (energetic) heads, and the pressures on the nodes. Head losses are determined automatically by routine, through the Hazen-Williams equation, with a roughness

coefficient C of 140, by default, referring to the PVC material for the pipes. The value of C can be changed if other pipe materials are used.

```
Digite a vazão em marcha: 0.0015
Digite a pressão no ponto A: 55
Digite o comprimento to trecho EG (m): 150
Digite a Cota Topográfica à Montate do trecho EG (m): 731
Digite a Cota Topográfica à Jusante do trecho EG (m): 750
Digite o Diâmetro do Trecho EG(mm²): 50

Digite o comprimento to trecho EF (m): 100
Digite a Cota Topográfica à Montate do trecho EF (m): 731
Digite a Cota Topográfica à Jusante do trecho EF (m): 738
Digite o Diâmetro do Trecho EF(mm²): 50

Digite o comprimento to trecho CE (m): 250
Digite a Cota Topográfica à Montate do trecho CE (m): 725
Digite a Cota Topográfica à Jusante do trecho CE (m): 731
Digite o Diâmetro do Trecho CE(mm²): 50

Digite o comprimento to trecho CD (m): 220
Digite a Cota Topográfica à Montate do trecho CD (m): 725
Digite a Cota Topográfica à Jusante do trecho CD (m): 741
Digite o Diâmetro do Trecho CD(mm²): 50

Digite o comprimento to trecho BC (m): 280
Digite a Cota Topográfica à Montate do trecho BC (m): 719
Digite a Cota Topográfica à Jusante do trecho BC (m): 725
Digite o Diâmetro do Trecho BC(mm²): 75

Digite o comprimento to trecho AB (m): 300
Digite a Cota Topográfica à Montate do trecho AB (m): 711
Digite a Cota Topográfica à Jusante do trecho AB (m): 719
Digite o Diâmetro do Trecho AB(mm²): 75
```

Fig. 3. Input data screen

	Trecho	Montante	Jusante	Comprimento (m)	CT Montante	CT Jusante	Diâmetro (mm²)	Ponto seco?	Marcha	Vazão Jusante	Vazão Montante	Vazão Fictícia	Perda de Carga Unitária [m/m]	Perda de Carga Total [m]	CP Montante	CP Jusante	Pressão Montante	Pressão Jusante
0	EG	E	G	150.0	731.0	750.0	50.0	Sim	0.225	0.000	0.225	0.1125	0.000122	0.018355	764.351261	764.332906	33.351261	14.332906
1	EF	E	F	100.0	731.0	750.0	50.0	Sim	0.150	0.000	0.150	0.0750	0.000058	0.005780	764.351261	764.345481	33.351261	14.345481
2	CE	C	E	250.0	725.0	731.0	50.0	Não	0.375	0.375	0.750	0.5625	0.002403	0.600752	764.952013	764.351261	39.952013	33.351261
3	CD	C	D	220.0	725.0	741.0	50.0	Sim	0.330	0.000	0.330	0.1650	0.000249	0.054676	764.952013	764.897337	39.952013	23.897337
4	BC	B	C	280.0	719.0	725.0	75.0	Não	0.420	1.080	1.500	1.2900	0.001549	0.433724	765.385737	764.952013	46.385737	39.952013
5	AB	A	B	300.0	711.0	719.0	75.0	Não	0.000	1.500	1.500	1.5000	0.002048	0.614263	766.000000	765.385737	55.000000	46.385737

[ ]

Fig. 4. Output data screen

The developed algorithm allows tests by students, with comparisons with solutions made by hand, with more direct and clear assimilation and verification between the varied impacts of the situations raised, approached and simulated by themselves, using different data.

5.1 Comparison Test

In order to verify the proper functioning of the proposed algorithm, it was contrasted with the SCALER software [20, 21]. For this purpose, the data for the network of the present work were arbitrated, and are presented in Table 1.

The length values of sections and diameters were taken randomly, however within a reasonableness of real situations. The pressure at the upstream node (A) was set as 55.000 mH2O, and the flow distributed along the sections was 0.0015 L/s/m, resulting from the total flow rate demanded by the network divided by its useful length (i.e., the length in which there is distribution).

Table 1: Hydraulic network data

Branch	Length (m)	Diameter (mm)	Upstream node terrain elevation (m)	Downstream node terrain elevation (m)
A-B	300	75	711.000	719.000
B-C	280	75	719.000	725.000
C-D	220	50	725.000	741.000
C-E	250	50	725.000	731.000
E-F	100	50	731.000	750.000
E-G	150	50	731.000	750.000

By using Python algorithm, the values of nodal pressures in nodes A, B, C, D, E, F, and G were, respectively, 55.000 (pressure set), 46.386, 39.952, 23.897, 33.351, 14.345, and 14.333 mH2O. Solving the network, with the same data, both manually and through the SCALER software, the same nodal pressure values were obtained as those generated by the Python algorithm. In this way, it was possible to verify its correct operation.

6. Conclusions

A computational algorithm for simulating water distribution networks in Python language was introduced. This has the function of contributing to the increase in the understanding of concepts on the topic by students, as it provides agility to the testing process and verification of results due to the different configurations of input data. The accuracy of the algorithm was validated by a simple situation and it is intended to be applied to larger networks, including networks with closed loop and distribution along the stretches, simultaneously.

Acknowledgments

The authors are grateful for the grant received from the Pesquisa Produtividade (Research Productivity) 2022 Estácio Juiz de Fora Program.

References

[1] Azevedo Netto, J. M., M. F. Fernandez, R. Araujo, and A. E. Ito. *Hydraulics Manual* (Manual de Hidráulica). São Paulo, Blucher, 2013.
[2] Wurbs, R. A. *Computer Models for Water Resources Planning and Management*. College Station, Texas A&M University, 1994.
[3] Kimura, A. *Computing Applied to Reinforced Concrete Structures* (Informática Aplicada a Estruturas de Concreto Armado). São Paulo, Oficina de Textos, 2018.
[4] Wagener, T., D. Savic, D. Butler, R. Ahmadian, T. Arnot, J. Dawes, S. Djordjevic et al. "Hydroinformatics education – the water informatics in science and engineering (WISE) centre for doctoral training." *Hydrology and Earth System Sciences* 25, no. 1 (May 2021): 2721–2738. https://doi.org/10.5194/hess-25-2721-2021.
[5] Muhammetoglu, A., H. Muhammetoglu, A. Adigüzel, Ö. İritaş, and Y. Karaaslan. "Management of water losses in water supply and distribution networks in Turkey." *Turkish Journal of Water Science and Management* 2, no. 1 (January 2018): 58–75. https://doi.org/10.31807/tjwsm.354298.
[6] Walski, T. M., D. V. Chase, D. A. Savic, W. Grayman, S. Beckwith, and E. Koelle. *Advanced Water Distribution Modeling and Management*. Bentley Institute Press, 2004.
[7] Walski, T. M. "Optimization and pipe sizing decisions." *Journal of Water Resources Planning and Management* 121, no. 4 (July/August 1995): 340–343. https://doi.org/10.1061/(ASCE)0733-9496(1995)121:4(340).
[8] Drumea, A. "Education in development of electronic modules using free and open source software tools." HIDRAULICA Magazine, no. 3-4 (2012): 54–60. https://hidraulica.fluidas.ro/2012/3_4/54_60.pdf.
[9] Gokyay, O. "An easy MS Excel software to use for water distribution system design: A real case distribution network design solution." *Journal of Applied Water Engineering and Research* 8, no. 4 (October 2020): 1–8. https://doi.org/10.1080/23249676.2020.1831975.
[10] Bermúdez, M., J. Puertas, and L. Cea. "Introducing Excel spreadsheet calculations and numerical simulations with professional software into an undergraduate hydraulic engineering course."

Computer Applications in Engineering Education 28, no. 1 (January 2020): 193–206. https://doi.org/10.1002/cae.22185.

[11] Demir, S., A. Karadeniz, H. C. Yörüklü, and N. M. Demir. "An MS Excel tool for parameter estimation by multivariate nonlinear regression in environmental engineering education." *Sigma Journal of Engineering and Natural Sciences* 35, no. 2 (2017): 265–273. https://sigma.yildiz.edu.tr/article/560.

[12] Demir, S., N. M. Demir, and A. Karadeniz. "An MS Excel tool for water distribution network design in environmental engineering education." *Computer Applications in Engineering Education* 26, no. 2 (August 2017): 203–214. https://doi.org/10.1002/cae.21870.

[13] Niazkar, M., and S. H. Afzali. "Analysis of water distribution networks using MATLAB and Excel spreadsheet: h-based methods." *Computer Applications in Engineering Education* 25, no. 1 (January 2017): 129–141. https://doi.org/10.1002/cae.21786.

[14] Niazkar, M., and S. H. Afzali. "Analysis of water distribution networks using MATLAB and Excel spreadsheet: Q-based methods." *Computer Applications in Engineering Education* 25, no. 2 (March 2017): 277–289. https://doi.org/10.1002/cae.21796.

[15] Zhang, H., X. Zhou, L. Wang, K. Wang, and W. Wang. "Development of a software tool for teaching real-time state simulation of water distribution networks." *Computer Applications in Engineering Education* 26, no. 3 (May 2018): 577–588. https://doi.org/10.1002/cae.21909.

[16] Yetilmezsoy, K. "IMECE - Implementation of mathematical, experimental, and computer-based education: A special application of fluid mechanics for civil and environmental engineering students." *Computer Applications in Engineering Education* 25, no. 5 (September 2017): 833–860. https://doi.org/10.1002/cae.21871.

[17] Wang, H., H. Xu, Q. Li, and Y. Fu. "PHP-based collaborative education and management system for water hydraulic laboratory." *Computer Applications in Engineering Education* 26, no. 2 (March 2018): 259–271. https://doi.org/10.1002/cae.21882.

[18] Matthes, E. *Python Crash Course: A Hands-On, Project-Based Introduction to Programming* (Curso Intensivo de Python: Uma introdução prática e baseada em projetos à programação). Translated into Portuguese by L. A. Kinoshita. São Paulo, Novatec Editora, 2016.

[19] McKinney, W. *Python for Data Analysis: Data Wrangling with Pandas, Numpy, and IPython*. Sebastopol, O'Reilly Media, 2017.

[20] Ignácio, J. P. C., M. V. Nascimento, P. H. G. Oliveira, R. Platz, and H. S. Pizzo. "SCALER - software for sizing water distribution networks (SCALER - software para dimensionamento de redes de distribuição de água)." *Brazilian Journal of Development* 7, no. 7 (July 2021): 71854–71877. https://doi.org/10.34117/bjdv7n7-387.

[21] Pizzo, H. S., J. P. C. Ignácio, and M. V. Nascimento. "Review of water network analysis and validation of SCALER hydraulic simulator." *Journal of Civil Engineering Frontiers* 3, no. 1 (January/June 2022): 1–11. https://doi.org/10.38094/jocef30142.

Determination of Energy Performance for a New Type of a Rotating Machine That Transports Fluids

PhD Student **Mariana Mirela STOICAN (PRISECARU)**[1,*], Prof. Dr. Eng. **Nicolae BĂRAN**[1], PhD Student **Gabriel FICHER-SZAVA**[1]

[1] University Politehnica of Bucharest

[*]mirela.prisecaru@yahoo.com

Abstract: *The paper presents a mathematical model of establishment for a constructive solution regarding:*
- the maximum flow rate transported by the machine;
- the power required to drive this machine, which is a volumetric pump with two specially processed rotors.
The aspects regarding the transport of multiphase fluids and the advantages of using this rotating machine are revealed.

Keywords: *Rotating machine, profiled rotor, rotating piston, volumetric pump*

1. Introduction

A current direction of research is to improve the performance of rotating machine that carry fluids. Optimizing the interior architecture of work machines is a very important issue, a problem studied both in our country and abroad.
Currently, existing machines in the art evolve over time to flow rate configurations that make them as imperfect as possible [1], [2].
Both motor and work machines evolve over time in the following direction:
- For motor machines, the aim is to produce the maximum mechanical work yielded outside.
- For work machines, the minimum consumption of mechanical work from the outside is sought.
For rotating work machines with profiled rotors, the problem regarding the architecture of the rotor is the optimization of its geometry and the choice of parameters that lead to a more efficient fluid transport.
Minimizing the drive power of volumetric rotor machines and finding a new profiled rotor architecture are key elements in designing and designing a new rotating machine.
The machines are aggregates used for the transformation of energies from one form to another with the help of a movable organ which can be: profiled rotor, piston, and blade.
Depending on their required purpose, the machines can be classified into two categories [3], [4]:
1. Power machines (motor machines) that convert a certain form of energy into mechanical energy; for example: internal combustion engines, steam turbines, gas turbines, etc.
2. Working machines that convert mechanical energy into another form of energy, for example: pumps, fans, compressors.
Both power and working machines are traversed by fluids; according to the flow variation parameters, they are classified as follows (table 1):
a. Hydraulic machines that drive or are driven by fluids, neglecting thermal phenomena.
b. Thermal machines that carry gases or vapors (or are driven by them) in which the thermal processes that occur cannot be neglected.
The achievement of high performance rotating machines (pumps, fans, blowers) is topical.
The researches aims to build machines to ensure the transformation of the motor moment received from the shaft into useful effects, but with small energy losses.
Table 1 presents the classification of rotating machines with profiled rotors according to the purpose pursued and the adopted constructive solution [5], [6].
Table 2 shows the rotating pumps in the category of rotating work machines for fluid conveyance.

Table 1. Classification of rotating machines with profiled rotors.

Working machines	Pumps for driving fluids or with suspensions
	Fans for transporting gases or vapors
	Blowers for gas and vapor compression
Force machines	Hydraulic motor
	Pneumatic motor
	Steam engine or combustion gases

Table 2. Pump categories

Volumetric pumps	Piston pumps	a) Single cylinder pumps
		b) Poly Cylinder pumps
		c) Axial piston pumps
	Rotating pumps	d) Blade pumps
		e) Gear pumps
		f) Screw pumps
		g) Lobe pumps
Non - volumetric pumps	Centrifugal pumps	
	Axial pumps	

A more difficult problem is to make a rotating machine that can be used as a working machine or a force machine that is theoretically a "reversible" machine.
Such a machine must provide:

- transforming the useful moment with minimal losses when it works as a working machine.
- maximum use of the energy of the working agent for shaft actuation when it is working as a force machine.

2. Determination of the maximum flow rate of fluid conveyed for a certain constructive solution

The machine consists of two identical rotors (3, 4) of special shape, which rotate at the same speed inside some casings (2, 5); the synchronous rotation of the two rotors is ensured by a cylindrical gear consisting of two toothed gear wheels with inclined teeth, located inside or outside the machine. The gears have the same diameter of division and are mounted on shafts 7 and 8; they provide a rotation motion so that the rotating pistons (6) of the upper rotor enters into the cavities (10) of the lower rotor.
The fluid in the chamber (1) is taken up by the rotating pistons (6) and transported to the discharge chamber (9).

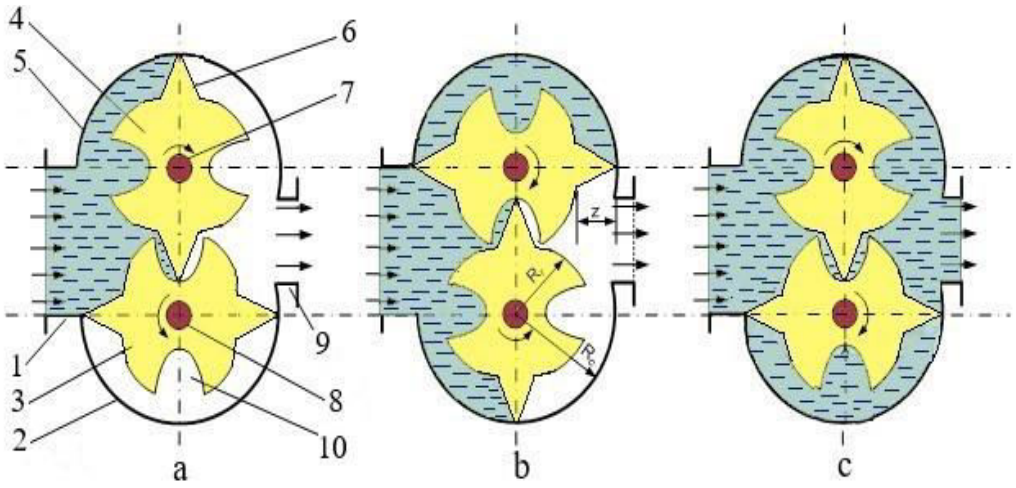

Fig. 1. The operating principle of the rotating volumetric machine
1 - suction chamber; 2 - lower casing; 3 - lower rotor; 4 - upper rotor; 5 - upper casing; 6 - rotating piston; 7 - driven shaft; 8 - discharge chamber; 9 - driving shaft; 10 - cavity in which the upper rotor piston enters

The constructive solution shown in figure 1 ensures a good resistance of the piston and two sealing areas: between the tip of the piston and the inside of the housing and between the tip of the piston and the cavity.

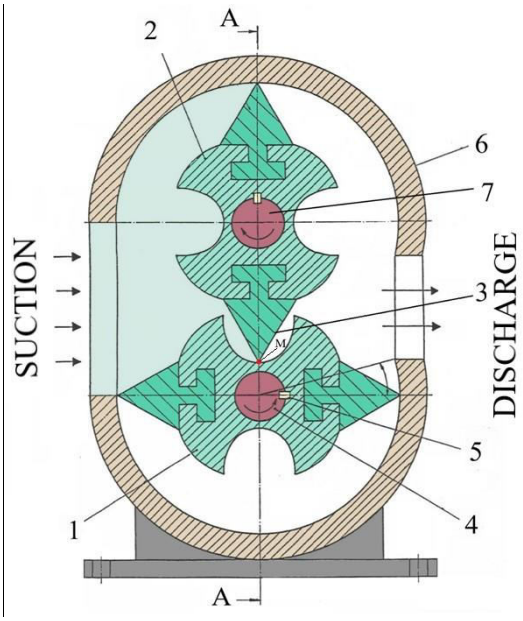

Fig. 2. Cross section through the rotating machine
1 - lower rotor; 2 – upper rotor; 3 - triangular piston; 4 - shaft; 5 - rectangular wedge; 6 - machine casing

Figure 2 shows that between the upper rotor (2) and the lower rotor (1) there is only one contact point noted with M; if the piston (3) is built with a larger base, it will lock in the cavity in the rotor (1). The fluid entering the suction chamber (4) is transported to the discharge chamber (9) by the rotating pistons (3, 6). Figure 3 shows the fluid flow after a 90 ° rotation of the two rotors. The useful volume of the fluid conveyed V_u is between the two rotating pistons and the lower housing. Figure 3 shows a cross section through the rotating machine [6], [7].

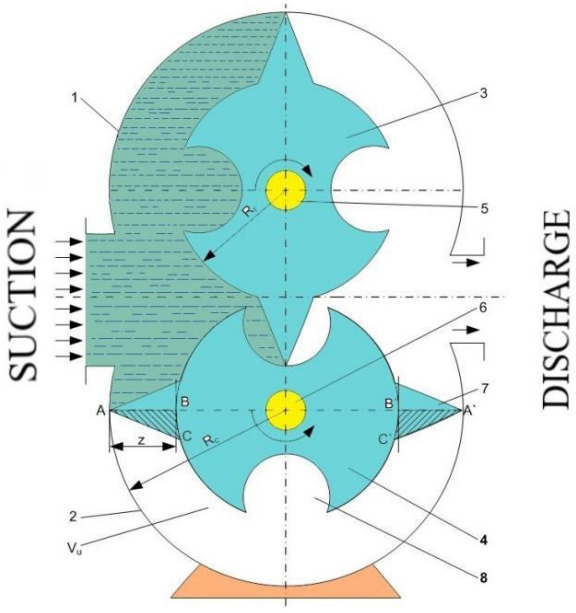

Fig. 3. Cross section through the rotating working machine
1 - upper casing; 2 - lower casing; 3 - upper rotor; 4 - lower rotor; 5,6 - shaft;
7 - rotating piston; 8 - cavity in which the upper rotor piston enters

Figure 3 shows that the useful volume V_u is reduced by the volumes of the prisms ABC and A'B'C'; the two equal prisms give the volume of a piston of triangular section, with the following dimensions: height: z = 30 [mm]; base: b = 30 [mm]; length: l = 50 [mm].

Neglecting the area of the section between the base of the prism and the rotor, the volume of the prism will be

$$V_p = A_{base} \cdot l = \frac{1}{2} \cdot b \cdot z \cdot l = \frac{1}{2} \cdot 0.03 \cdot 0.03 \cdot 0.05; \qquad V_p = 0.0225 \cdot 10^{-3} \quad [m^3/rev] \tag{1}$$

Theoretical flow rate of the machine with triangular pistons $\bar{V} = \pi lz(z + 2R_r) \cdot \frac{n_r}{30}$ [m³/s] will be reduced by V_p.
where: V_p - the prism volume of a piston of triangular section.
The volumetric flow rate of fluid conveyed by a single rotor of length l [m] and speed n_r [rev/min] will be

$$\bar{V}_u = \left[\pi lz\left(z + 2R_r\right) - V_p\right] \quad [m^3/rev]. \tag{2}$$

The rotating machine has two identical rotors, so the fluid flow rate will be:

$$\bar{V} = \left[\pi lz(z + 2R_r) - \frac{1}{2} bzl\right] \cdot \frac{n_r}{30} \quad [m^3/s], \tag{3}$$

$$V = \left[\pi \cdot 0.05 \cdot 0.03(0.03 + 2 \cdot 0.05) - \frac{1}{2} \cdot 0.03 \cdot 0.03 \cdot 0.05\right] \cdot \frac{500}{30} \tag{4}$$

$$V = 0.00983\ [m^3/s] = 35.388[m^3/h] \tag{5}$$

Table 3. Values $V = f(n_r)$

n_r [rev/min]	100	200	300	400	500
$\bar{V}$ [m³/s]	0.001966	0.003932	0.005898	0.007864	0.00983
$\bar{V}$ [m³/h]	7.0776	14.1552	21.2328	28.3104	35.388

3. Mathematical determination of the relationship between the rotor radius and the height of the rotating piston

The main dimensions of the pump, which has two identical rotors, must first be determined; must be known [7], [8]: *l* - rotor length [m]; R_r - rotor radius [m]; *z* - height of the rotating piston [m].
The radius of the housing R_c results from the sum of the radius of the rotor R_r and the height of the piston *z* (figure 1).
What is the connection between z and R_r? How big can *z* be in relation to R_r?
To solve this problem we will consider a single piston (5) fixed to the lower rotor (figure 4).
The rotor radius (1) is extended by a length (*z*) and thus the line *01B* reaches the rotor (2) at point *A*. Theoretically, when point *K* reaches point *D*, point A reaches *K*, respectively point *N* reaches *K*, because the length of the circle arcs *AK*, *KD* and *KN* is the same. When the piston (5) exits the gap created in the rotor (2), points *A* and *N* reach point *K*; the sealing between the two rotors being ensured by the direct contact between the lateral surfaces of the rotors.
From the rectangular triangle O_1O_2A results:

$$O_1O_2^2 = AO_2^2 + AO_1^2 \tag{6}$$

$$(2R_r)^2 = R_r^2 + (R_r + z)^2 \tag{7}$$

relations that becomes:

$$z^2 + 2R_r z - 2R_r^2 = 0 \quad (8)$$

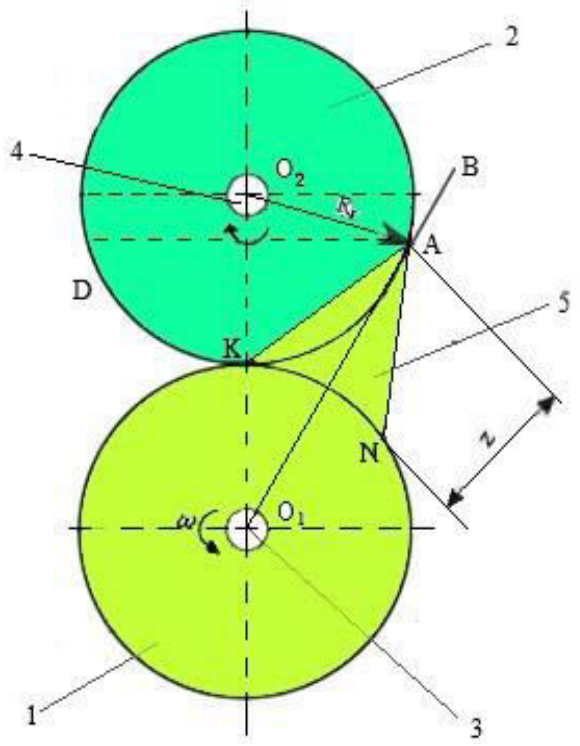

Fig. 4. Calculation notations.
1 - lower rotor; 2 - upper rotor; 3 - driving shaft;
4 - driven shaft; 5 - rotating piston of triangular shape [9]

4. Determination of the driving power of the rotating machine with profiled rotors

For calculating the driving power of the rotating machine, it is known from the literature [13]:

$$P = \bar{V} \cdot \Delta p \ \text{[W]}, \quad (9)$$

where Δp – pressure increase [N/m^2], $\Delta p = \rho g H$ [N/m^2];
H – pumping height [m];
ρ_l – the density of the conveyed fluid [kg/m^3].
In the next paragraph we will analyze this relationship.
Analyzing the formula of the volume flow circulated by the rotating machine:

$$\bar{V}_u = \left[\pi l z\left(z + 2R_r\right) - V_p\right] \cdot \frac{n_r}{30} \quad \text{[m}^3\text{/s]} \quad (10)$$

and the driving power of the rotating machine:

$$P = \bar{V} \cdot \Delta p = \left[\pi \cdot l \cdot z \cdot (z + 2R_r) \cdot \frac{n_r}{30} - V_p\right] \cdot \Delta p \ \text{[W]}. \quad (11)$$

it is found that the volume flow rate $\bar{V}$ and the driving power *P* of the rotating machine are influenced by the constructive parameters (rotor length, piston height, rotor radius) and functional parameters (rotating machine speed, pressure increase).

From the relationship: $R_c = R_r + z$ [m], it is replaced in the relationship (11): $R_r = R_c - z$ [m] and it results

$$P = \left[\pi l\left(2R_c \cdot z - z^2\right) - V_p\right] \cdot \frac{n_r}{30} \cdot \Delta p \quad \text{[W]} \tag{12}$$

$$P_H = 0.00983 \cdot 0.3924 \cdot 10^5 = 385.729 \quad [W]. \tag{13}$$

Neglect the volume of the piston prism, perform the function derivative and equal 0.

$$P'(z) = 0 \Rightarrow 2R_c - 2z = 0 \tag{14}$$

It results $$z = R_c\,. \tag{15}$$

In conclusion, the driving power of the machine is maximum when $z = R_c$ (figure 5).

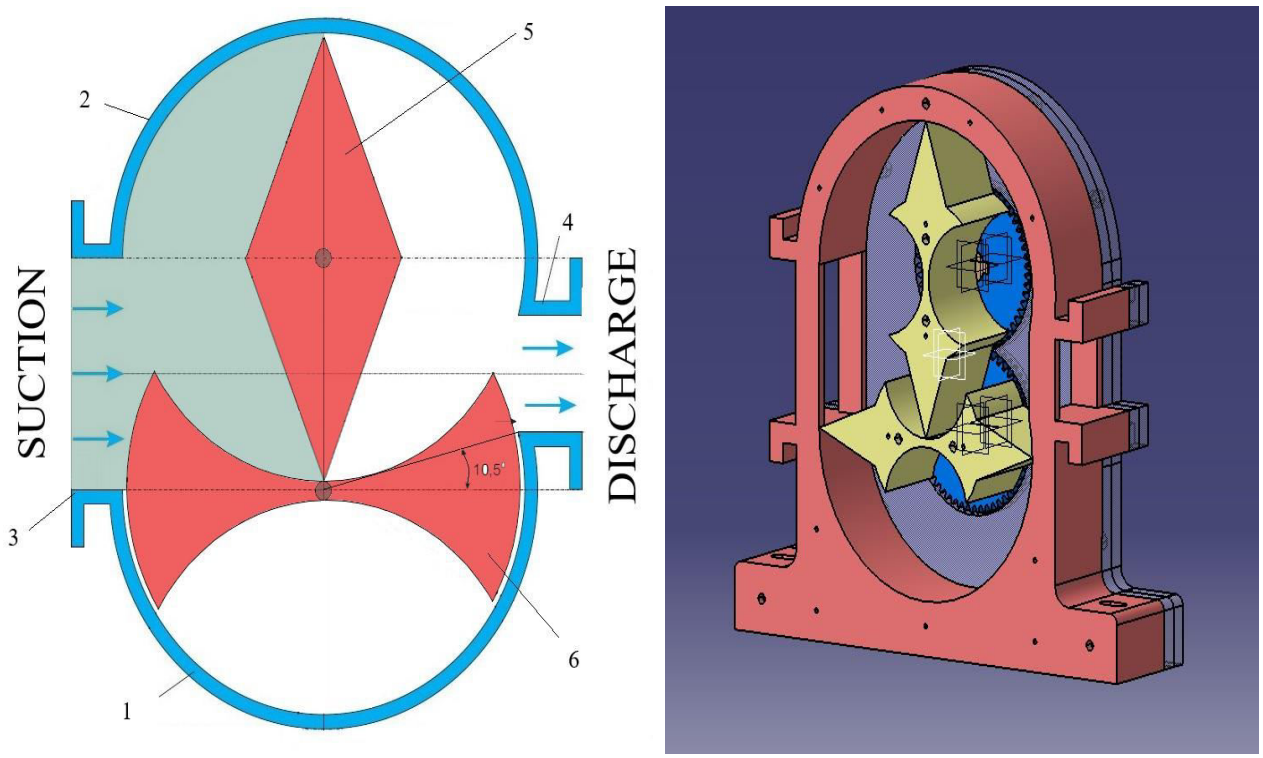

Fig. 5. Cross section through the rotating machine
1 – lower housing; 2 – upper housing; 3 – fluid suction connection;
4 – fluid discharge connection; 5 – upper rotor with two rotating pistons; 6 – lower rotor

5. Conclusions

1. Choosing the shape of the rotors leads to an increase in the flow rate of this rotating machine with profiled rotors.

2. In order to achieve the constructive solution proposed, increased precision is required due to the fact that if there are large clearances between the rotor and the housing, the volume efficiency of the pump will decrease.
3. The driving power is influenced by the flow rate, by the increase of pressure (Δp) made by the rotating machine between suction and discharge, by the nature of the fluid conveyed.

References

[1] Băran, N. *Rotating thermic machines. Working machines. Force machines* / Masini termice rotative. Masini de lucru. Masini de forta. Bucharest, MATRIXROM Publishing House, 2001.
[2] Băran, N. *Working rotating thermic machines. Machines with profiled rotors. Blade machines* / *Mașini termice rotative de lucru. Mașini cu rotoare profilate. Mașini cu palete*. Bucharest, MATRIXROM Publishing House, 2003.
[3] Dobrovicescu, Alexandru, Nicolae Băran, Alexandru Chisacof, Mircea Marinescu, Petre Răducanu, and Alin Ovidiu Motorga. *Bases of Technical Thermodynamics. Elements of Technical Thermodynamics* / *Bazele termodinamicii tehnice*. *Elemente de termodinamică tehnică*. Bucharest, Politehnica Press Publishing House, 2010.
[4] Exarhu, M. *Hydraulic and pneumatic machines and installations* / *Masini si instalatii hidraulice și pneumatice*. Bucharest, ANDOR TIP S.R.L. Publishing House, 2006.
[5] Hanlon, Paul C. (editor). *Compressor Handbook*. Library of Congress Cataloging-in-Publication Data. New York, McGraw Hill, 2001.
[6] Motorga, A. *Influence of constructive and functional parameters on the performances of rotating machines with profiled rotors* / *Influența parametrilor constructivi și funcționali asupra performanțelor mașinilor rotative cu rotoare profilate*. PhD Thesis, Faculty of Mechanical Engineering and Mechatronics, Politehnica University of Bucharest, 2011.
[7] Băran, Nicolae, Despina Duminica, Daniel Besnea, and Antonios Detzortzis. „Theoretical and Experimental Researches Regarding the Performances of a New Type of Rotating Machine with Profiled Rotors." *Advanced Materials Research* 488-489 (2012): 1757-1761.
[8] Burchiu, V., I. Santău, and O. Alexandrescu. *Pumping installations* / *Instalaţii de pompare*. Bucharest, Didactic and Pedagogical Publishing House, 1982.
[9] Hâncu, S. *Fluid Mechanics - Mécanique des fluides: contributions*. Bucharest, CONSPRESS Publishing House, 2011.
[10] Reynolds, A. J. *Turbulent Flows in Engineering* / *Curgeri turbulente în tehnică*. Bucharest, Technical Publishing House, 1982.
[11] Băran, N., D. Besnea, and A. Motorga. "Elements of computing the architecture and manufacturing technology for a new type of profiled rotor." Paper presented at the International Conference, 6th Workshop on European Scientific and Industrial Collaboration on promoting Advanced Technologies in Manufacturing WESIC'08, Bucharest, Romania, September 25-26, 2008.
[12] Stoican (Prisecaru), Mariana Mirela, and Nicolae Băran. "Designing and dimensioning of a new type of pump that can be used in the field of land reclamation*."* Paper presented at the 10th International Conference on Thermal Equipment, Renewable Energy and Rural Development TE-RE-RD 2021, Bucharest, Romania, June 10-12, 2021.
[13] Baran, N., D. Besnea, R. Mengher, and E. Munteanu. "Research on establishing the contour shape of the rotor profile in a new type of rotary compressor" / "Cercetari privind stabilirea formei conturului profilului rotorului la un nou tip de compresor rotativ." Paper presented at the 7-th International Conference on Mechatronics and Precision Engineering (COMFIN 7), Bucharest, Romania, May 27 – 29, 2004.
[14] Stoican (Prisecaru), M. M., N. Băran, D. Besnea, and A. F. S. Almaslamani. "Calculation elements for establishing the design of a rotating machine that transports fluids." *International Journal of Mechatronics and Applied Mechanics*, no. 7 (2020): 61-64.
[15] Almaslamani, Ammar Fadhil Shnawa, and Mariana Mirela Stoican (Prisecaru). "Calculation relations regarding the architecture of a rotating machine for transports fluids." *International Journal for Research in Applied Science and Engineering Technology (IJRASET)* 8, no. 3 (March 2020): 61 - 66.

Constructive and Technological Considerations on the Realization of a Prototype of a Rotary Valve Made with 3D Printed Components with UV Resin

Prof. habil. dr.eng. ec. **Mircea Dorin VASILESCU**[1,*]

[1] Polytechnic University Timisoara, Mechanical Faculty, Department MMUT, Sq. Victoriei, no. 2

* mircea.vasilescu@upt.ro

Abstract: *This study is intended to be the first part of a series of technological studies to determine the possibility of realizing pneumatic and/or hydraulic components using 3D additive manufacturing processes with photopolymerizable resins. Since the problem of the environment protection is an important component, the author initiated a study on the structural and technical aspects of the efficient realization of a rotary valve prototype. Finally, considering the correlation and determination of dimensional repeatability of 3D printed parts using a polymerization process with a mask (MSLA) with light-emitting diodes, it is possible to transfer this study to industrial fabrication of this component. At this stage of the study, aspects of alignment in the printing of the analysed part assembly are also identified, as well as the way to determine its positioning and to subsequently correct it for surfaces with changes in flatness or cylindricity.*

Keywords: *MSLA, 3D printing, resin, pneumatic/hydraulic valve*

1. Introduction

In the current economic conjuncture, determined both by the energy costs of manufacturing aluminium components, but also from other metallic and non-metallic materials, the approach of some technological manufacturing alternatives is becoming more and more important.
The present work addresses both the CAD design part of such components made of aluminium and steel respectively [1], but also the practical realization of these components taken into consideration the CAM and additive manufacturing.
For the present study, a valve with two paths and two positions was chosen. At the same time, it is important to note that the realization of this component will be integrated into more complex constructive solutions that use as an active environment air with pressures of up to 10 atmospheres and water with pressures of up to 50 atmospheres.
It should also be emphasized that the technology envisaged is that of additive manufacturing by optical photopolymerization with an LCD screen. This manufacturing technology was chosen for several reasons. The first is determined by the fact that compared to the other additive manufacturing methods, especially the one performed by the thermoplasty method, which has been encountered more frequently so far in the specialized literature [2, 3], the generated layer is much more compact both vertically and horizontally. Also, the dimensional accuracy of surface realization is in the range of 50 microns, and the quality of the surface generated is the best [4].

2. Constructive CAD-CAM consideration

From a constructive point of view, a rotary valve has a relatively parallelepiped or cubic construction depending on its functional role, one or more inputs, and one or more outputs, respectively. The overall constructive solution is presented in (Figure 1) where it can be observed that we have a lower prismatic body and a rotating cylindrical element, with the possibility of rotation at 360° degree [5].

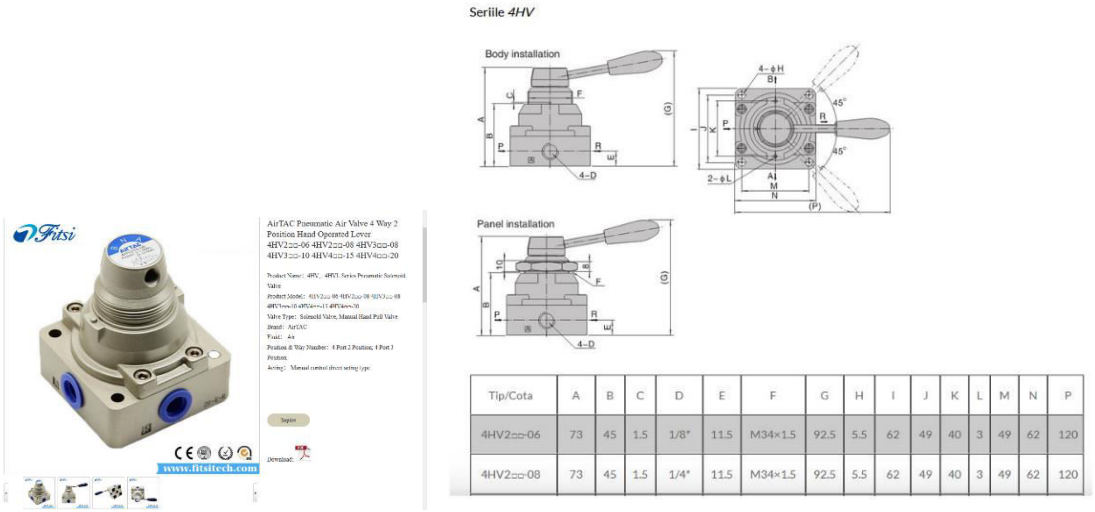

Tip/Cota	A	B	C	D	E	F	G	H	I	J	K	L	M	N	P
4HV2□□-06	73	45	1.5	1/8"	11.5	M34×1.5	92.5	5.5	62	49	40	3	49	62	120
4HV2□□-08	73	45	1.5	1/4"	11.5	M34×1.5	92.5	5.5	62	49	40	3	49	62	120

Fig. 1. Constructive solution [5]

2.1 CAD consideration for constructive solution

To be able to use these elements in a constructive solution, we have the manufacturer generate them in a 3D CAD solution. The second solution is to generate them based on the size of these elements and an image of the constructive solution. It should be noted that usually the second solution is faster and, in some condition, safer as will be seen below given the aspects of mounting the components.
For a given case (rotary valve), the body of valve has two entry and two exit orifices, depending on the position of the central rod.
To understand its construction and how to assemble or use it, let us consider the individual components. This element is presented in the logical order of its position in the design where the construction valve is created.
The first of these is the body of the valve (Figure 2). For the constructive CAD design solution, the method used was based on scaling the view of the constructive element and inserting it into the side view. The advantage of the method is determined by the fact that it is no longer necessary to measure the dimensions of the element in the scaled picture, thus reducing the design time. The program used to design the component was the educational version of Inventor 2022 [6].

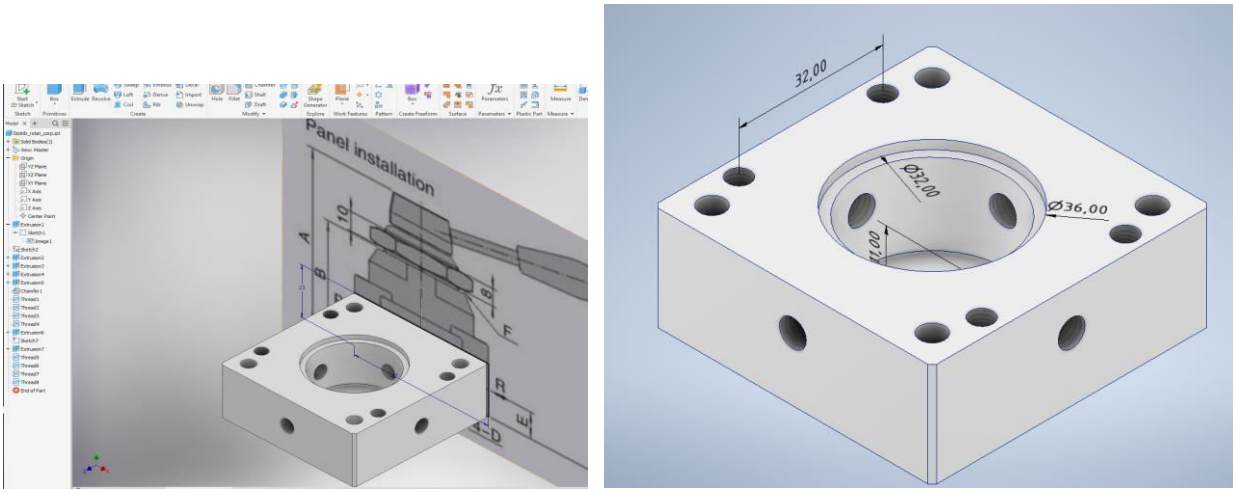

Fig. 2. Constructive body of the valve left picture and CAD construction, right important dimensional surface

The second element that comes into contact with the body is the clamps of the centring element (Figure 3). It can be seen from the picture on the left side of (Figure 3) that the realization of important surfaces is obtained by using the commands for cutting some circular areas. It is

important to consider that the dimensions of the circular areas to be made with a play of at least 0.5 mm within the radius of the homologous dimensions on the body with which it comes into contact. The corresponding connecting dimensions are arranged on the body of the generated 3D part in order to correlate them with those of the parts with which it comes into contact, namely the body of the valve and the conic element for fixing and positioning the rotating central element.

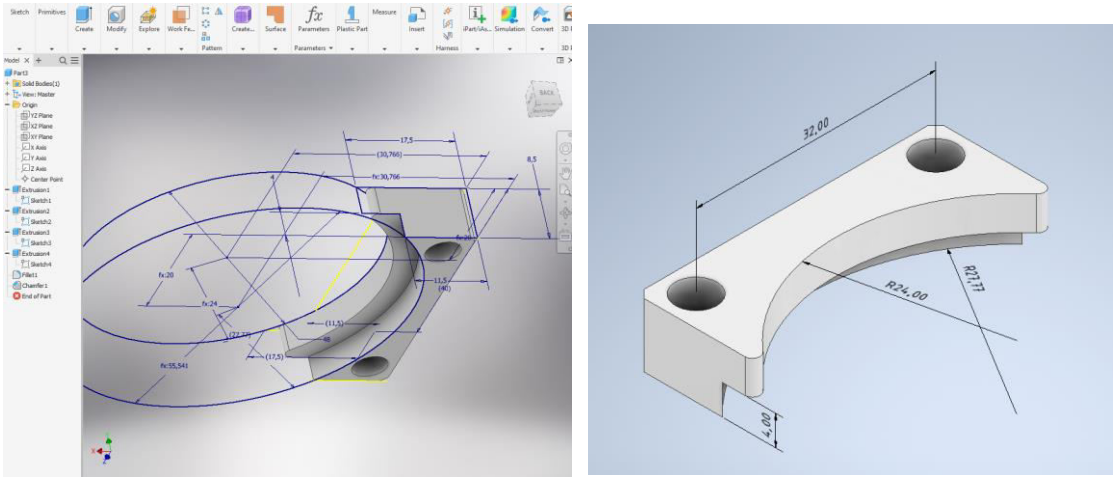

Fig. 3. Constructive clamp body of the valve left picture and CAD construction, right important dimensional surface

The truncated cone element is presented in (Figure 4 left), which is intermediate between the clamps and the rotating centre element which can be seen in (Figure 4 right). This element is positioned on the surface of the rotating valve body.

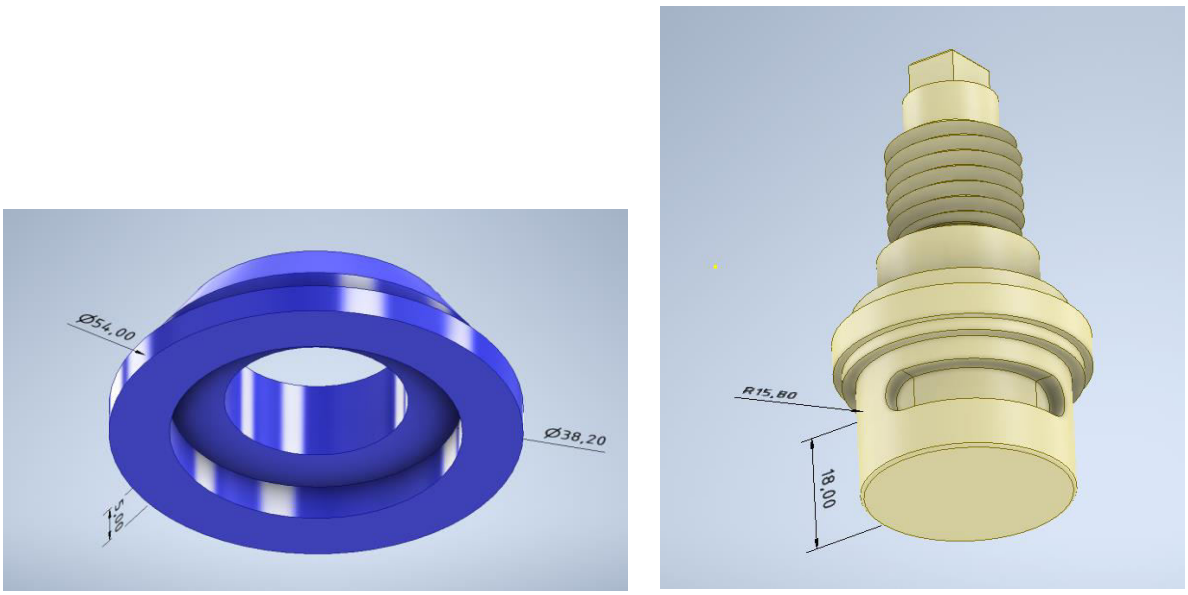

Fig. 4. Constructive body of the left truncated cone element and right the rotating center element

After generating these elements, we will proceed to position the 3D designed elements in order to start the construction of the rotary valve. The assembly order is that of inserting the rotating element into the body of the rotating valve, after which the ring-truncated cone element of fastening and pressing is inserted, respectively, into the fastening and positioning clamps on the side (Figure 5).

To be able to see whether the circuit is properly positioned in relation to the holes in the body, the transparency in the property command of the above-mentioned component will be assigned (Figure 6). It can be seen that the holes are below the median level of the canal, and the easiest way is to change the position of the four holes by changing the position of the centre of the holes. The final assembly with the control rod and the upper tightening nut can be seen mounted on (Figure 7).

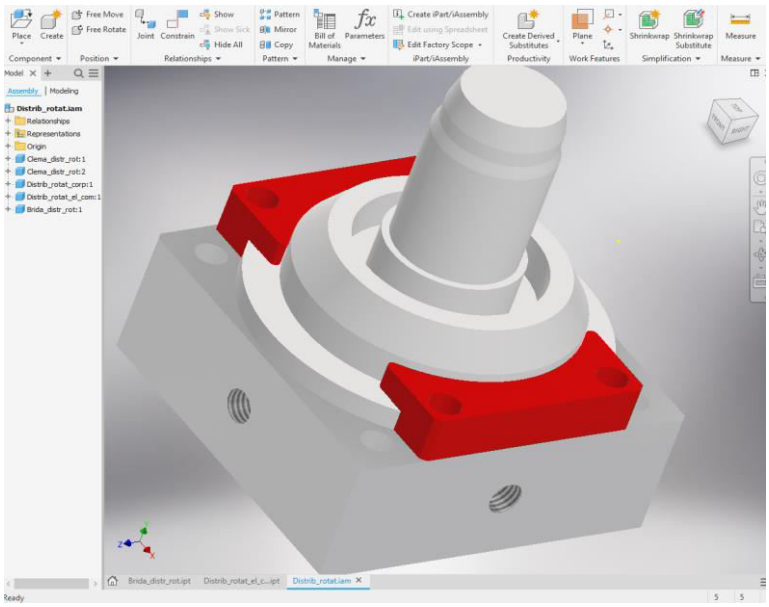

Fig. 5. Mounting of the CAD generated elements

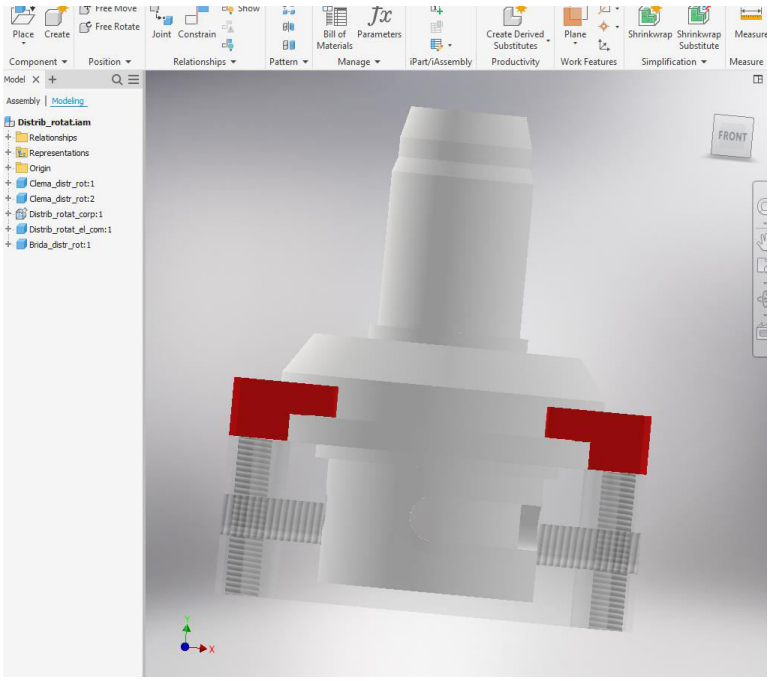

Fig. 6. Transparency of inferior mounting of the CAD generated elements

At this point the design part of the construction is completed and the previously presented parts are exported in solid format for preparation for printing.

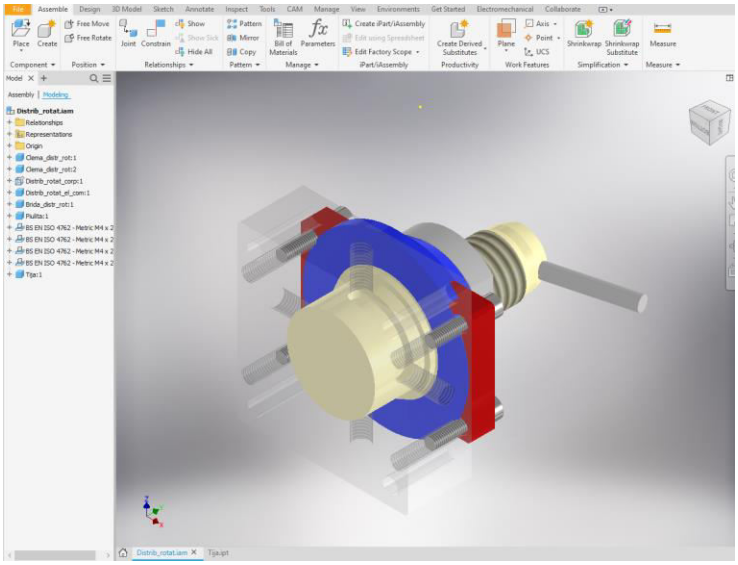

Fig. 7. Assembly mounting of the CAD generated elements

2.2 CAM consideration for elements of constructive solution

The first aspect that is taken into consideration is the roll of the generated components. If the role is for didactical mounting, the generation of the element can be made with a structure with a large dimension inside the body generated. If there is a functional role of this component them must have a smaller dimension, or the body must have a solid structure construction. At the same time, if the component has a static mounting function without mechanical or dynamical functionality, the dimension must be larger.

From the point of view of the mounting dimensions for the realization of the assembly, it is recommended the solution of modifying the dimensions by decreasing or increasing them from the program of generating the structure for printing for the parts that have a symmetry axis (Figure 8). In the other situations, it is recommended to make the correction from the CAD generation part because independent corrections can be made to increase or decrease the different functional dimensions on each area that will be manufactured additively.

The program used to design the layers of polymerized material is of open-source type [7] and is in agreement with both the type of resin used [8] and the printer used for generating the components [9].

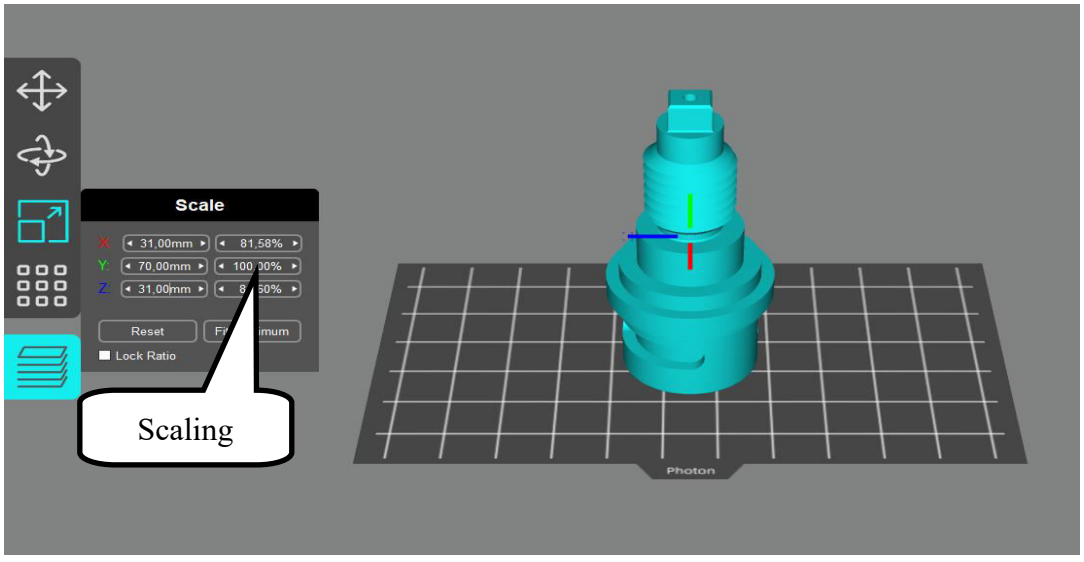

Fig. 8. Scaling of the STL rotating center generated

It is also very important to orient the parts according to the functional role of the printed surfaces because if the printed surface is oriented with supports after this the surface is damaged after the cut of the supporting elements of the part (Figure 9). In the left position of (Figure 9) it can be seen that the functional surface is not affected by the support structures normally used for resin printing (they are placed in the opposite position). The quality of the printed side is very good. After removing them put in the functional surface in right picture from (Figure 9), a different surface quality can be seen on the surface after removing the support's structure.
An important aspect to consider when 3D printing is the actual value of the surface obtained by printing. It can be seen that the resulting dimensions are different from those designed CAD. For example, if we consider the diameter of the hole in the body of the part that is 32.00 mm, the actual value resulting from 3D printing is 31.96 mm. For the central part considered and which ensures by rotating it the stopping or transmission of air/oil, the value resulting from the design is 31.00mm and the one obtained from 3D printing is 31.34 mm.
A very important stage considering the previous observations of real 3D printed and designed dimensional differences is to ensure the functionality and installation of the valve components. Such a step can be seen in (Figure 10) where the possibilities of fixing the side fastening elements are checked, but also the provision of a clearance large enough to allow the rotating central element to position itself coaxially in the body of the valve and to allow the easy positioning of the axial locking element.

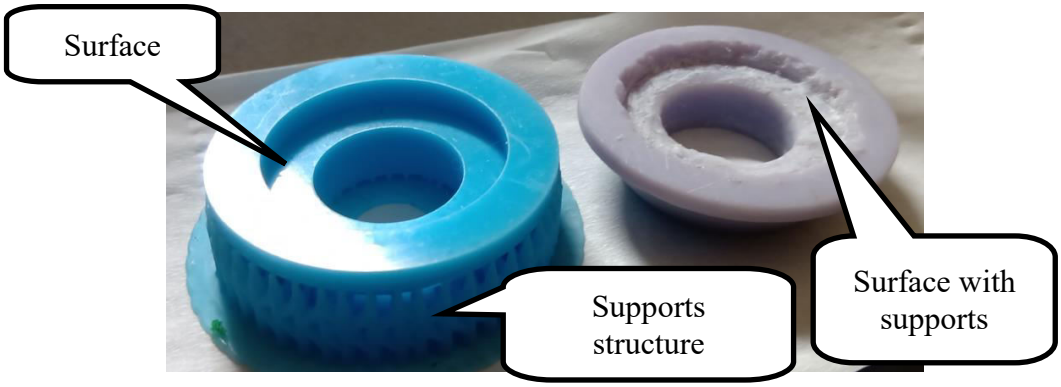

Fig. 9. Surface printed left without supports, right with supports after removing it

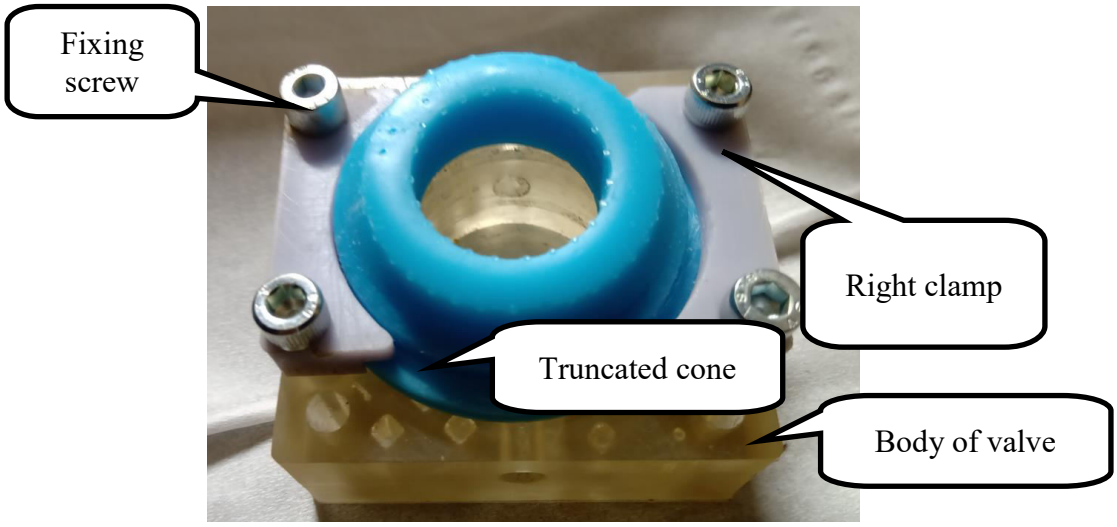

Fig. 10. Functionality and fixing of the valve components

One of the most important phases is the realization of the supporting structure of the part subjected to the printing process. As can be seen from (Figure 11) for the central command element automatic generation is often not with good accuracy. From the figure it can be seen that there are areas of red colour at the bottom that are not supported. This situation may cause surface or

printed material deformations in the printing process. A second important aspect is the one related to the arrangement of the supporting structures. From the figure it can be seen that the conical part of such elements is arranged on the cylindrical edge area, and not on the flat surfaces of red colour. As presented in the quality of the surfaces generated at the truncated conic element, this aspect must be corrected by repositioning the supporting elements, or by deleting some of the automatically generated parts, or by moving the tip of the cone to the desired position (Figure 12).

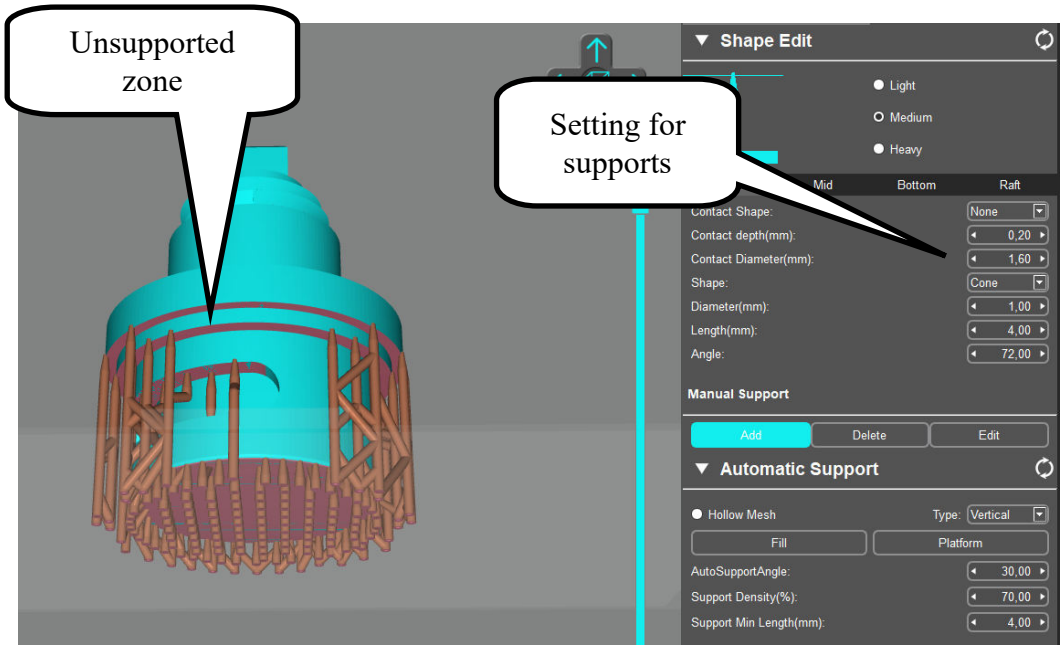

Fig. 11. Automatic generating supports for rotating center component

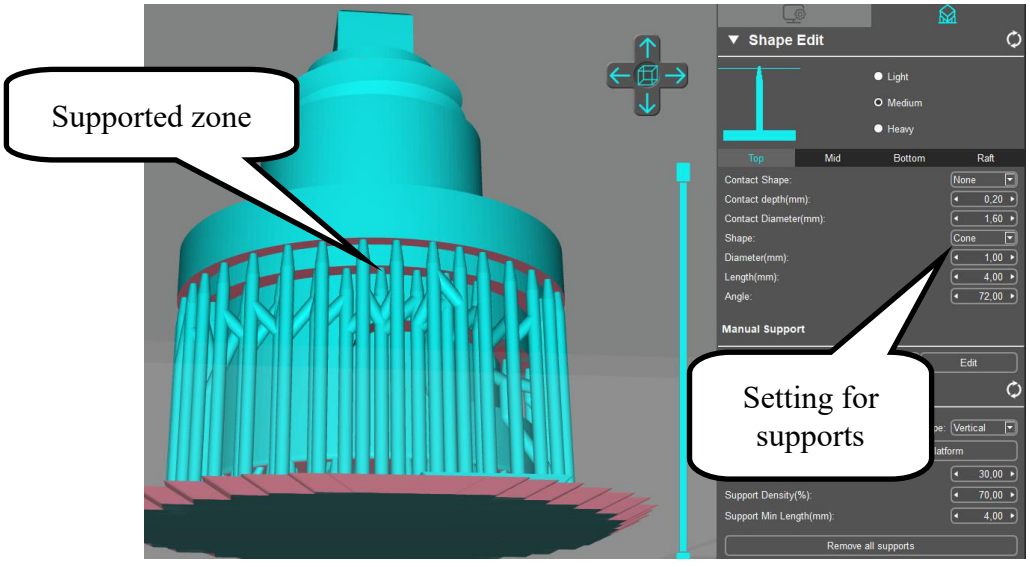

Fig. 12. Manual generating supports for rotating center component

3. Conclusions

Starting from the design part, but also the 3D generation of the part with the related support structure, it can be stated that through this work the bases of the possibilities of conception and technological realization with resin-based additive manufacturing technologies have been laid. The components under consideration are those in the command part specific to pneumatic drive systems, but also hydraulic.

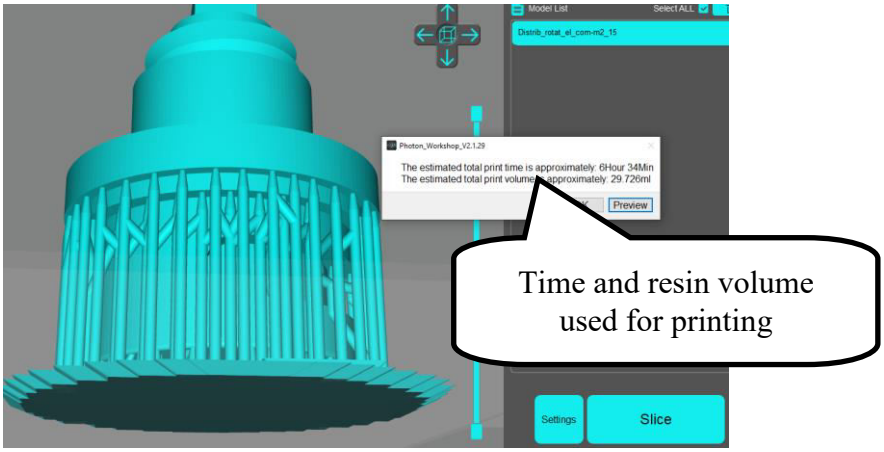

Fig. 13. Slice for generating structure for rotating center component

It should also be noted that the technology of 3D generation by photopolymerization is one of the most accurate both in terms of the surfaces obtained, but also in terms of characteristics of dimensional deviations and form. Based on these conclusions, the research process will be extended by following both the behaviour of the designed components at the flow and pressure demands of the gas or liquid medium used, but also in the comparative study in relation to other additive manufacturing technologies from the economic point and ecological efficiency of the industrial implementation of such a manufacturing solution.

References

[1] Vasilescu, M.D., Tiberiu Aurel Vasilescu, and Ioan Vasile Groza. "Economical considerations over 3D printing components for abrasive water jet machinery." *Advanced Materials Research* 1146 (2018): 84-91, https://doi.org/10.4028/www.scientific.net/AMR.1146.84.

[2] Vasilescu, M.D. "Technological and Constructive Considerations on the Realization of Components and Parts Using 3D Printing FDM-Type Technology." *Hidraulica Magazine*, no. 4 (December 2018): 55-62.

[3] MacCurdy, R., R. Katzschmann, Y. Kim, and D. Rus, "Printable hydraulics: A method for fabricating robots by 3D co-printing solids and liquids." Paper presented at the 2016 IEEE International Conference on Robotics and Automation (ICRA), Stockholm, Sweden, May 16-21, 2016, pp. 3878-3885, doi: 10.1109/ICRA.2016.7487576.

[4] Vasilescu, M.D. "Constructive and technological consideration on the generation of gear made by the DLP 3D-printed method." *MATERIALE PLASTICE* 56, no. 2 (2019): 440-444.

[5] ***. "Manually Actuated Valves" --- for details, please see: http://www.fitsitech.com/4hv-4hvl-AirTAC-Pneumatic-Air-Valve.html, accessed 08.2022.

[6] ***. "Unlock educational access to Autodesk products" --- for details, please see: https://www.autodesk.com/education/edu-software/overview?sorting=featured&filters=individual, accessed 08.2022.

[7] ***. "Slicer: Photon Workshop" --- for details, please see: https://drive.google.com/file/d/1EShd4LmAZ9OZyjxIEsMCUVg99yUmUuPx/view, accessed 08.2022.

[8] ***. "Anycubic Plant-based UV Resin 3KG" --- for details, please see: https://www.anycubic.com/products/anycubic-plant-based-uv-resin-3kg?currency=USD&utm_medium=cpc&utm_source=google&utm_campaign=Google%20Shopping&gclid=EAIaIQobChMIlZeL35r_-QIVtpBoCR3MOgTHEAsYAiABEgKPePD_BwE, accessed 08.2022.

[9] ***. "Anycubic Photon" --- for details, please see: https://www.anycubic.com/products/anycubic-photon-3d-printer, accessed 08.2022.

A Volumetric Working Machine with Profiled Rotors for Fluids Circulation

PhD Std. **Gabriel FISCHER-SZAVA**[1], Prof. Dr. Eng. **Nicolae BĂRAN**[1],
Șl. Dr. Eng. **Mihaela CONSTANTIN**[1,*]

[1] University Politehnica of Bucharest, Romania

* i.mihaelaconstantin@gmail.com

Abstract: *The paper presents a constructive solution of a new type of volumetric rotating machine, with two profiled rotors, which can transport clean fluids or polyphasic fluids. The operation principle of the machine is set out and the computation relations are established for:*
- the rotating machine flow rate;
- the power required to drive the rotating machine.
At the end of the paper, the advantages of this machine are highlighted compared to other machines for fluids circulation.

Keywords: *Rotating machine, Profiled rotors, Polyphase fluids*

1. Introduction

The paper presents a type of rotating working machine with profiled rotors that can operate [1], [2]:
- As a fan, for the circulation of different gas mixtures with or without suspensions.
- As a low-pressure compressor.
- As a rotating volumetric pump for the transport of any type of fluid, liquid, or gas, namely:
- general fluids: water, air, steam, etc.
- polyphasic fluids: water and air, water and sand, water, and ash, etc.
- viscous fluids: oil, diesel, oil, etc.

Table 1 presents a general classification of rotating machines.

Table 1: A general classification of rotating machines

According to the pursued purpose	**Depending on the constructive solution**	**According to the working parameters**
Working machines	With profiled rotors	a) Fans, blowers, pumps
	With pallets	b) Fans, blowers
Force machines	With profiled rotors	c) Internal combustion engines, steam or gas engines, pneumatic engines
	With pallets	d) Steam turbines, gas turbines

The construction of rotating working machines (pumps, fans, blowers) with high performance is topical.
The research aims to build machines that ensure the transformation of the engine torque received from the shaft into useful effects, but with energy losses as small as possible.

Table 2 presents the classification of rotating machines with profiled rotors according to the intended purpose and the constructive solution adopted [1].

Table 2: Classification of rotating machines with profiled rotors

According to the pursued purpose	Depending on the constructive solution
Working machines Force machines	Fans for the circulation of gases or vapors
	Blowers for gas and vapor compression
According to the pursued purpose	Hydraulic motors
	Pneumatic motors
	Steam or flue gas engines

2. Presentation of the constructive solution and the operating principle of the rotating machine with two profiled rotors

The machine consists of (figure 1) two identical rotors (2, 5) of special shape, which rotate at the same speed inside some housings (1, 4). The synchronous rotation of the rotors is ensured by two gears fixed on the shafts 7 and 9 which form a cylindrical gear mounted on the outside of the rotating machine [2] [3].
The determination of the contour shape of the two rotors is performed based on a calculation program [3] [4], and the construction of the rotors takes place on a numerically controlled centre [5] [6].

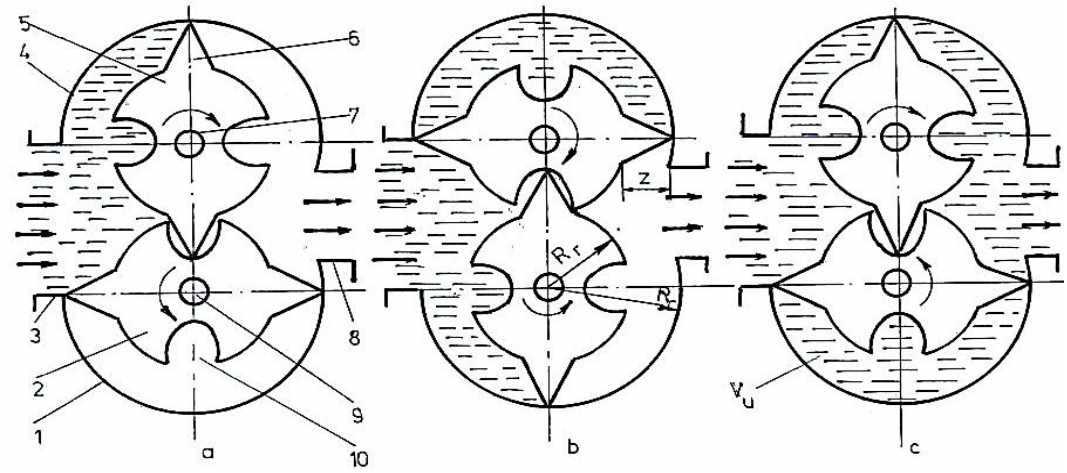

Fig. 1. Rotor position after a 90°rotation
1-lower case; 2-lower rotor, 3-suction chamber; 4-upper case; 5-rotor top; 6-rotating piston; 7-driven shaft; 8-discharge chamber; 9- driving shaft; 10-cavity into which the upper rotor piston enters

The aspirated fluid (figure 1.a) is transported for discharge and after a 90° rotation of both rotors, it reaches the situation in figure 1.b and later in figure 1.c.

3. Establishing the calculation relation of the flow rate transported by the machine

After a 180 ° rotation, the fluid in the useful volume V_u (figure 1.c), i.e., in the space between the pistons, the lower case (1) and the lower rotor (2), will be sent to the discharge chamber. At a complete rotation of the shaft (9) two such volumes will be transported from suction to discharge [1] [2] [3]:

$$\dot{V}_u = 2 \cdot \left(\frac{\pi R_c^2}{2} - \frac{\pi R_r^2}{2} \right) \cdot l \quad \left[m^3 / rot \right] \tag{1}$$

The case radius of the (R_c) is the sum of the rotor radius (R_r) and the piston height (z), (Figure 1.b).

$$R_c = R_r + z \quad [m] \tag{2}$$

it results:

$$\dot{V}_u = \pi \cdot l \cdot z\left(z + 2R_r\right) \quad \left[m^3 / rot\right] \tag{3}$$

The volumetric flow rate of the fluid discharged by a single rotor of length l [m] and speed n_r [rot/min] will be:

$$\dot{V}_u = \pi \cdot l \cdot z\left(z + 2R_r\right) \cdot \frac{n_r}{60} \quad \left[m^3 / s\right] \tag{4}$$

Since the machine has two identical rotors, the fluid flow rate transported by the machine will be:

$$\dot{V}_u = 2 \cdot \dot{V}_u = \pi \cdot l \cdot z\left(z + 2R_r\right) \cdot \frac{n_r}{30} \quad \left[m^3 / s\right] \tag{5}$$

From relation (5) one can observe that the flow rate transported by the rotating machine will increase exponentially when the parameters change: l - rotor length [m];z - rotating piston height [m];R_r - rotor radius [m]; n_r - machine speed [rpm].
Obviously, a certain ratio must be established between the rotor radius (R_r) and the piston height (z).

4. Establishing the calculation relation of the driving power of the rotating machine

The presented rotating machine is a volumetric pump, which must achieve a pressure increase equal to Δp [N / m^2]. In this case, the relation (7) will give the theoretical driving power of the machine [8]:

$$P = \dot{V}_m \cdot \Delta p \quad [W] \tag{6}$$

Substituting from relation (5), one can obtain:

$$P = \pi \cdot l \cdot z \cdot \left(z + 2R_r\right) \cdot \frac{n_r}{30} \cdot \Delta p \quad [W] \tag{7}$$

From relation (7) one can observe that the machine power varies according to the following parameters:
* Constructive parameters: l - rotor length [m]; R_r - rotor radius [m]; z - rotating piston height [m].
* Functional parameters: n_r - machine speed [rpm]; Δp- the increase in pressure achieved by the pump between suction and discharge.
The actual driving power of the rotating volumetric pump will be higher [9] [10]:

$$P_r = \frac{P}{\eta_e} \quad [W] \tag{8}$$

where η_e is the effective efficiency of the pump:

$$\eta_e = \eta_v \cdot \eta_m \cdot \eta_h \tag{9}$$

where:
η_v is the volumetric efficiency of the pump.
η_m is the mechanical efficiency of the pump.
η_h is the hydraulic efficiency of the pump.

5. Advantages of the rotating machine compared to other machines used to transport fluids

The evaluation of a technical solution must consider the following aspects:
a) Increased installation efficiency.
b) Increased reliability.
c) A wide field of operation.

d) The value of the investment should be as small as possible.
- The aspirated fluid is conveyed to the discharge with minimal energy losses; thus, the engine torque is $\vec{M} = \vec{F} \times \vec{b} \rightarrow M = Fb\sin\alpha$, where F is the force pressing on the rotating piston; b is the arm force: $b = R_r + \frac{z}{2}[m]$.

The force F is always perpendicular to the arm, so the angle α between the force and the arm will be 90°; as a result, sin90° = 1. This leads to an advantage over piston machines where α is variable over 360°. As a result, neglecting the friction between the rotors and the case, the entire engine torque received from the drive motor is used to convey the fluid.
- The constructive solution presented in the paper has only rotating moving parts; it has a safe operation and easy maintenance.
- This type of rotating volumetric pump can carry any fluid:
* In the field of constructions: different solutions, diesel, etc.
* In the field of hydrotransport: water + sand, water + ash.
* In the food field: oil, syrups, etc.
* Rheological fluids.
* Other pure or polyphase fluids with low or high viscosity; once they reach the pump suction, they are conveyed to the pump discharge.
- The investment for the construction of a pumping installation [9] is not large; this is because a calculation program is available for the construction of the rotors [4] and their construction can be performed on a numerically controlled computer centre [5].

6. Conclusions

- The constructive solution presented in the paper was designed and built in the laboratory of the Department of Thermotechnics, Engines, Thermal and Refrigeration Equipment within the Faculty of Mechanical and Mechatronics Engineering; after its construction, the pump was tested.
- The results of experimental researches are presented in the paper [11]; it is important that for this type of rotating volumetric pump an effective efficiency $\eta_e = 0.77$ was experimentally determined, a value that exceeds the results obtained for piston pumps, centrifugal pumps, etc. [9] [10] [11].
- This type of pump can be used in the following fields: in agriculture for irrigation, in energy for hydrotransport, in civil or industrial constructions for the circulation of high viscosity fluids; this type of machine can also be used as a fan or low-pressure compressor.

References

[1] Dobrovicescu, Al., N. Băran, Al. Chisacof, M. Marinescu, and P. Răducanu. *Bases of Technical Thermodynamics / Bazele termodinamicii tehnice*. Bucharest, Politehnica Press Publishing House, 2010.
[2] Dobrovicescu, Al., N. Băran, Al. Chisacof, S. Petrescu, E. Vasilescu, D. Isvoranu, M. Costea, C. Petre, A. Motorga. *Basics of Technical Thermodynamics. Vol. 1 Elements of Technical Thermodynamics* / *Bazele termodinamicii tehnice. Vol. 1 Elemente de termodinamică tehnică*. Bucharest, Politehnica Press Publishing House, 2009.
[3] Stoican (Prisecaru), M. M., and N. Băran. "A constructive solution that can function as a force machine or as a work machine." *Asian Journal of Applied Science and Technology (AJAST)* 4, no. 2 (April-June 2020): 97-107.
[4] Almaslamani, A., and M. M. Stoican (Prisecaru). "Calculation relations regarding the architecture of a rotating machine for transports fluids." *International Journal for Research in Applied Science and Engineering Technology (IJRASET)* 8, no. 3 (March 2020): 61 - 66.
[5] Donţu, O. *Manufacturing technologies for mechatronics* / *Tehnologii de fabricaţie pentru mecatronică*. Bucharest, Printech Publishing House, 2003.
[6] Donţu, O. *Laser processing technologies* / *Tehnologii de prelucrare cu laser*. Bucharest, Technical Publishing House, 1985.
[7] Motorga, A. *Influence of constructive and functional parameters on the performances of rotating machines with profiled rotors* / *Influența parametrilor constructivi și funcționali asupra performanțelor mașinilor rotative cu rotoare profilate*. PhD Thesis, Faculty of Mechanical Engineering and Mechatronics, Politehnica University of Bucharest, 2011.

[8] Hawas, M. *The influence of fluid viscosity on the performance of rotating machines with profiled rotors* / *Influența vâscozității fluidului asupra performanței mașinilor rotative cu rotoare profilate*. PhD Thesis, Faculty of Mechanical Engineering and Mechatronics, Politehnica University of Bucharest, 2015.

[9] Burchiu, V., I. Santău, and O. Alexandrescu. *Pumping installations* / *Instalații de pompare*. Bucharest, Didactic and Pedagogical Publishing House, 1982.

[10] Bale, M. P. *Pumps and Pumping - A Handbook for Pump Users Being Notes On Selection, Construction And Management*. Hawthorne, CA, Joseph. Press, 2009.

[11] Gheorghe, G., D. Besnea, N. Băran, M. Constantin, and Malik N. Hawas. "Experimental research on the determination of the effective efficiency of a new type of positive displacement pump with profiled rotors" / „Cercetări experimentale privind determinarea randamentului efectiv al unui nou tip de pompă volumică cu rotoare profilate." Paper presented at the 7th International Conference on Innovations, Recent Trends and Challenges in Mechatronics, Mechanical Engineering and New High-Tech Products Development MECAHITECH, Bucharest, Romania, September 10-11, 2015.

Chassis with Installed Hydraulics for Multifunctional Vehicles Intended for Public Utility Works

PhD. Student Eng. **Ștefan Mihai ȘEFU[1,*],** PhD. Eng. **Radu Iulian RĂDOI[1],**
PhD. Student Eng. **Liliana DUMITRESCU[1],** Eng. **Ioan BĂLAN[1],**
PhD. Student Eng. **Mihail PETRACHE[2],** Dipl. Eng. **Elena IORDAN[3]**

[1] INOE 2000 – Subsidiary Hydraulics and Pneumatics Research Institute (INOE 2000-IHP) Bucharest / Romania

[2] Lyra Hydraulics Consulting SRL, Bucharest / Romania

[3] HIAROM INVEST SRL, Dragomirești-Vale / Romania

* sefu.ihp@fluidas.ro

Abstract: *The article presents a solution for the hydrofication of a small capacity truck chassis (total authorized mass of max 7.5 tonnes), i.e. equipping it with a hydraulic system (installation, aggregates, components, electrical control devices, etc.), to actuate various pieces of mechanical-hydraulic equipment (plow, snow cutter, salt spreader, sweeping brush, mower, etc.), intended for carrying out public utility works (snow removal, street sweeping, mowing of the roadsides, etc.).*

Keywords: *Hydrostatic transmission, utility vehicle, interchangeable pieces of work equipment, low fuel consumption*

1. Introduction

The utility vehicles intended for carrying out various works of public utility, such as: snow removal, street sweeping, mowing of the roadsides, etc., have been developed in two stages.

Fig. 1. Utility vehicles [2]

In the first stage, these vehicles were made by mounting a piece of equipment (plow or snow cutter, salt spreader, rotating brush for sweeping, tank with installation for street spraying, etc.), in front of or behind the vehicle operated by a hydraulic installation dedicated to each type of equipment [1].

In the current stage of development, the utility vehicles intended for carrying out public utility works are equipped with interchangeable work equipment, which offers flexibility when using the vehicle carrying various pieces of equipment, so that the same chassis is equipped, for example, in summer, with a rotating brush for sweeping and a street spraying installation, and in winter, with a snow plow or blower and salt spreader.
Fig. 1 shows a utility vehicle designed to perform public utility works, on which interchangeable work equipment pieces - mowers, sprinklers, snow blade and salt spreader - were mounted [2].

2. The structure of the chassis with installed hydraulics

The chassis proposed for being equipped with hydraulics parts has a total authorized mass of 7.5 tonnes.
The capacity of the chassis was limited to max. 7.5 tonnes of the total authorized mass, for reasons of overall size, so that it has access to small spaces or narrow streets.
The small capacity chassis, max. 7.5 tonnes, are manufactured with the motor rear axle and the steered front axle. The work equipment that is mounted in front of the vehicle "unloads" the rear axle, traction, which reduces the grip of the rear wheels especially when the road is slippery. For this reason, it is necessary to modify the front axle and turn it into a steering axle and motors with the possibility of decoupling when it does not need to be used.
Fig. 2 shows the structure of a utility vehicle made on a 7.5 tonne chassis, equipped with a blade for removing snow in front and with a salt spreader for spreading the anti-skid material in the back.

1. Hydraulic system for the operation of the interchangeable work equipment;
2. Salt spreader for spreading anti-skid material;
3. Blade for snow removal;
4. Front axle steering and decoupled motors;
5. 4x2/4x4 Chassis;
6. Rear axle motors.

Fig. 2. The structure of the chassis with installed hydraulics [2]

The power required for the hydraulic system implemented on the chassis is provided by its heat engine, through the power take-off (PTO) and the transfer case.
The chassis with installed hydraulics proposed for the development of the utility vehicles for carrying out public utility works, brings the following innovative elements:

- It offers the possibility to use the vehicle carrying interchangeable work equipment pieces to its maximum potential throughout the year, in summer with equipment specific to this season and in winter with snow equipment;
- It uses a single hydraulic drive system to operate all interchangeable work equipment;
- The power required for the hydraulic drive system of the interchangeable work equipment is provided by the heat engine of the chassis. The fact that there is no second heat engine dedicated to the hydraulic system for operating the interchangeable work equipment leads to the following advantages:
  - The cost price of the entire vehicle is reduced;
  - The fuel consumption is reduced when carrying out the public utility works, because a single heat engine is used;
  - The polluting emissions are lower, since there is no pollution caused by a potential second heat engine.

- The hydraulic system for operating the interchangeable work equipment has high energy efficiency, which is achieved by:

- Implementing hydraulic drive schematic diagrams that reduce the energy losses produced by the throttling of the working fluid to a minimum;
- Storing the energy during the inactive phases in pneumo-hydraulic accumulators, and supplying it during the working phases of the equipment.

3. The structure of the hydraulic equipment of the chassis with installed hydraulics

The structure of the hydraulic equipment of the chassis with installed hydraulics is shown in Fig. 3. The equipment [3, 4] consists of six subassemblies: Pumping group A; Pumping group B; Distribution subassemblies 1, 2 and 3; equipped basin to which the pipes that connect the components of the equipment are added; connection elements (joints, nipples, fittings, etc.) and fastening and assembly elements (clamps, bridles, etc.).
Pumping group A provides the necessary flow rate for the positioning of interchangeable work equipment (snow plough, mowers, etc.).
Pumping group B ensures the flow rate required to drive the equipment (snow cutter, rotating brush, etc.).
Distribution subassembly 1 and Distribution subassembly 2 direct the flow rate of pumping group A, for the positioning of the equipment.
Distribution subassembly 3 directs the flow rate of pumping group B, for driving the work equipment.

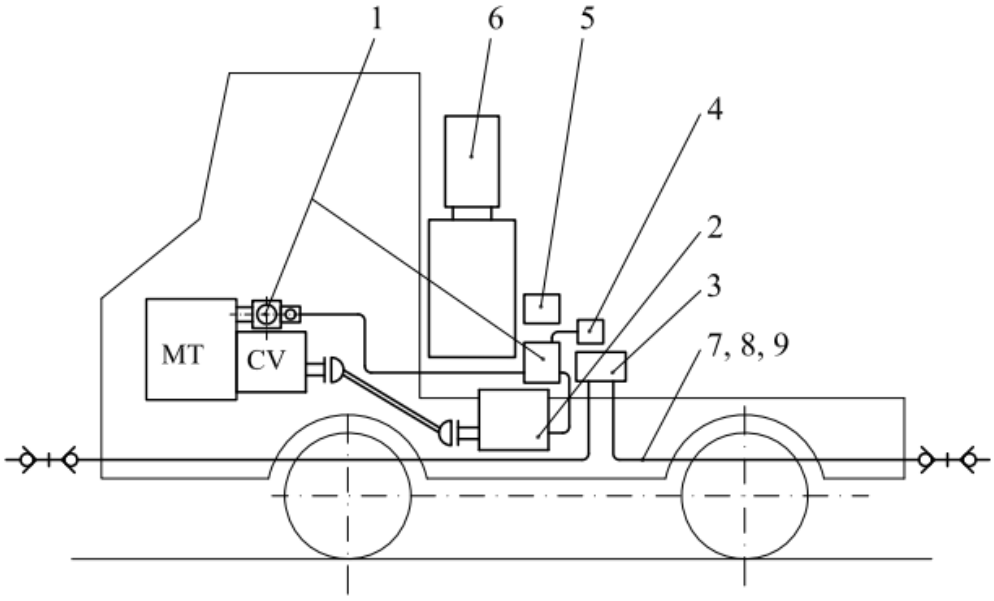

Fig. 3. The structure of the hydraulic equipment of the chassis with installed hydraulics [3, 4]

1. Pumping group A; 2. Pumping group B; 3. Distribution subassembly 1; 4. Distribution subassembly 2; 5. Distribution subassembly 3; 6. Equipped basin; 7. Pipelines; 8. Connection elements; 9. Fastening and assembly elements.

4. Operation of the hydraulic equipment of the chassis with installed hydraulics

The operation of the hydraulic equipment of the chassis with installed hydraulics is presented in accordance with the hydraulic block diagram in Fig. 4 and the hydraulic diagrams of the component subassemblies.

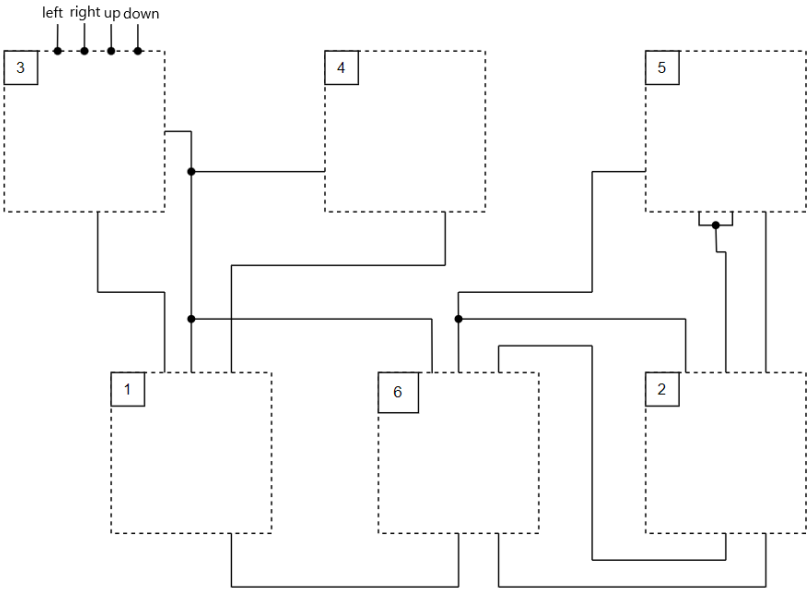

1. Pumping group A;
2. Pumping group B;
3. Distribution subassembly 1;
4. Distribution subassembly 2;
5. Distribution subassembly 3;
6. Equipped basin.

Fig. 4. Operating mode of the equipment - block diagram

4.1 Pumping group A – Fig. 5

Pumping group A consists of a double gear pump 1-P_1+P_2 driven from heat engine-MT, gearbox-CV, distribution box-CD via pneumatic clutch 9, controlled with the help of pneumatic directional control valve 8.

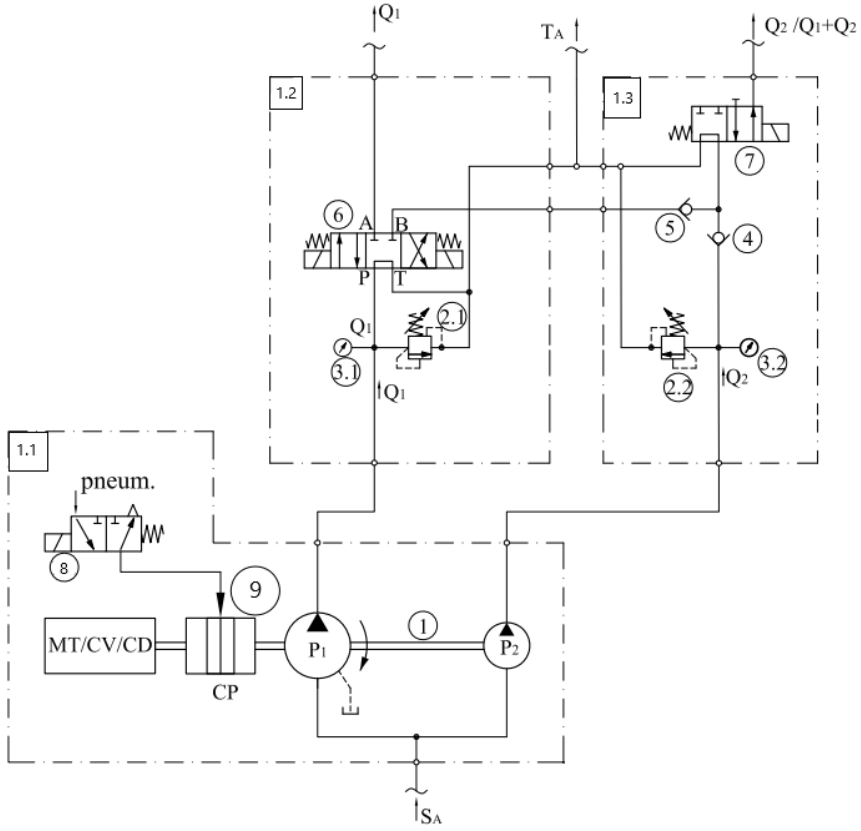

1. Double gear pump;
2. Safety valve;
3. Pressure gauge;
4. Check valve;
5. Check valve;
6. 4/3 Directional control valve;
7. 4/2 Directional control valve;
8. Pneumatic directional control valve;
9. Pneumatic coupling.

Fig. 5. Hydraulic diagram of pumping group A

Safety valves 2.1 and 2.2 limit the pressure on the discharge circuit of the gear pumps P_1 and P_2. Gauges 3.1 and 3.2 indicate the pressure on the discharge circuits of pumps P_1 and P_2. The check valves 4 and 5 allow the flow rate of the pumps to circulate in one direction only - from the double

gear pump to the consumers. The directional control valve 6 directs the flow rate of pump P_1 to the distribution subassembly 1 or the distribution subassembly 2.

4.2 Pumping group B – Fig. 6

Pumping group B ensures the working flow rate for the multifunctional equipment and consists of variable flow pump 1-P_3, pneumatic clutch 2-HP, pneumatic distributor 3, pressure gauge 4 and safety valve 5.
Pump 1 is equipped with LS flow regulator and pressure regulator [5]. It is driven from heat engine-MT, gearbox-CV, distribution box-CD, through pneumatic coupling 2-HP led with the help of pneumatic directional control valve 3.
Pressure gauge 4 indicates the pressure on the pump discharge circuit, and safety valve 5 limits the pressure on the pump discharge circuit.

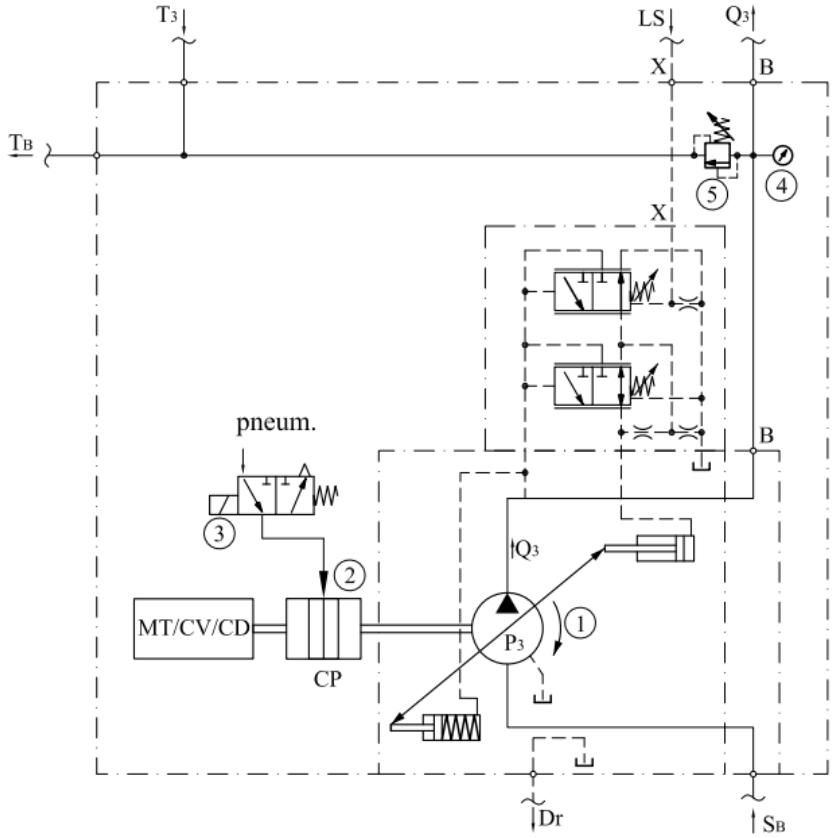

1. Variable flow pump;
2. Pneumatic clutch;
3. Pneumatic 3/2 directional control valve;
4. Pressure gauge with glycerin;
5. Safety valve.

Fig. 6. Hydraulic diagram of pumping group B [5]

4.3 Distribution subassembly 1 – Fig. 7

Distribution subassembly 1 is dedicated to the positioning of the snow plough equipment and consists of 4/3 directional control valves, items 1.1 and 1.2, and 4/2 directional control valve, item 2.
Directional control valve 1.1 directs the plow to remove snow on the left or right side of the utility vehicle.
Directional control valve 1.2 lifts or lowers the snow plow.
Directional control valve 2 provides the "flat-out" position of the snow plow if the electromagnet is electrically powered.

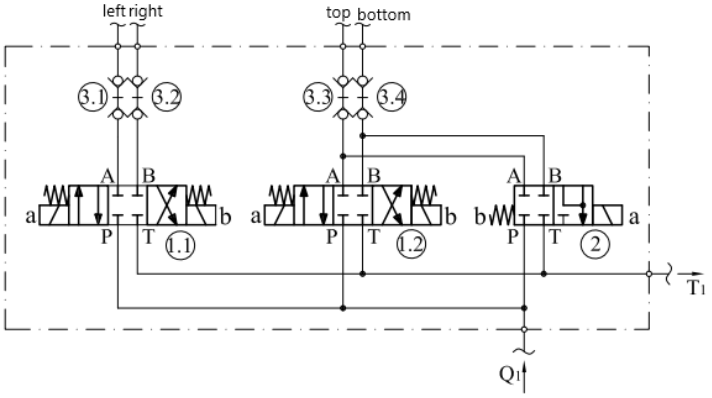

1. 4/3 Directional control valve;
2. 4/2 Directional control valve;
3. Quick couplings.

Fig. 7. Hydraulic diagram of distribution subassembly 1

Quick couplings 3 ensure the rapid hydraulic connection of the interchangeable equipment, the snow plow, in this case, and the hydraulic installation.

4.4 Distribution subassembly 2 – Fig. 8

With the help of distribution subassembly 2, interchangeable equipment positioned in front of or behind the chassis can be positioned / operated.

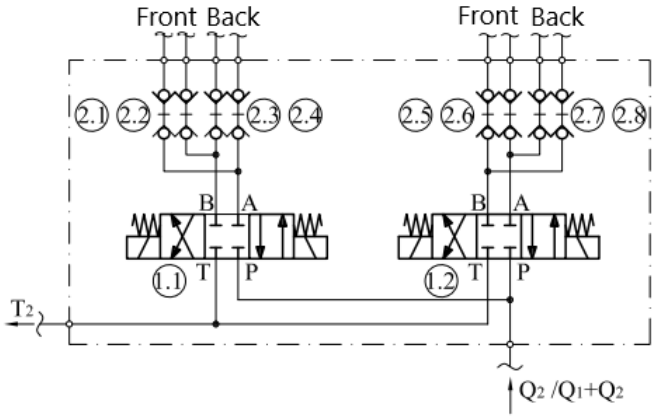

1. 4/3 Directional control valves;
2. Quick couplings.

Fig. 8. Hydraulic diagram of distribution subassembly 2

The subassembly is composed of two 4/3 directional control valves, items 1.1 and 1.2, and the quick couplings 2.1....2.8, which ensure the fast connection of the interchangeable equipment to the hydraulic installation.

4.5 Distribution subassembly 3 – Fig. 9

Distribution subassembly 3 directs the flow rate provided by pumping group B, for the operation of the interchangeable equipment located in front of or behind the chassis. It consists of monoblock hydraulic directional control valve 1 and quick couplings 2.1……2.6.
The monoblock directional control valve has three work sections, one of which supplies the equipment in front of the chassis, another - the ones on the rear, and the third is the reserve. The monoblock directional control valve sends the LS hydraulic signal to the pump of pumping group B, for the variation of its capacity. The pump flow rate of pumping group B is proportional to the electric signal of 0 ...10V, with which the proportional electromagnets of the monoblock directional control valve are supply. Quick couplings ensure fast connection of the equipment to the hydraulic installations.

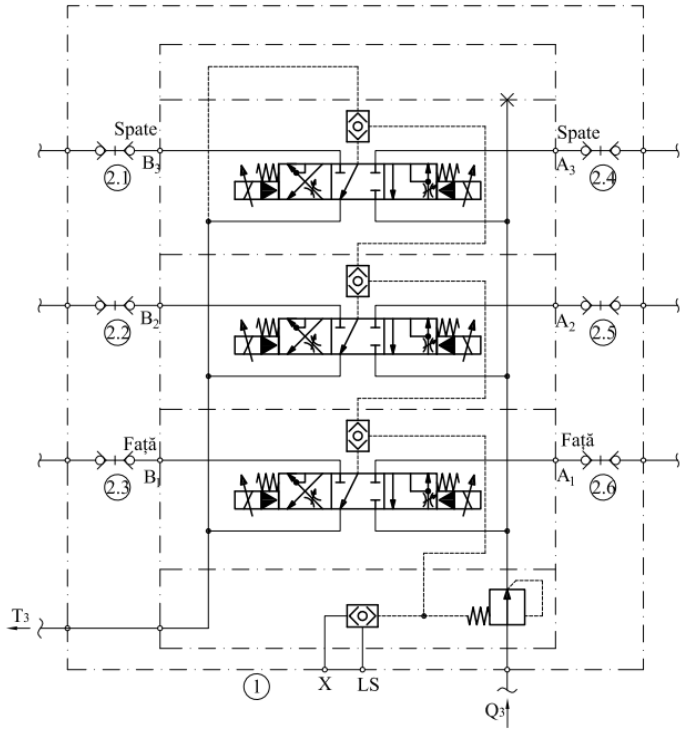

Fig. 9. Hydraulic diagram of distribution subassembly 3

4.6 Equipped basin – Fig. 10

The "Equipped basin" subassembly provides the working fluid necessary for the hydraulic installation, which equips the utility vehicle. The cooling of the hydraulic oil is provided by heat exchanger 1.1, for pumping group A, and heat exchanger 1.2, for pumping group B, and the filtration by return filter 2. Basin 3 has a capacity of 160 liters. Minimum level sensor 4 emits an alarm beep if the oil level drops below the minimum suction value of the pumps.

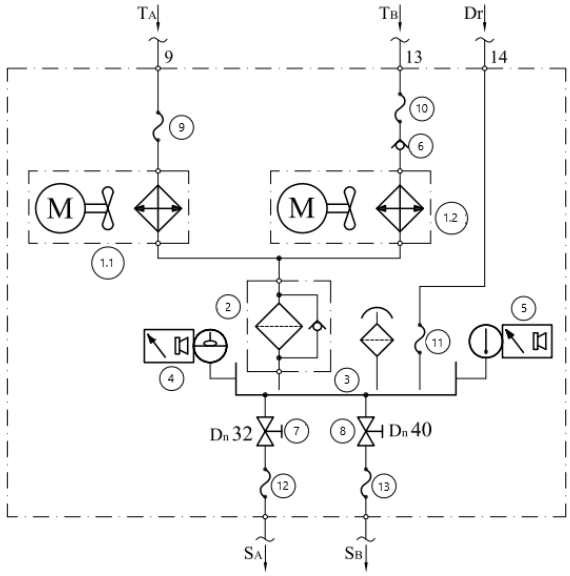

1. Air-oil heat exchanger;
2. Return filter;
3. Oil tank;
4. Minimum level sensor;
5. Maximum temperature sensor;
6. Check valve;
7. Suction valve A;
8. Suction valve B;
9. Flexible connection D_n 10;
10. Flexible connection D_n 20;
11. Drainage connection D_n 10;
12. Suction connection D_n 32;
13. Suction connection D_n 40.

Fig. 10. Hydraulic diagram of the equipped basin

Temperature sensor 5 turns on the fan of the coolers, if the oil temperature exceeds the value of 50 °C.

Suction valves 7 and 8 isolate the pumps from the oil tank. Flexible connections 8...13 ensure the connection between the basin and the rest of the devices, with the damping of the vibrations produced by the components in rotational motion.

5. Conclusions

The chassis with installed hydraulics presented in this article comes with the following innovative ideas:

• It uses a single hydraulic drive system for all interchangeable pieces of work equipment that equip utility vehicles designed to perform public utility works;

• It offers the possibility to make full use of the vehicle carrying interchangeable work equipment throughout the year, in summer with equipment specific to this season, and in winter with snow equipment;

• The power required for the hydraulic drive system of the interchangeable work equipment is provided by the heat engine of the chassis. The fact that there is no second engine dedicated to the hydraulic system for operating the interchangeable work equipment, leads to the following advantages of the utility vehicle:

- The cost price of the entire vehicle is reduced;
- The fuel consumption is reduced when carrying out public utility works, because a single heat engine is used;
- The polluting emissions are lower, since there is no pollution caused by a potential second heat engine.

Acknowledgments

This work was carried out under the project ASHEUP - *Hydro powered motor chassis for high energy efficiency operation of interchangeable equipment intended for performing public works / Autoșasiu hidroficat pentru acționarea cu eficiență energetică ridicată a echipamentelor interschimbabile destinate realizării unor lucrări de utilitate publică*, Grant no. 53PTE/2020, PN III: Programe 2 - Increasing the competitiveness of the Romanian economy through research, development and innovation, Subprogramme 2.1 - Competitiveness through research, development and innovation, Project type - Transfer project to the economic operator. The paper has been developed in INOE 2000-IHP, as part of a project co-financed by the European Union through the European Regional Development Fund, under Competitiveness Operational Programme 2014-2020, Priority Axis 1: Research, technological development and innovation (RD&I) to support economic competitiveness and business development, Action 1.2.3 – Partnerships for knowledge transfer, project title: *Development of energy efficient technologies in niche applications of the manufacture of on-demand mechanical-hydraulic subassemblies and maintenance of mobile hydraulic equipment*, project acronym: MENTEH, SMIS code: 119809, Financial agreement no. 6/25.06.2018, subsidiary contract no. 413/05.05.2022. It has also received financing under a project funded by the Ministry of Research, Innovation and Digitalization through Programme 1- Development of the national research & development system, Subprogramme 1.2 - Institutional performance - Projects financing the R&D&I excellence, Financial Agreement no. 18PFE/30.12.2021.

References

[1] INOE 2000-IHP. *Electrohydraulic equipment (EHE) with high energy efficiency (HEE) for multipurpose motor vehicles (MPV) / Echipamente electrohidraulice (EEH) cu eficienta energetica ridicata (EER) pentru autovehicule multifunctionale (AMF)*. Financing agreement no: 11 PTE /2016, Project code: PN-III-P2-2.1-PTE-2016-0077.

[2] KAERCHER. "Holder S Series." Accessed August 4, 2022. https://www.kaercher-municipal.com/en/s-series.

[3] Lepădatu, Ioan, Corneliu Cristescu, Liliana Dumitrescu, and Polifron – Alexandru Chiriță. "Numerical simulation of dynamic behavior of a multifunction motor vehicle equipped with a primary adjustment hydrostatic transmission." Paper presented at the 6-th International Conference on Thermal Equipment, Renewable Energy and Rural Development TE-RE-RD 2017, Moieciu de Sus, Romania, June 8-10, 2017.

[4] Lepădatu, Ioan, Corneliu Cristescu, Polifron – Alexandru Chiriță, and Cristian Mărculescu. "Four-wheel drive high efficiency hybrid transmission for multipurpose motor vehicles." Paper presented at the 23rd International Conference on Hydraulics and Pneumatics HERVEX 2017, Băile Govora, Romania, November 8-10, 2017.

[5] Bosch Rexroth AG. "Variable displacement." Accessed August 5, 2022. https://store.boschrexroth.com/Hydraulics/Pumps/Axial-piston-pumps/Variable-displacement?cclcl=ro_RO.

Damping of the Rainwater Runoff by Small Underground Reservoirs in Subdivision Lots

Sc. Eng. **Tayline BONANE**[1], Prof. Dr. Eng. **Henrique PIZZO**[2,3,*], Sc. Eng. **Marcela MEIRELES**[2], Prof. M.Sc. Eng. **Lucas ROCHA**[2,3,4]

[1] Fire and Panic Safety Engineering, Juiz de Fora, Minas Gerais, Brazil

[2] Estácio University of Juiz de Fora, Minas Gerais, Brazil

[3] Municipal Water and Sewage Company of Juiz de Fora, Minas Gerais, Brazil

[4] Vértix Trirriense College, Três Rios, Rio de Janeiro, Brazil

* henriquepizzo.estacio@gmail.com

Abstract: *The present work aims to evaluate the effect of small flow dampening reservoirs installed in the front of the lots in subdivision, regarding the reduction of the discharge peak and eventual decrease of the diameters of the drainage galleries, in relation to a conventional drainage system. After a review of the literature on the subject, the calculation of the drainage network of a certain street is carried out in the conventional way, with the presentation of the respective dimensioning worksheet. In sequence, the Routing Simulator Application is used in order to verify the reductions in the flows caused by the damping devices, with the presentation of the new dimensioning worksheet with damping. Finally, the flow values for gallery sections and diameters are compared, considering both scenarios. Lot reservoirs were responsible for a reduction rate of 21% to 35% in flow rates, with a decrease in diameter in 50% of the evaluated galleries.*

Keywords: *On-site stormwater detention, urban drainage, reservoir routing, floods, sustainable development*

1. Introduction

Drainage systems in expanding metropolitan areas are becoming insufficient as population rises, necessitating more occupation. The growth in impermeability has a direct effect on the peak and volume of water discharged superficially, necessitating work to extend the drainage system. Because of the enormous expenditures and physical constraints, this extension is frequently impracticable. The Urban Drainage Master Plans have identified issues and pointed to solutions incorporated within urban basins, with the goal of resolving them as near to the source as feasible. One of the plans' recommendations is to prevent the increasing of natural flow at the exit of the lots by applying control techniques at the source. The use of this type of measure has some objectives such as dampening the flood peak, by improving infiltration and storage conditions [1].

This decrease has a significant beneficial effect on downstream communities by lowering the peak discharge and postponing the arrival of floods. Reservoir routing is a mathematical approach for calculating the amount and form of a flood wave transition via a water retention facility over time [2].

As stated by [3], the absence of urban planning, along with chaotic population expansion and a rise in surface runoff, has considerably contributed to flooding concerns in metropolitan areas. The existing drainage system, which is primarily concerned with plumbing, is built on a rapid flow of rainfall downstream, which adds to increased peak flows and exacerbates the situation. As a result, alternative strategies for pluvial water management are required.

According to [4], a more recent concept of urban drainage has been used, based on the principle of storing and delaying the surplus in order to provide a better flow distribution over time. The main sustainable measures at source have been detention in lots, with the use of small reservoirs, and infiltration into the soil.

During a rain event, the detention tanks collect and store storm water runoff from roofs, pavements, and other impervious surfaces. The collected water will be discharged into the downstream drainage system at a regulated rate, lowering the peak discharge [5].

As per [6], low impact development strategies are used across the world to offset the effects of urbanisation on the hydrological cycle. Aside from their widespread use, the public's understanding

of these strategies and stormwater management is limited. People's awareness of flood control approaches and use of those techniques leads to greater acceptance and involvement.
In [7] a short script is suggested with general guidelines for the incorporation of detention reservoirs to new projects, in order to guide and facilitate the use of these devices, improving their acceptance by society.

2. Applications: Theoretical and Field Situations

Reference [5] introduces an article where 88 detention tanks are supposed to be uniformly spaced throughout the section, collecting stormwater from 44 ha of effective impervious area (one detention tank every 0.5 ha of impervious surfaces on average).
Using a mathematical hydrological model of precipitation flow, six types of reservoirs implanted in typical and subjected to increases in impermeable regions lots of a city were analysed [8]. The required volumes of implantation and maintenance expenses were determined using the typical precipitations of micro drainage and the hydraulic behaviour of each device. The results revealed that for the biggest simulated lot, 600 m2, with 100% waterproofing, quantities in the range of 2.5 to 3.0 m3 would be required, and for 50% waterproofing, volumes in the region of 1.0 to 1.5 m3 would be required.
A work is presented in [9], in which the volume of the damping reservoir required for a lot with 360 m2, fully waterproofed was 3.24 m3. For less impermeability values the volume of the reservoir was 0.97 m3. The study carried out showed that it is possible to obtain a reduction in peak flows from 13.31% to 40.69% through variations in dimensions of the outlet pipes.
As stated by [10], underground stormwater detention chambers (USDC) are a stormwater detention and treatment technology that can eliminate the thermal difficulties associated with sun-exposed detention facilities while still offering a similar degree of stormwater pollution treatment services. A field study of an USDC was undertaken to characterise its treatment performance and effect on water temperature. It was found that the USDC provided results, in terms of level of stormwater treatment, similar to those of the wet detention ponds. Outlet maximum temperatures were 5 °C colder than intake maximum temperatures on average, and outlet water temperatures stayed within the thermal range for cold water fish habitat across the study period.
Reference [11] presents an article in which they compare the monitoring data of an on-site stormwater detention device (OSD) installed in a hospital with the findings derived by theoretical approaches often employed in the construction of this type of structure. The OSD filling was studied during 48 precipitation occurrences. The measured values were greater than theoretical values in the maximum heights of water level comparison, and the results using the Rational Method were closer to monitoring data than the results using the SCS-HU Method.
The use of OSD in aspects of regulations, technical details and management matters is evaluated in [12]. Based on it, all administrations, in general, have the same management challenges. There is no regulation for the quantity of OSD installed in cities or even their condition. As a result, the authors provided several recommendations for improving OSD policy.
In order to evaluate OSD performance on a real scale as well as its hydrological and hydraulic parameters, two devices were monitored, with results described in [13]. Based on measuring data analysis, it was discovered that the OSD mean efficiencies in discharge attenuation were greater than 50%; the storage quantity per catchment area was close to 25 L/m2; the short pipes discharge coefficients were around 0.90; and the shape of inflow hydrographs was similar to hyetographs. The Unit Hydrograph Modified Rational Method was used to accurately portray the rain-runoff transition. The findings might be utilised in OSD design to calculate the inlet hydrograph, pre-sizing the storage capacity based on contribution area, and selecting the appropriate discharge coefficient value for the output device.
Reference [14] investigates the attenuation impact of household rainwater storage reservoir implementation in a typical square using Visual Basic for Applications (VBA) programming, where two damping volumes for the storage device in lot condition settings were built. The household reservoir was sized for initial rains of 05 and 10 year return period and tested for maximum project rains of 02, 05, 10, 15, 20, 25, 50, and 100 year return period, of which the temporal distribution used was the largest storm recorded at that place. The detention reservoir with a damping volume

of 3.25 m3 provided attenuation, at the end of the simulated stretch, of 37.38, 24.02, 21.74, 20.99, 18.51, 16.70, 11.73, and 7.52 percent, for the rains 02, 05, 10, 15, 20, 25, 50 and 100 year return period, respectively, while for the detention reservoir with a damping volume of 5.015 m3 the attenuation was 64.72, 65.10, 63.96, 63.23, 62.71, 62.32, 61.11, and 59.98 percent. In a subsequent work [15], another home detention reservoir, this one with a volume of 1.5 m3, was added to the study mentioned in [14], whose efficiency was 15.47% attenuation in the peak flow of the respective maximum rainfall.

A study that aimed to simulate and evaluate the impact of implementing a sustainable drainage system, more specifically distributed detention facilities, in a small contribution area, is presented in [16]. The simulations were carried out in a subdivision, from which a block was delimited for the implementation of the reservoirs, in order to assess the impact on the gallery system. Two blocks influenced by 24 lots were selected, being subdivided into 6 sub-basins with areas of 0.16 hectares each, covering 4 lots, with the reservoirs provided with 35 mm outlet orifices. Data were obtained from two series of precipitation with different intensities and durations, in order to verify the behaviour of the detention reservoir in different situations. For the simulations, the EPA SWMM software was used, which made it possible to implement the scenarios under study as well as the compensatory measure. The results showed that the distributed detention basins were efficient in mitigating the peaks of surface runoff in a sustainable way, from almost 45.0 L/s to approximately 7.5 L/s, in addition to increasing the peak time of the area considered in the simulations.

A research presented in [17] addresses the flow dampening microreservoirs, seeking to size and assess their impact at the lot and subdivision level and, subsequently, at the macrodrainage scale. In the subdivision used in the study, for a 10-minute rainstorm, the peak flow dampening was 63%, while for a 60-minute rainstorm and for the critical rain, it was reduced by 54% and 44%, respectively.

A study described in [18] evaluated the effect that the implementation of control measures at the source can provide in the abatement of flood peaks in densely occupied urban areas. The analyses were done through 209 scenarios, using a decision support system for SWMM, and contemplated permeable pavements, green roofs, and rain gardens as alternatives for retention.

In accordance with [19], an on-site stormwater detention system was constructed in a house's car porch with a 4.40 m x 4.70 m x 0.45 m tank filled with precast-concrete modular units with an effective storage volume of 3.97 m3. The system received water from a 95 m2 house roof via 0.1 m diameter pipe, discharged water via 0.05 m diameter pipe. It had been recorded six observed storm events, that consisted 20 - 50 mm peak hourly rainfall, 0.7 - 1.8 L/s inflow, 0.5 - 1.2 L/s outflow, and 0.21 - 0.47 m water level. Previous four historical storm events were sourced to augment the analysis. A computer model developed using the storm water management model was calibrated and verified using the six observed events. As such, the calibrated and verified model was used to simulate the historical storm events with 40 - 50 mm peak hourly rainfall and produced 1.0 - 1.3 L/s inflow, 0.72 - 0.76 L/s outflow, and 0.41 - 0.45 m water level.

A similar study, mentioned in [20], focuses on the probability of OSD below a residential vehicle porch. The space given in the vehicle porch area can be utilised by installing an OSD beneath it to temporarily store rainwater from the roof while raining in the hopes of decreasing surface runoff. The OSD is exposed to 15-minute, 10-year return periods interval design rains. SWMM is used to illustrate this process in urban hydrology. The performance of the OSD is further examined by varying the number of orifice exits. According to modelling efforts, one orifice exit is ideal, resulting in a 95% discharge decrease at the outfall.

An article published in [21] describes the findings of a study comparing the efficiency of three retention devices with different hydraulic systems: the standard single-chamber reservoir, the modified multi-chamber reservoir with an accumulation and flow compartment implemented as a channel with overflow, and a reservoir that works together with a drainage system via a certain degree of retention capacity availability of its channels itself. The simulation study's research revealed that the usage of ordinary single-chamber reservoirs is the less efficient approach. A contrast of the functions of various hydraulic systems of retention reservoirs under equal circumstances revealed that the required retention volume of a single-chamber reservoir is many times bigger than that of highly efficient alternatives, and it can account for up to 582% of the reservoir's capacity when used in conjunction with the channel retention system. Simultaneously, it

has been proved that using channel retention is not the most efficient approach for all hydraulic circumstances in a drainage network or for all hydrological conditions. Furthermore, the research presents a set of retention performance measures that may be used to evaluate particular rainwater storage technologies in the prospective.
Reference [22] states that it is well known that OSD can have adverse effects when it is installed at inappropriate locations, ending up exacerbating the problems of floods. Issues about relying on OSD for regional hydrology control are increased by parameter uncertainty and the requirement for a statistical method to hydrograph development. It introduces research that serves to spread awareness of these concerns as well as providing a realistic solution to the issue. Using interconnected modules, a hydrologic framework for Monte Carlo simulation of regional watershed hydrographs was built. A sample of ten regional watersheds was modelled with the scenarios of current situation, with plots of land of varying sizes and urbanised points in different locations within the regional catchment basin, and with such urbanised points containing OSD. The results have been focused on the discovery and evaluation of two important factors that affect the peak runoff of regional watersheds, namely the size and position of the urban areas land parcel.
The article presented in [23] expresses concern that many existing OSD systems created using the singular temporal pattern for creation storms can fail to meet their claimed aims when tested against a range of other temporal patterns. Following an investigation of the performance of twenty genuine OSD systems, it was determined that expanding the number of temporal patterns for the design and evaluation of OSD systems improved the success rate of accomplishing objectives. In practice, as many different temporal patterns as feasible should be explored as a proposed solution.
In [24], a design technique is suggested that establishes certain new criteria that connect impervious portions of the lots to tank design parameters. The efficiency concept was developed on the assumption that the tanks should offer the restoration of flows from an impervious region to its pre-urbanization situation. This was determined to be 70% of the local maximum discharge. Based on flow routing simulations using the Puls Method, the ideal geometric properties of the tanks (volume, area, water depth, and orifice diameter) were determined to ensure a decrease in the peak. When compared to the results of the municipal legislation plan, the new technique proved to be more efficient, with a 24% reduction in storage tank.
The efficiency of rainwater detention tanks with specific design configurations (insertion into the rain sewerage system; capacity per impermeable area) and operating circumstances (constant and irregular emptying criteria) was analysed using an integrated methodology presented in [25]. Different performance measures have been used to quantify the decrease of pollution impact on the natural environment, the reduction of maintenance and management costs for the urban drainage system, the preservation of regular purifying reliability, and the restriction of expenses at the treatment system. The impact of the primary parameters of the urban catchment and the drainage system (area of the basin and system inclination) on the performance of different design and operational approaches has also been investigated. According to it, stormwater detention tanks combined with discharge controls demonstrated positive results in terms of environmental damage: adequate performance metrics can be achieved with relatively low flow rates of flow regulators (0.5 - 1.0 L/s per hectare of impervious area) and tank volumes of about 35 - 50 m3 per impervious surface. Constant emptying ensured the least amount and length of overflows, but discontinuous operation reduced the amount sent for purification, lowering costs and chances of degradation in the plant's regular treatment efficiency. Generally, simulation results demonstrated that the extent of the watershed and the slope of the drainage system have little effect on efficiency indicators.

3. Methodology

The aim of this article is to present a theoretical comparative study, in terms of peak flow and required pipe diameters, between a conventional drainage system and another one equipped with small underground reservoirs for rainwater runoff attenuation, located at the front of the lots in an urban subdivision. Six stretches of pluvial gallery, receiving contributions from sub-basins delimited by the bottom of the lots and by the drain inlets, which follow each sequence of 03 lots on the

same side of the street (06 on both) were considered. The lots have a frontage of 15 metres and a depth of 32 metres. The cross section of the street and sidewalks is 12 metres, and the longitudinal slope of the street, which coincides with that of the drainage galleries, is 0.01 m/m. The system described is schematized in Figure 1.

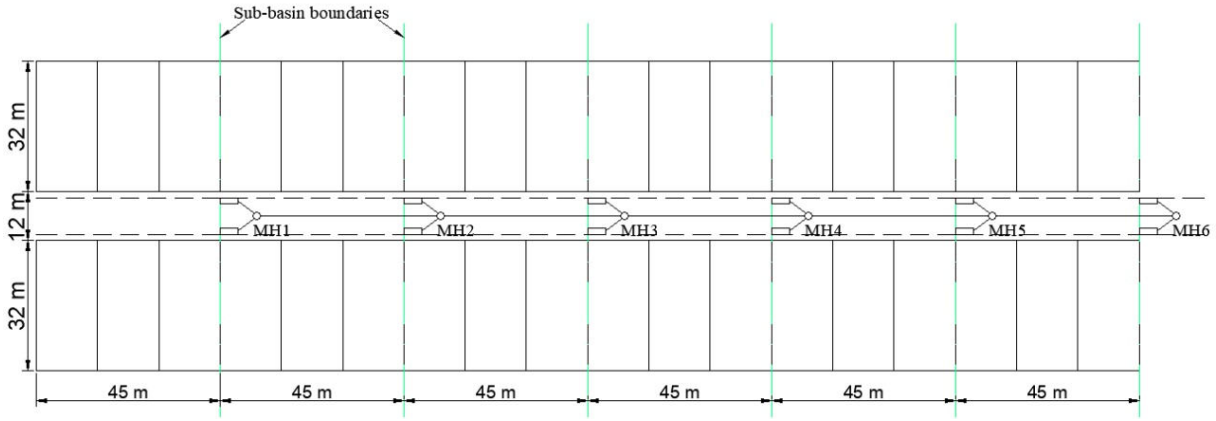

Fig. 1. Schematic of the conventional rainwater drainage system

The process adopted for flow rates calculation was the Rational Method, with time of concentration of 12 minutes in the headwater sub-basin for residential areas with gutter slope less than 03% [26], and 18-year recurrence time, according to that recommended for micro-drainage works (05-20-year). Intensity-duration-frequency equation for the city of Juiz de Fora was used. The runoff coefficient C is 0.5. A uniform steady state is assumed in sections between manholes, and the hydraulic calculations were made using the Manning equation, with a relative roughness coefficient of 0.013. For the hydraulic sizing of pipes, a water depth of at most 85% of the diameter is allowed, in accordance with technical standards. Figure 2 illustrates the worksheet for calculating the drainage gallery, inspired by the worksheet for the dimensioning of sanitary sewage networks [27].

UPSTREAM RUNOFF											DOWNSTREAM GALLERY								
Manhole	A lot (ha)	A st+sw (ha)	A_{accum} (ha)	DC	tc (min)	I (mm/h)	C	Q lot (L/s)	Q st+sw (L/s)	Q total (L/s)	S (m/m)	D_{theor} (m)	D_{real} (m)	K1´	h/D_{real}	h (m)	V (m/s)	L (m)	T_{tl} (min)
1	0,288	0,054	0,342	1	12,00	158,7	0,5	63,5	11,9	75,5	0,01	0,27	0,40	2,266	0,42	0,168	1,50	45	0,50
2	0,288	0,054	0,684	1	12,50	156,6	0,5	62,7	11,8	149,9	0,01	0,35	0,40	1,751	0,63	0,250	1,81	45	0,41
3	0,288	0,054	1,026	0,9962	12,91	154,9	0,5	61,8	11,6	223,3	0,01	0,41	0,50	1,885	0,55	0,275	2,02	45	0,37
4	0,288	0,054	1,368	0,9541	13,28	153,5	0,5	58,6	11,0	292,9	0,01	0,45	0,50	1,703	0,66	0,331	2,13	45	0,35
5	0,288	0,054	1,71	0,9227	13,64	152,1	0,5	56,2	10,5	359,6	0,01	0,49	0,50	1,577	0,78	0,392	2,18	45	0,34
6	0,288	0,054	2,052	0,8978	13,98	150,8	0,5	54,2	10,2	423,9	0,01	0,52	0,60	1,779	0,61	0,365	2,36	45	0,32

Fig. 2. Calculation worksheet of the conventional rainwater drainage system

The worksheet in Figure 2 lists, for each sub-basin and the respective downstream gallery, the areas of the lots and the street and sidewalks; the accumulated area from the headwater sub-basin; the distribution coefficient, which takes into account the irregular distribution of rainfall; the time of concentration; the rainfall intensity; the runoff coefficient; the flow rates of lots, of the street and sidewalks, and total; the slope of the rainwater gallery; the theoretical diameter, for a water depth of 85% of the diameter; the real diameter, immediately superior to the theoretical one; an auxiliary coefficient; the relationship between water height and the chosen diameter; the height of the water depth; the average velocity of the flow; the length of the gallery; and the travel time.
The flow rates from the rains on the lots had to be treated separately from those generated from the streets and sidewalks, due to the fact that, as the reservoirs are placed in the lots, only the flows originating there will have their flow rates attenuated.
It is also important to keep in mind that the damped flow rates of the lots must be those that occur in the same time of concentration considered for the flow rates of the streets and sidewalks, since they will be added.
Figure 3 illustrates a scheme similar to that of Figure 1, however with the small underground damping reservoirs in the front part of the lots. The reservoirs were given the full dimension of the width of the lot, 15.0 m, and a length of 1.0 m, making up an area of 15.0 m2. Each reservoir is provided with a 75 mm orifice at the bottom, for the discharge of the flows.

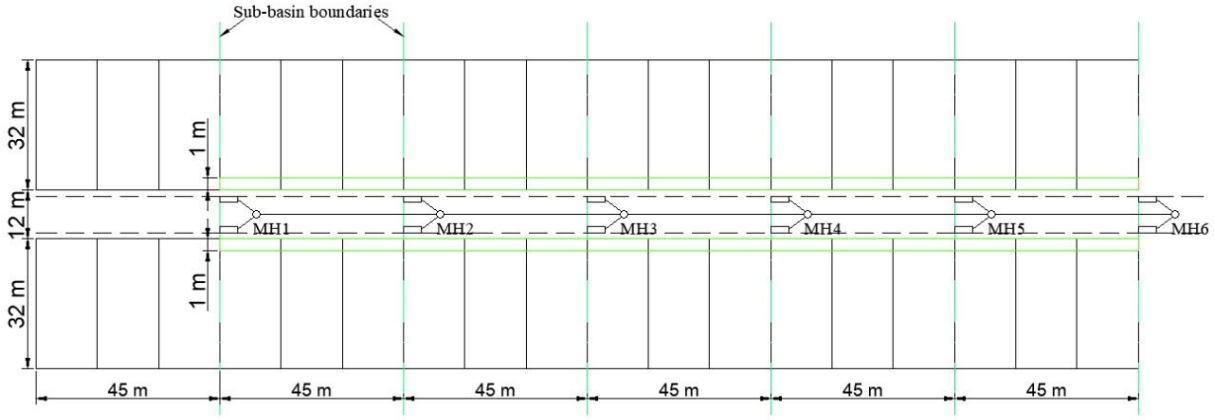

Fig. 3. Schematic of the rainwater drainage system with damping

Using the Routing Simulator Application, introduced in [28, 29], it is possible to determine the flows damped by the lot reservoirs, in each of the sub-basins. Consequently, the total flows of each section will be reduced in relation to the scheme without damping, and it is possible that the diameter previously designated for each section between manholes (MH) can also be reduced in relation to the conventional drainage system, still meeting the criterion that the maximum depth of water is 85% of the diameter.
Figures 4 and 5 show a simulation by the Routing Simulator of the lots flow rate attenuation, from 62.7 L/s to 30.6 L/s, referring to the second upstream sub-basin, which contributes to the gallery section MH2-MH3, the values being in m3/s.

Fração	Tempo Inicial [s]	DT [s]	QA_i	QA_f	QEi	$V_{i\,[m^3]}$	V_f	QE_f	K_1	K_2	Tentativa
1	60	60	0.00	0.01	0.00	0.00	0.08	0.0026	0.27	0.16	21
2	120	60	0.01	0.01	0.00	0.08	0.32	0.0051	0.27	0.47	10
3	180	60	0.01	0.02	0.01	0.32	0.72	0.0077	0.27	0.95	7
4	240	60	0.02	0.02	0.01	0.72	1.28	0.0102	0.27	1.59	11
5	300	60	0.02	0.03	0.01	1.28	2.00	0.0128	0.27	2.38	7
6	360	60	0.03	0.03	0.01	2.00	2.88	0.0153	0.27	3.34	13
7	420	60	0.03	0.04	0.02	2.88	3.92	0.0179	0.27	4.46	14
8	480	60	0.04	0.04	0.02	3.92	5.12	0.0204	0.27	5.74	14
9	540	60	0.04	0.05	0.02	5.12	6.48	0.0230	0.27	7.17	9
10	600	60	0.05	0.05	0.02	6.48	8.00	0.0255	0.27	8.77	9
11	660	60	0.05	0.06	0.03	8.00	9.68	0.0281	0.27	10.53	13
12	720	60	0.06	0.06	0.03	9.68	11.52	**0.0306**	0.27	12.44	15
13	780	60	0.06	0.06	0.03	11.52	13.27	0.0329	0.27	14.26	15
14	840	60	0.06	0.06	0.03	13.27	14.69	0.0346	0.27	15.73	15
15	900	60	0.06	0.05	0.03	14.69	15.81	0.0359	0.27	16.89	16
16	960	60	0.05	0.05	0.04	15.81	16.66	0.0369	0.27	17.76	16
17	1020	60	0.05	0.05	0.04	16.66	17.25	0.0375	0.27	18.38	14
18	1080	60	0.05	0.04	0.04	17.25	17.60	0.0379	0.27	18.74	15
19	1140	60	0.04	0.04	0.04	17.60	17.73	0.0380	0.27	18.87	17
20	1200	60	0.04	0.03	0.04	17.73	17.65	0.0379	0.27	18.78	14
21	1260	60	0.03	0.03	0.04	17.65	17.37	0.0376	0.27	18.50	14
22	1320	60	0.03	0.03	0.04	17.37	16.90	0.0371	0.27	18.02	14
23	1380	60	0.03	0.02	0.04	16.90	16.26	0.0364	0.27	17.35	14
24	1440	60	0.02	0.02	0.04	16.26	15.46	0.0355	0.27	16.53	12
25	1500	60	0.02	0.02	0.04	15.46	14.51	0.0344	0.27	15.54	13
26	1560	60	0.02	0.01	0.03	14.51	13.43	0.0331	0.27	14.42	13
27	1620	60	0.01	0.01	0.03	13.43	12.22	0.0316	0.27	13.17	13
28	1680	60	0.01	0.01	0.03	12.22	10.90	0.0298	0.27	11.80	13
29	1740	60	0.01	0.00	0.03	10.90	9.48	0.0278	0.27	10.32	11
30	1800	60	0.00	0.00	0.03	9.48	7.98	0.0255	0.27	8.75	10

Fig. 4. Routing Simulator numeric output screen

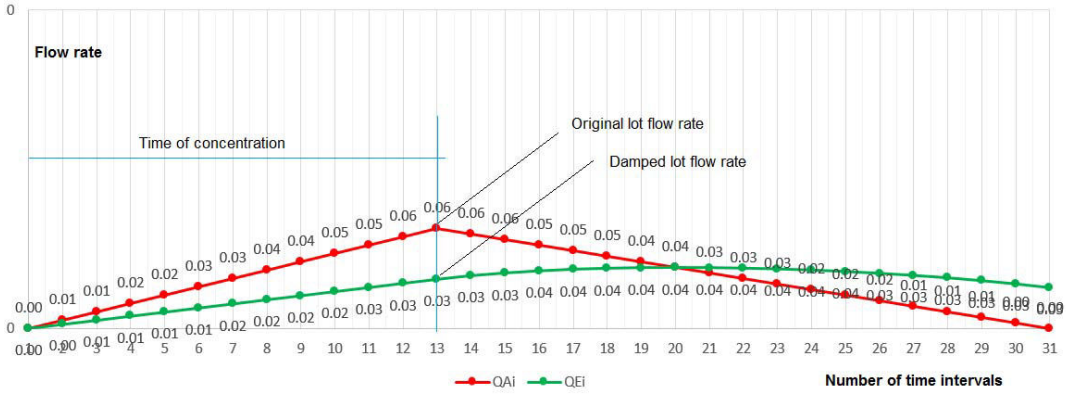

Fig. 5. Routing Simulator graphical output screen

Assigning the damped values to a spreadsheet as in Figure 2, a new spreadsheet is generated, representing the proposed drainage system, shown in Figure 6.

UPSTREAM RUNOFF											DOWNSTREAM GALLERY								
Manhole	A lot (ha)	A st+sw (ha)	A_{accum} (ha)	DC	tc (min)	I (mm/h)	C	Q lot (L/s)	Q st+sw (L/s)	Q total (L/s)	S (m/m)	D_{theor} (m)	D_{real} (m)	K1	h/D_{real}	h (m)	V (m/s)	L (m)	T_u (min)
1	0,288	0,054	0,342	1	12,00	158,7	0,5	63,5	11,9	75,5	0,01	0,27	0,40	2,266	0,42	0,168	1,50	45	0,50
2	0,288	0,054	0,684	1	12,50	156,6	0,5	30,6	11,8	117,8	0,01	0,32	0,40	1,917	0,54	0,214	1,72	45	0,44
3	0,288	0,054	1,026	0,9962	12,94	154,9	0,5	30,4	11,6	159,8	0,01	0,36	0,40	1,71	0,66	0,262	1,83	45	0,41
4	0,288	0,054	1,368	0,9541	13,35	153,2	0,5	29,4	11,0	200,2	0,01	0,39	0,40	1,571	0,79	0,316	1,88	45	0,40
5	0,288	0,054	1,71	0,9227	13,74	151,7	0,5	28,4	10,5	239,1	0,01	0,42	0,50	1,838	0,57	0,287	2,05	45	0,37
6	0,288	0,054	2,052	0,8978	14,11	150,3	0,5	27,8	10,1	277,0	0,01	0,44	0,50	1,739	0,63	0,317	2,11	45	0,36

Fig. 6. Calculation worksheet for the damped rainwater drainage system

Figure 6 expresses the flow values in L/s, unlike the Routing Simulator, where they are represented in m3/s.

4. Results and Discussion

As verified in the simulations, the maximum level reached by the water in the damping reservoir was 20.0 cm. A recess in the bottom is suggested to accommodate the 75 mm discharge orifice, to be protected with mesh to prevent the ingress of solids, with consequent flow to the street drainage gallery. In this way, the reservoirs could have a total depth of 30 cm.
Table 1 summarises the values of the worksheet in Figure 6 and shows the total flow rates in each section between manholes and their respective diameters of the rain gallery, respecting the maximum depth limits of 85% of the diameter, both for the conventional drainage system and for the drainage system with damping in the lot reservoirs.

Table 1: Flow rates and diameters of conventional and damped systems

Gallery section	Q (L/s) conventional system	Q (L/s) damped system	D (mm) conventional system	D (mm) damped system
1 - (MH1-MH2)	75.5	75.5	400	400
2 - (MH2-MH3)	149.9	117.8	400	400
3 - (MH3-MH4)	223.3	159.8	500	400
4 - (MH4-MH5)	292.9	200.2	500	400
5 - (MH5-MH6)	359.6	239.1	500	500
6 - (MH6-MH7)	423.9	277.0	600	500

Flow data were expressed graphically and are represented in Figure 7.

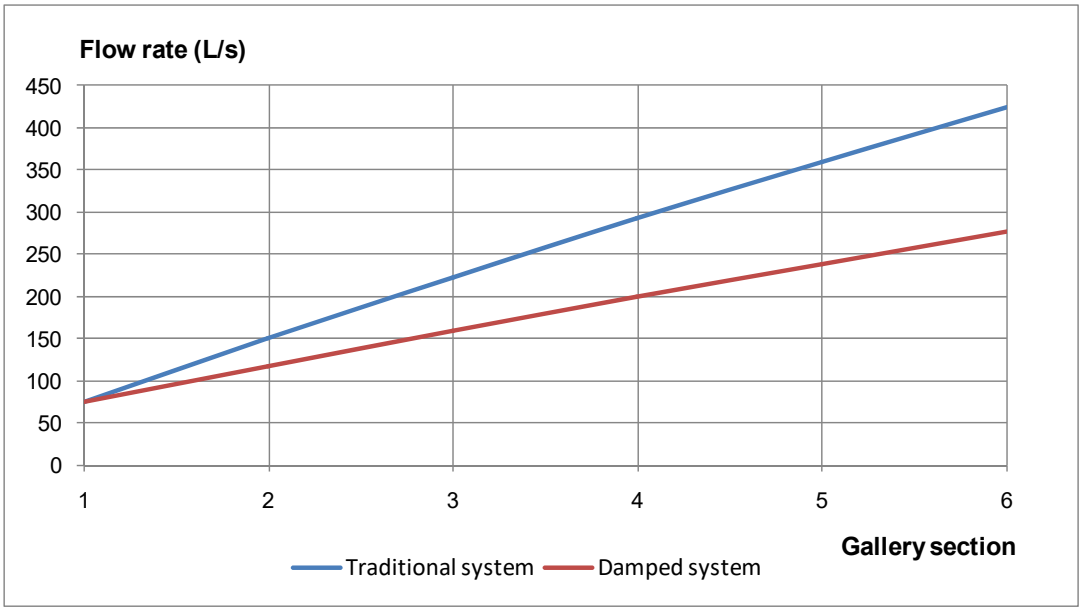

Fig. 7. Evolution of flow damping per section of rainwater gallery

It was found that, with the adoption of damping reservoirs, the flow rates were reduced from 21% to 35% in relation to those of traditional systems, with such percentages of reduction increasing as one went from upstream to downstream. This behaviour suggests that there could be even greater damping if the number of sections were greater than that represented here.
The design of the drainage galleries using the traditional system resulted in diameters of 400 mm for the two initial sections, 500 mm for the three following sections, and 600 mm for the last section. Using the proposal of damping reservoirs in the lots, the design indicated diameters of 400 mm for the first four sections and 500 mm for the last two sections. That is, with the methodology, there was a gain in relation to the diameter reduction in the third and fourth sections, from 500 to 400 mm, and in the last section, from 600 to 500 mm.

5. Conclusion

A work was presented and discussed on the installation of small reservoirs in the lots to dampen the flows, with an impact on reducing the diameters of the drainage galleries. Simply aiming at a matter of financial advantage, it would be enough for the person responsible for the subdivision's infrastructure to verify if it would be more interesting, financially speaking, to save the amount referring to the reduction of the diameters of the galleries and bear the cost of building the damping units, or proceed from the traditional way.
However, this issue can be presented in a much more complex way, where not only the micro level, internal to the subdivision, is the one to be evaluated, but also the macro level, that of the city where it is inserted. Although the issues inherent to the subdivision, referring to the correct drainage of rainwater can be fully satisfied, greater or lesser flow rates may be released in the already consolidated galleries of the city, providing conditions for the occurrence or not of flooding. The matter may involve social policies and urban development interests. It is not just a necessarily punctual approach. This can, and perhaps should, also be seen as an environmental, public health, welfare and social responsibility issue.

References

[1] Tassi, Rutinéia, and Adolfo O. N. Villanueva. "Analysis of the impact of lot microreservoirs in the costs of an urban drainage network (Análise do impacto dos microrreservatórios de lote nos custos de uma rede de drenagem urbana)." *Revista Brasileira de Recursos Hídricos* 9, no. 3 (July-September 2004): 89–98. http://dx.doi.org/10.21168/rbrh.v9n3.p89-98.

[2] Ionescu, Cristina S., and Daniela E. G. Nistoran. "Influence of reservoir shape upon the choice of hydraulic vs. hydrologic reservoir routing method." *E3S Web of Conferences* 85 (February 2019): 1–8. http://dx.doi.org/10.1051/e3sconf/20198507001.

[3] Dias, Gilmara E. L. "Feasibility study of collective reservoirs in damping peak flows in drainage of rainwater for a condo in Curitiba - PR (Estudo de viabilidade de reservatórios coletivos no amortecimento de vazões de pico em drenagem de águas pluviais para um condomínio em Curitiba - PR)." Undergraduation final report, Federal Technological University of Paraná, Curitiba, 2015. https://repositorio.utfpr.edu.br/jspui/handle/1/7962.

[4] Carrera, Carolina M. A., Catherine A. Miyazaki, Daniel N. Guerra, and Guilherme G. Silva. "Non-conventional structural solutions in urban drainage (Soluções estruturais não convencionais em drenagem urbana)." Undergraduation final report, University of São Paulo, São Paulo, 2016. https://repositorio.usp.br/bitstreams/771dd72a-f7e6-429b-be3d-ceacb4617bca.

[5] Chen, Weicheng. "Efficiency of urban water detention methods in downstream cities." Student report, Delft University of Technology, Delft, 2017. https://repository.tudelft.nl/islandora/object/uuid%3A2bcff4aa-75c2-4265-8590-661a19471eb9.

[6] Drumond, Pedro P., Priscilla M. Moura, Talita F. G. Silva, Juliana C. Ramires, and Lucas R. V. Silva. "Citizens's perception on stormwater management and use of on-site stormwater detention in Belo Horizonte/Brazil." *Brazilian Journal of Water Resources* 27 (2022): 1–15. https://doi.org/10.1590/2318-0331.272220210137.

[7] Nakazone, Lucia M. "Implementation of stormwater storage facilities for low income dwelling: the CDHU experiences (Implantação de reservatórios de detenção em conjuntos habitacionais: a experiência da CDHU)." Master thesis, University of São Paulo, São Paulo, 2005. https://www.teses.usp.br/teses/disponiveis/3/3147/tde-13042006-210759/pt-br.php.

[8] Cruz, Marcus A. S., Carlos E. M. Tucci, and André L. L. da Silveira. "Runoff control with detention in urban lots (Controle do escoamento com detenção em lotes urbanos)." *Revista Brasileira de Recursos Hídricos* 3, no. 4 (October-December 1998): 19–31. http://dx.doi.org/10.21168/rbrh.v3n4.p19-31.

[9] Della, Juliano P., Carlos R. Bavaresco, and Álvaro J. Back. "Control of flow through micro reservoirs in urban lots (Controle de escoamento através de micro reservatórios em lotes urbanos)." In *Territorial Planning and Management: the role and instruments of territorial planning at the interface between urban and rural* (*Planejamento e Gestão Territorial: o papel e os instrumentos do planejamento territorial na interface entre o urbano e o rural*), edited by Nilzo I. Ladwig, and Juliano B. Campos, 306–322. Criciúma, UNESC Press, 2019.

[10] Drake, Jennifer, Dean Young, and Nicholas McIntosh. "Performance of an underground stormwater detention chamber and comparison with stormwater management ponds." *Water* 8, no. 5 (2016): 1–13. https://doi.org/10.3390/w8050211.

[11] Drumond, Pedro P., Priscilla M. Moura, and Márcia M. L. P. Coelho. "Comparison the monitoring data of an on-site stormwater detention (OSD) and the results in the use of theoretical methods for its design." *Brazilian Journal of Water Resources* 23 (2018): 1–12. https://doi.org/10.1590/2318-0331.231820170149.

[12] Drumond, Pedro P., James E. Ball, Priscilla Moura, and Márcia M. L. P. Coelho. "Are the current on-site stormwater detention (OSD) policies the best solution for source control stormwater management? A case study of Australian and Brazilian cities." *Urban Water Journal* 17, no. 3 (2020): 273–281. https://doi.org/10.1080/1573062X.2020.1760321.

[13] Drumond, Pedro P., Priscilla M. Moura, and Márcia M. L. P. Coelho. "Improving the understanding of on-site stormwater detention performances." *Urban Water Journal* (2022): 1–19. https://doi.org/10.1080/1573062X.2021.2020300

[14] Francischet, Marcelo M., and José E. Alamy Filho. "Analysis of the influence of household detention reservoirs on urban surface runoff applied to the estimation of critical flows generated in a standard block (Análise da influência dos reservatórios de detenção domiciliares no escoamento superficial urbano aplicados na estimativa de vazões críticas geradas em uma quadra padrão)." Paper presented at the XIX Brazilian Symposium on Water Resources, Maceió, Brazil, November 27 - December 01, 2011. https://www.abrhidro.org.br/SGCv3/publicacao.php?PUB=3&ID=81&SUMARIO=970.

[15] Francischet, Marcelo M. "Analysis of the influence of household detention reservoirs on urban surface runoff (Análise da influência dos reservatórios de detenção domiciliares no escoamento superficial urbano)." Master thesis, Federal University of Uberlândia, Uberlândia, 2012. https://repositorio.ufu.br/bitstream/123456789/14168/1/d.pdf.

[16] Sangalli, Nayara C. R., Loriane C. B. Kalinoski, and Cesar A. M. Destro. "Evaluation of the use of distributed detention reservoirs in residences in the mitigation of surface runoff peak in a periurban microbasin in Pato Branco/PR (Avaliação do uso de reservatórios de detenção distribuída em residências na mitigação de pico de escoamento superficial em uma microbacia periurbana em Pato

Branco/PR)." Paper presented at the XIV Italian-Brazilian Symposium on Sanitary and Environmental Engineering, Foz do Iguaçu, Brazil, June 18-20, 2018. https://abesnacional.com.br/XP/XP-EasyArtigos/Site/Uploads/Evento40/TrabalhosCompletosPDF/IX-006.pdf.

[17] Silva, Daniele F. "Analysis of micro-reservoirs influence in a residential land and its effects in a catchment scale (Análise da influência de microrreservatórios em um loteamento e seus efeitos em escala de bacia)." Master thesis, University of São Paulo, São Carlos, 2016. https://www.teses.usp.br/teses/disponiveis/18/18138/tde-23032017-111325/pt-br.php.

[18] Tominaga, Erika N. S. "Urbanization and flood: low impact development practices (Urbanização e cheias: medidas de controle na fonte)." Master thesis, University of São Paulo, São Paulo, 2013. https://www.teses.usp.br/teses/disponiveis/3/3147/tde-19092014-120127/pt-br.php.

[19] Mah, Darrien Y. S., Johnny O. K. Ngu, Rosmina A. Bustami, and Frederik J. Putuhena. "Case study of modular pre-cast concrete on-site stormwater detention system during monsoon season in southeast Asia." *Applied Environmental Research* 43, no. 1 (2021): 28–40. https://doi.org/10.35762/AER.2021.43.1.3.

[20] Ngu, Johnny O. K., Darrien Y. S. Mah, Ching V. Liow, and Ik T. Ngu. "Modelling of On-Site Stormwater Detention Underneath a Car Porch." *International Journal of Innovative Technology and Exploring Engineering* 8, no. 12 (October 2019): 4304–4307. http://doi.org/10.35940/ijitee.L2718.1081219.

[21] Pochwat, Kamil. "Assessment of rainwater retention efficiency in urban drainage systems—model studies." *Resources* 11, no. 2 (2022): 1–23. https://doi.org/10.3390/resources11020014.

[22] Ronalds, Rodney, and Hong Zhang. "Assessing the impact of urban development and on-site stormwater detention on regional hydrology using Monte Carlo simulated rainfall." *Water Resources Management* 33 (2019): 2517–2536. https://doi.org/10.1007/s11269-019-02275-y.

[23] Ronalds, Rodney, Alex Rowlands, and Hong Zhang. "On-site stormwater detention for Australian development projects: Does it meet frequent flow management objectives?" *Water Science and Engineering* 12, no. 1 (2019): 1–10. https://doi.org/10.1016/j.wse.2019.03.004.

[24] Souza, Ricardo C. C., Flávio B. Freire, and Michael Mannich. "Design guidelines for on-site stormwater detention." *Ciência e Natura* 43 (2021): 1–20. https://doi.org/10.5902/2179460X63494.

[25] Todeschini, Sara, Sergio Papiri, and Carlo Ciaponi. "Performance of stormwater detention tanks for urban drainage systems in northern Italy." *Journal of Environmental Management* 101 (2012): 33–45. https://doi.org/10.1016/j.jenvman.2012.02.003.

[26] Tourasse, Enio. *Urban Drainage*. Rio de Janeiro: unpublished, 1994.

[27] Nascimento, Marcus V., Mayara R. Nascimento, and Henrique S. Pizzo. "Electronic worksheet for sizing and verification of sewage networks (Planilha eletrônica para dimensionamento e verificação de redes de esgoto)." *Estação Científica* 26 (August-December 2021): 1–18. https://doi.org/10.6084/m9.figshare.20406258.v2.

[28] Galil, Vinícius M., and Henrique S. Pizzo. "Flood damping curve modeling by flood routing method using Visual Basic for Applications-VBA." *International Journal of Science and Engineering Investigations* 10, no. 115 (August 2021): 50–55. https://doi.org/10.6084/m9.figshare.20406213.v2.

[29] Pizzo, Henrique S., and Vinícius M. Galil. "Detention reservoir: proposal for flood control in the Ipiranga stream basin, Juiz de Fora, MG, Brazil." *Journal of Mechanical, Civil and Industrial Engineering* 2, no. 2 (2021): 34–43. https://doi.org/10.32996/jmcie.2021.2.1.6.

Remote Control of an Automatic System for Handling Fragile Objects

Ph.D. Eng. **Ionel Laurențiu ALBOTEANU**[1,*], Eng. **Ionel Bogdan ILIE**[1]

[1] University of Craiova, Faculty of Electrical Engineering

* lalboteanu@em.ucv.ro

Abstract: *The paper presents a remote control solution based on wireless technology of a small-scale fragile object handling system. The description of the handling system and the local control solution by means of a PLC have been published in Hidraulica Magazine no. 4/2020 [1].*

Keywords: *Remote control, wireless, automatic system, handling, electro-pneumatic drive, vacuum technology*

1. Introduction

The term wireless communication was introduced in the 19th century, and wireless communication technology developed over the following years. It is one of the most important means of transmitting information from one device to another. In this technology, information can be transmitted through the air without requiring cable or wires or other electronic conductors by using electromagnetic waves such as IR, RF, satellite, etc. [2].
Currently, wireless communication technology refers to a variety of wireless devices and communication technologies, from smartphones to computers, tabs, laptops, Bluetooth technology, printers.
Wi-Fi is a low-power wireless communication that is used by various electronic devices such as smartphones, laptops, etc. In this configuration, a router acts as a wireless communications hub. These networks only allow users to connect in close proximity to a router. WiFi is very common in networking applications that provide wireless portability [2].
The aim of the work is remote monitoring and control of an automatic fragile object handling system through the Blynk application. This is achieved by attaching a wireless module to the automatic handling system designed to remotely monitor and control the handling of various fragile objects using a vacuum suction cup [3], [4].
The wireless module used is NodeMCU ESP8266, as it provides a complete and self-contained Wi-Fi network solution, allowing it to host the application or offload all Wi-Fi network functions from another application processor.

2. Structure of the handling system

The proposed automatic fragile object handling system consists of a stock of fragile plates at the entrance, an output stock and a manipulator system that transfers the plates to be processed from the input stock to the output stock (Fig.1).

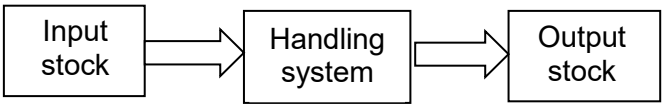

Fig. 1. Structure of handling system

Starting from the previously presented structure of the fragile object handling system, it is proposed to create a manipulating system that performs the handling operation for a single piece per work cycle, and the input stock has a capacity that can include several fragile plates.
The entire structure is integrated in an electro-pneumatic drive system with linear (pneumatic cylinder) and rotary (electric motor) actuators, controlled by monostable and bistable valves [5],[6], [7], [8].

The block diagram of the handling system is shown in Fig. 2.

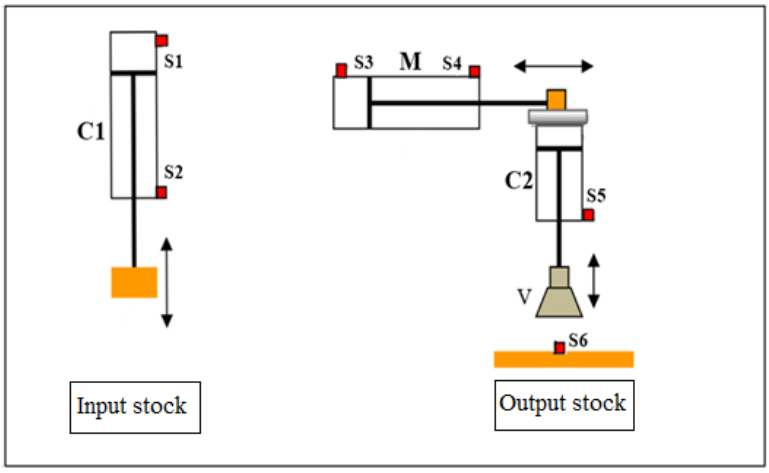

Fig. 2. Block diagram of handling system

Based on the structure of the pneumatic drive, the general scheme of the automatic handling system (Fig. 3) has been drawn up.

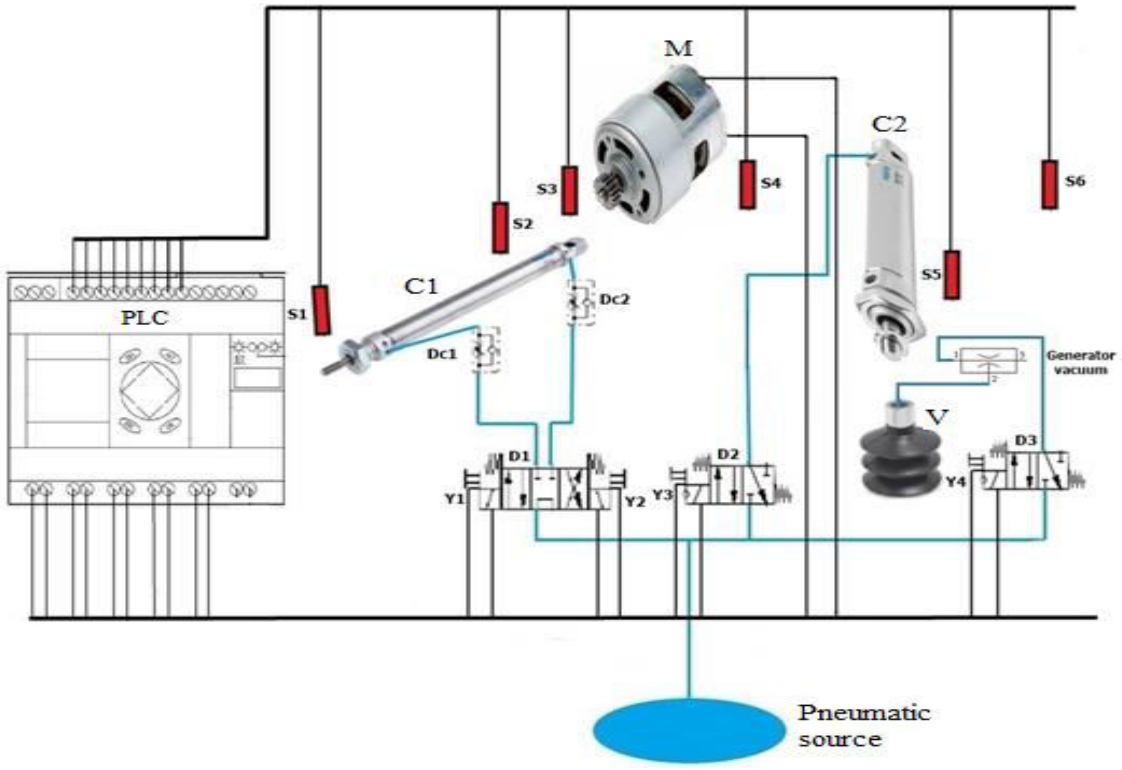

Fig. 3. Schematic diagram for the interconnection of the elements of the handling system

The meaning of the elements used in the scheme is as follows:
PLC – programmable logic controller;
D1...D3 – pneumatic valve;
C1, C2 – pneumatic cylinders;
M – electric motor;
DC1...DC3 – one-way flow control valves;
S1...S6 – sensors;
Y1...Y4 – relays valve control;
V – vacuum suction cup.

3. Structure of remote control system

3.1. Hardware structure

One of the most challenging problems in the design of control systems is the development of the system architecture, namely the choice of hardware components (e.g.: sensors, actuators, integrated circuits, microcontrollers) [9], [10].
To design the system, several tests have been carried out with various types of development boards, among which we can list: ESP8266 NodeMCU, Arduino UNO WIFI Rev2 and ESP-01 ESP8266.
Following the tests carried out, it has been proven that the best solution that lends itself to implementation is the use of the ESP8266 NodeMCU development system.
The main advantage of this system, compared to the two tested modules, is given by the multitude of analog and digital outputs that are arranged on the same board, by the size but also by the technical characteristics that will be presented next.

1) Development board ESP8266 NodeMCU

The NodeMCU ESP8266 development board comes with the ESP-12E module which contains the ESP8266 chip having Tensilica Xtensa 32-bit LX106 RISC microprocessor. This microprocessor supports RTOS and operates at an adjustable clock frequency from 80 MHz to 160 MHz. The NodeMCU has 128 KB of RAM and 4 MB of Flash memory to store data and programs. Its high processing power with built-in Wi-Fi/Bluetooth and sleep mode operation functions make it ideal for IoT (Internet of Things) projects [11].
The NodeMCU can be powered using a Micro USB plug but also a VIN pin (external power pin).
ESP8266 NodeMCU development board is based on a wireless ESP8266 microcontroller with Wi-Fi 802.11 compatible IDE-Arduino development environment. The structure of this board is based on a standard Arduino hardware design with similar proportions to the Arduino Uno and Leonardo.
The low price of the device has made it very popular, being included in modules, but also in development boards for IoT applications. The ESP8266 contains a 32-bit processor clocked at 80 MHz, with 32kB instruction RAM and 80kB user RAM.

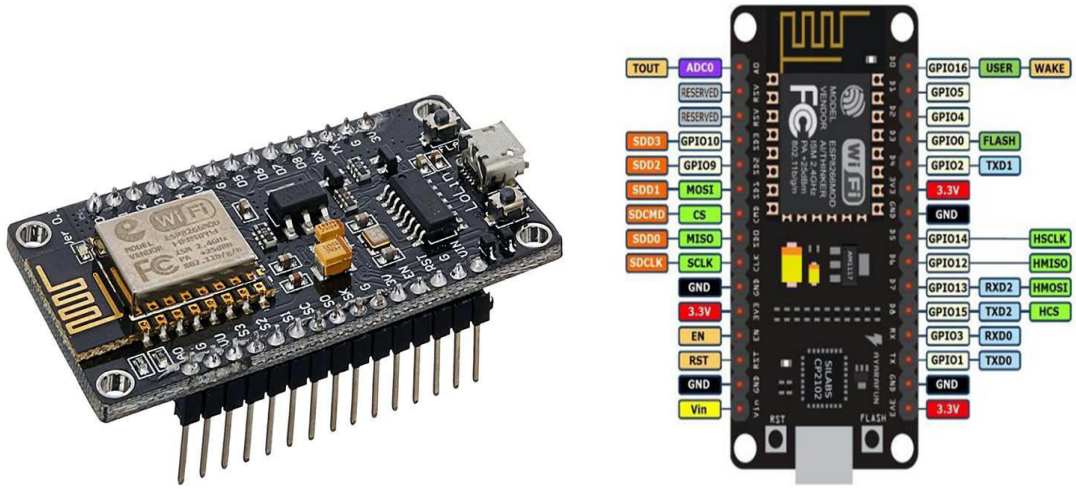

Fig. 4. ESP8266 NodeMCU development board

2) Expansion module

For the control of the component elements that make up the hardware part of the handling system, the solution of building an expansion board consisting of the supply part and the control part has been adopted (Fig. 5). This board has been designed using the Targhet 3001 program [12].
The module is useful for controlling several devices operating at different voltages (12V, 24V) using the NodeMCU ESP8266 development board.

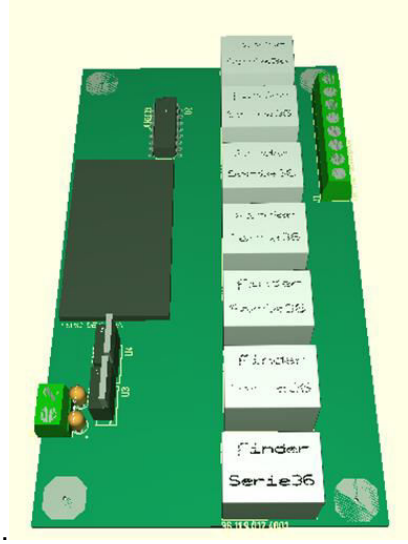

Fig. 5. Expansion module

3.2. Software structure

For the software part, the Blynk application has been used, an application that can be installed on almost any smartphone or tablet [13].
This is to create a user interface and provide a way to control the manipulation system.
The Blynk app has been designed for the Internet of Things. It can remotely control hardware, display sensor data, store data and visualize it.
There are three major components in the platform (Fig. 6):

- *Blynk application* - allows the creation of project interfaces using various widgets that it provides.
- *Blynk Server* - responsible for all communications between smartphone and hardware. One can use any Blynk cloud or run a local Blynk private server.

It is open-source and can easily manage thousands of devices.

- *Blynk libraries* - for all popular hardware platforms - allow communication with the server and process all incoming and outgoing commands.

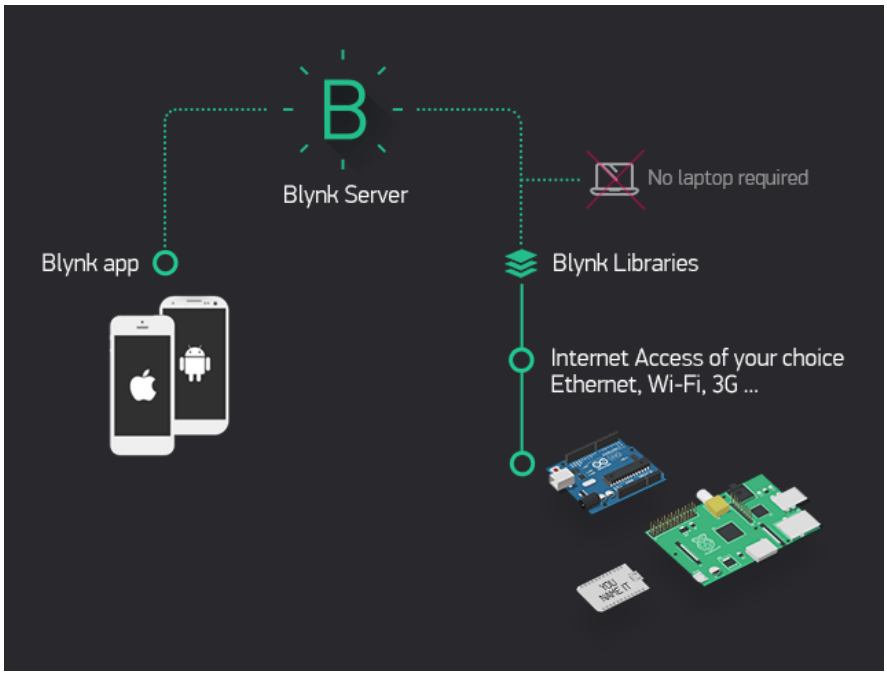

Fig. 6. Structure of the Blynk application

Every time a button is pressed in the Blynk app, the message reaches the Blynk Space Cloud, where it finds its way to the hardware, working the same way in the opposite direction, all happening in an extremely short time.
To create the virtual control panel in the Blynk application, buttons are created using widgets.
Widgets are pre-designed pieces of the graphical user interface. Each widget performs a specific input/output function when communicating with hardware or the end user.
Two types of widgets have been used for the chosen application:

Button widget
It works in push or switch modes. Allows sending any numeric value to clicks and button release events. By default, the button uses values 0/1 (LOW/HIGH). The button sends 1 (HIGH) when pressed and 0 (LOW) when released.
It is also possible to change the state of the button from the hardware side. For example, turn on the button assigned to virtual pin V1:

```
Blynk . virtualWrite ( V1 , HIGH );
```

Can change the hardware button labels with:

```
Blynk.setProperty(V1, "onLabel", "ON");
Blynk.setProperty(V1, „offLabel", „OFF")
```

or change the colour:

```
//#D3435C - Blynk RED
Blynk . setProperty ( V1 , „culoare" , „#D3435C" );
```

Button status can be obtained from the server if the hardware has been disconnected with Blynk Sync:

```
BLYNK_CONNECTED() {
Blynk.syncVirtual(V1);
}
BLYNK_WRITE(V1) {
int buttonState = param.asInt();
  }
```

Led widget
A simple indicator (similar to an LED).
- if the value is equal to the DataStream min setting, the indicator is OFF
- if the value is equal to the DataStream max setting, the indicator is ON
- intermediate values are used for brightness control (such as PWM)

```
// DataStream is configured to 0..255 range
// LED light setting is to 50%
  Blynk.virtualWrite(V1, 127)
```

It can change the color of the LED with:

```
//#D3435C - Blynk RED
Blynk.setProperty(V1, „culoare", „#D3435C");
```

The outputs have been configured as custom widgets (windows) for each movement in the form of virtual buttons for manipulator movements, and for the system status a led has been added for the status of the presence of the piece on the output stock.
The virtual control panel in the Blynk application is illustrated in Fig. 7.
After completing the previous steps, proceed to programming the NodeMCU Esp8266 development board.
On the development board there is a program written in the native Arduino language. It has the role of processing the information received wirelessly and commanding the movement of the manipulator.
This programming is done using the Arduino IDE program [14].

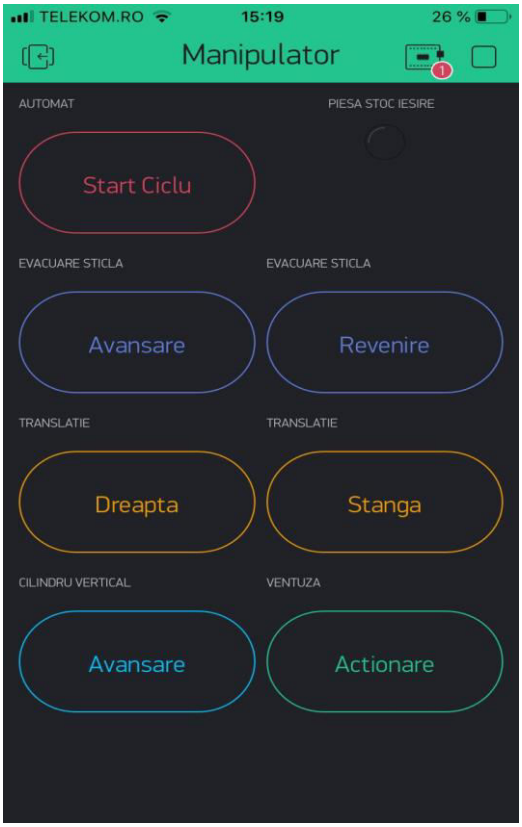

Fig. 7. Virtual control panel in the Blynk app

4. Achievement and testing of the automatic handling system

The achieved automatic handling system (Fig. 8) can work in the following ways:
- local manual mode:
- local automatic mode;
- remote manual mode;
- automatic remote mode.

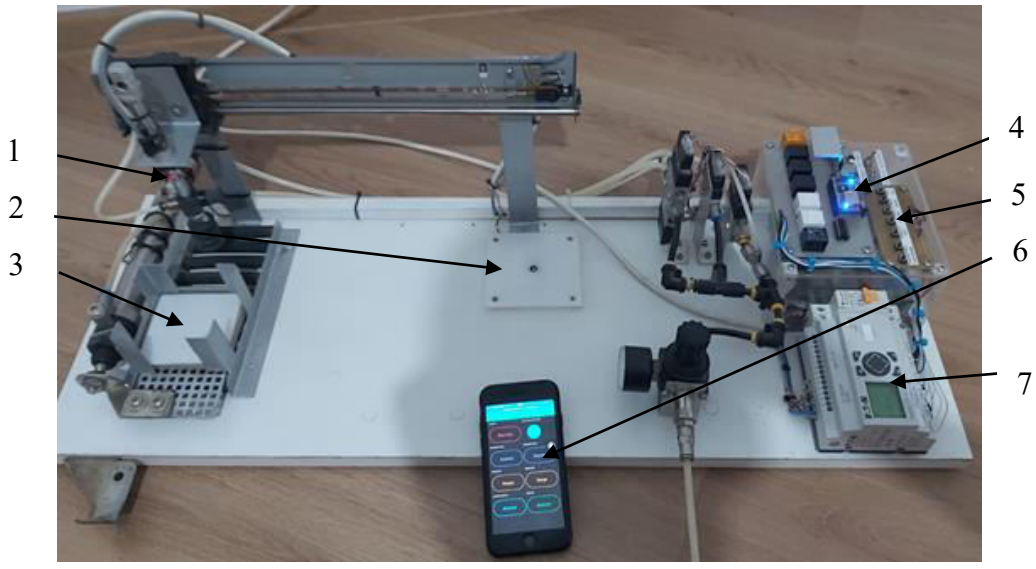

Fig. 8. Automatic handling system achieved: 1- manipulator; 2- output stock; 3- input stock; 4- NodeMCU Esp8266 development board; 5- push button board; 6- smartphone; 7- PLC

Experimenting with the operation mode of the remote monitoring and control system has been physically carried out on the experimental model made, through a series of tests. They captured all the stages of the process of handling fragile objects through the Blynk application, which aims to monitor and control the system remotely.

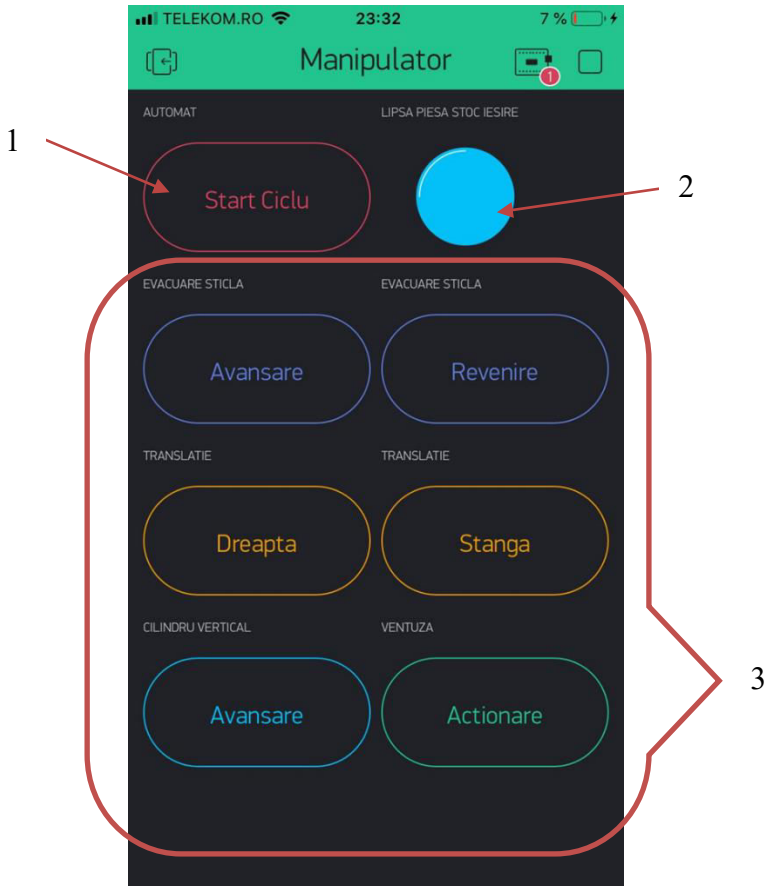

Fig. 9. Virtual control panel of remote control system: 1- start button of automat mode; 2- LED status of output piece stock; 3- buttons of manual remote control

Figure 9 shows the screen of the application during operation. The blue colour of LED 2 shows the lack of piece in the output stock, which means that button 1 can be activated to start the automatic cycle.

5. Conclusions

The main goal of the research presented in the paper has been to create a wireless module that has been attached to an automated fragile object handling system to be able to remotely monitor and control the handling of various fragile objects using a vacuum suction cup.
Taking into account the composition of the wireless module, its programming has been carried out using the Blynk application.
The design consisted of the use of widgets from the Blynk application through which all stages related to the handling of fragile objects can be monitored and controlled.
For the remote monitoring and control of the fragile object handling system, the following steps have been taken: designing the control system for a pneumatic manipulator and choosing the component elements, making the handling system, and using widgets in the Blynk app to program the wireless module.
Experimentation with remote monitoring and control of the automated fragile object handling system has led to the conclusion that the system is operating correctly according to the established operating protocol.

References

[1] Alboteanu, L. "Automatic System for Handling Fragile Objects." *Hidraulica Magazine,* no. 4 (December 2020): 26-32.
[2] FMUSER International Group INC. "Diferite tipuri de comunicații fără fir cu aplicații"/ "Various types of wireless communication with applications." May 29, 2020. Accessed February 20, 2021. https://ro.fmuser.net/.
[3] ***. "About flexible production systems and complex automation." *Plant Engineering*, XIII Year, no. 11 (118) (2013): 42-45.
[4] Hucknall, D. J. *Vacuum Technology and Applications*. Oxford, Butterworth-Heinemann, 2013.
[5] Alboteanu, L., Gh. Manolea, and F. Ravigan. "Automatic sorting and handling station actuated by pneumatic drive." *Annals of the University of Craiova, Electrical Engineering Series,* no. 1 (2018): 1-8.
[6] Alboteanu, L. "Automatic Processing Station Actuated by Pneumatic Drive." *Hidraulica Magazine*, no. 1 (March 2019): 16-22.
[7] Alboteanu, L. "Modeling an Automatic Processing Station Using Fluidsim Software." *Hidraulica Magazine*, no. 3 (September 2017): 27-30.
[8] Alboteanu, I. L. "Pneumatic Tracking System for Photovoltaic Panel." *Hidraulica Magazine,* no. 1 (March 2015): 32-39.
[9] Gorton, Ian. *Essential Software Architecture*. Springer Publishing House, 2006.
[10] Carnegie Mellon University, Software Engineering Institute. "What Is Your Definition of Software Architecture?" January 22, 2017. http://www.sei.cmu.edu/architecture/definitions.html.
[11] ElectronicWings. "Introduction to NodeMCU." https://www.electronicwings.com/nodemcu/introduction-to-nodemcu.
[12] ***. Target 3001 Software. http://server.ibfriedrich.com/.
[13] ***. Blynk software. https://blynk.io/.
[14] ***. Arduino software. https://www.arduino.cc/en/software.

Thermal Rehabilitation of an Educational Building in the Context of the Adaptation of Buildings to the Effects of Climate Change. Case Study

PhD. student Eng. **Nicoleta-Elena KABA**[1], Prof. Emeritus PhD. Eng. **Adrian RETEZAN**[1], Assoc. Prof. PhD. Eng. **Adriana TOKAR**[1,*]

[1] University Politehnica Timisoara

* adriana.tokar@upt.ro

Abstract: *In view of the Directive 2006/32/EC of the European Parliament and of the Council of 5 April 2006 on energy end-use efficiency and energy services, it is requested, as a consequence, to ensure the Energy Audit of the building and propose energy improvement measures in order to access structural funds, inclusively for functional and structural rehabilitation. This article proposes to analyse the energy survey aimed at the issuing of the Energy Efficiency Certificate of the building, and finally the Energy Efficiency Audit of the thermally rehabilitated school building, in view of improving the energy efficiency of the building and of the related installations.*

Keywords: *Energy efficiency audit, energy certificate, rehabilitation, thermal insulation*

1. Introduction

Mitigation of the climate changes felt in the last period is a worldwide concern that in order to stabilize the global temperature would take about 20-30 years (approximately 1.1°C of warming since 1850-1900, and finds that averaged over the next 20 years, global temperature is expected to reach or exceed 1.5°C of warming) and hundreds of years to thousands of years in terms of continued sea level rise (Coastal areas will see continued sea level rise throughout the 21st century, contributing to more frequent and severe coastal flooding in low-lying areas and coastal erosion). It is already proven that the strong and sustained reduction of carbon dioxide emissions (CO_2) and other greenhouse gases would limit the effects of these climate changes [1].
In this context, it can be said that in the field of construction a rapid adaptation to the pace of climate changes is needed, both in terms of existing buildings and in terms of the decreasing environmental impact, with an emphasis on reducing CO_2 emissions. Vulnerability of buildings to climate change manifests itself through negative effects on the structural characteristics of building and indoor comfort conditions [2].
As far as Romania is concerned, it is estimated that a high percentage of buildings (77% [3]) do not meet the energy efficiency criteria related to the building envelope and therefore the application of energy renovation measures is necessary. Regarding Romania's total energy consumption, it is estimated that the building sector represents a percentage of 45% [3], so the energy efficiency of this sector will certainly contribute to reaching the targets, established by European and national strategies, in terms of energy efficiency.
Unfortunately, the rehabilitation rate of buildings in Romania is quite low, but it is worth appreciating the fact that buildings in the tertiary sector are given a lot of attention.
The urgent application of measures to combat climate change and implicitly their consequences also implies the energy efficiency of buildings, which is also a basic element in ensuring a sustainable energy future. Thus, the UN's 2030 Agenda for Sustainable Development will establish 17 sustainable development goals (SDGs) and 169 targets for their achievement. Figure 1 shows the progress registered in the EU until 2022, of objective 7 relating to energy (Fig. 1 a) and of objective 11 relating to climate change (Fig. 1 b) [4].
In achieving these objectives, from the point of view of the stock of existing buildings, their energy audit plays an important role. Thus, by establishing the energy performance of a building, correct and effective energy rehabilitation measures can be proposed. For this reason, the article proposes a case study that addresses the energy audit of an educational building.

a) b)

Fig. 1. SDG progress in the EU [4]
a) SDG7, b) SDG 11

The object of this audit is the Primary and Lower Secondary School of Giera (Fig. 2). The building was built in the 60s, but various improvements have been performed over the years. The school has two floors, having 664.80 m^2 footprint, gross building area of 1150.10 m^2 and 943.10 m^2 net area [5].

Fig. 2. Primary and Lower Secondary School of Giera

The building has one main entrance and several secondary entrances from the yard. The floor has an equal height of 3m, the roof is truss-type and has ceramic roof tiles. The framework of the building is made of burned brick masonry placed on a continuous concrete foundation. The interior floor is made partially of mosaic concrete and the rest is a boarding floor. The ceiling slab of the 1st floor is made of wood revetment nailed on the wooden boards placed over the rooms and covered in plaster on reed net support. The rooms have the ceiling made of resinous wood logs, platen with wood board and reinforced plaster on reed net. The slab under the roof truss is made of plastered wood, with beaten clay thermal insulation. The following finishing works are made in the interior of the building: warm floors; wood flooring; cold floors; hallways and pathways and the footsteps are

plated with mosaic precast plates. The entrance doors in the building are made of PVC joinery with double-glazed windows, being in very good shape [5, 6].
As a consequence of the Energy Efficiency Audit, the exterior wall, the floor slab and ceiling slab will be thermally insulated, and the installation will be modified. The main elements of the supporting structure are [5, 6]:

- Load-bearing walls made of full brick masonry;
- Concrete continuous foundations under the load-bearing walls;
- The floor under the roof truss is made of wood;
- The ceiling of the first floor is insulated with beaten clay. It is a structure of wood logs and boards, plaster on reed net support and beaten clay to provide thermal insulation.

2. Assessment

The building as a whole has remained in good shape over the time (from the point of view of load-bearing structure). No cracks due to unequal settlement of earth or to seismic effects have been noticed until now [5].
After the visual control, the building has no structural damages to the main elements. The interior and exterior finishing works of the building floors and ceilings are damaged [6].
The building also has non-load-bearing damages and depreciation signs of the ceramic tiles (without negatively affecting the load-bearing structure of the roof truss) and of the rain water gutters. The ceiling of the entire building is made of wood revetment nailed under the wood logs covering the ground floor; the ceiling is plastered on a Rabitz plastering net. Earth has been introduced among the wood logs serving as thermal insulation [6].
The interior floors also have signs of tear. The interior floor boarding of the building is made of wood board covered by carpet and other types of floor covering.
Dark stains are visible inside the building due to growth of microorganisms on wet surfaces. Therefore, the exterior thermal insulation is insufficient mainly at corners and in between.
The thermal insulation of the ground floor ceiling is made of beaten clay, but it is damaged due to the age of the building and to the roof truss defects [6].

2.1 Heating and hot water installation

The building has a functional heating installation, using hot water as thermal carrier and a distribution system of steel radiators. The heat carrier is supplied by a functional boiler. The calculation of thermal losses has been made according to the applicable standard [7]. All the afore mentioned facts are representing the motivation to perform this survey, according to the Construction Quality Law [8], considering the inefficient performance from an energy point of view. We mention that the survey of the building has been already done and requires the thermal rehabilitation. The evaluation of the building was done in accordance with the regulations and norms in force in Romania [9-18].

3. Information regarding the building

The total heated volume of the building is 3160.00 m^3 and the geometrical, thermal and technical characteristics of the actual building covering is presented in Table 1. The main elements of the building that refer to the walls (PE), joinery, ground slabs and loft floor are analyzed from the point of view of their orientation and thermal resistance [5, 6].

Table 1: Geometrical, thermal and technical characteristics of the actual building covering

Building elements	Orientation	Surface [m^2]	Total surface [m^2]	Thermal resistance [m^2K/W]
PE 1	N	210.70	817.80	3.634
	S	107.60		
	E	209.50		
	V	290.00		
PE 2	N	83.50	374.30	2.384

Building elements	Orientation	Surface [m²]	Total surface [m²]	Thermal resistance [m²K/W]
	S	38.50		
	E	108.70		
	V	143.60		
PE 3	N	-	161.20	4.53
	S	93.90		
	E	67.30		
	V	-		
PVC Joinery	N	22.50	228.60	0.50
	S	57.20		
	E	100.30		
	V	48.60		
Ground slab	O	928.80	928.80	3.055
Loft floor	O	928.80	928.80	4.226
Total			**3439.50**	-

The average resistance of the actual building covering is: $\bar{R} = 2.459$ m²K/W and compactness index of the building: S_{ext} / V = 0.56 [6].

From the point of view of the existing system for space heating, it was found [6]:

- Energy source for heating: gas fuel;
- Type of heating system: heating station;
- Distribution of heat carrier: two tubes;
- Computed heating requirements: 120 kW;
- Connection to the central heating source: -;
- Heat meter for heating system: -;
- Thermal and hydraulic automation elements: yes.

For annual heat consumption for heating (Q) and specific annual heat consumption for heating the rooms of the building (q), it is known [6]:

- at the level of the heated spaces: Q_{inc} = 223.50 MW/an;
- at the level of the heat source connection: Q_{inc} = 294.111 MW/a;
- at the level of the heated spaces: q_{inc} = 236.98 MW/m² an;
- at the level of the heated spaces: q_{inc} = 311.86 MW/m² an.

The performances of the distribution system and the heating installation are:

- η_d = 0.95 - distribution;
- η_{inc} = 0.80 - heating installation.

3.1. Information concerning the heating installation for domestic hot water

The consumption points for hot / cold water (16/32) are equipped with 12 sinks, 2 shower tubs, 24 lavatories and 8 toilet bowls [6].
For average specific normalized heat consumption of hot water, it was established the value of 15.00 kWh/m² an and in addition it was established for lighting, that the average specific electricity consumption is 32.81 kWh/m² an [6].

4. Calculation the global coefficient of thermal insulation, G_1 [W/m³K]

Calculation of the global coefficient of thermal insulation was performed both for the current building and for the reference building [6].

4.1. Actual Building

The thermal resistance of the elements of the actual building covering is presented in Table 2 and the coefficients of heat loss through transmission (thermal coupling), in Table 3.

Table 2: Thermal resistance of the building, elements of the actual building covering

Building element /Symbol	R_j [m^2 K/W]	τ_j [-]	R'_j [m^2K/W]
North Wall (P N)	0.724	0.85	0.615
South Wall (P S)	0.724	0.85	0.615
East Wall(P E)	0.724	0.85	0.615
West Wall (P V)	0.724	0.85	0.615
North Facade (FT N)	0	0	0.5
South Facade (FT S)	0	0	0.5
East Facade (FT E)	0	0	0.5
West Facade (FT V)	0	0	0.5
Ground Slab (PLS)	1.131	1	3.18
Ceiling (PLF)	1.54	0.85	1.309
Average corrected thermal resistance of the covering [m^2K/W]			**0.96**

Table 3: Coefficients of heat loss through transmission (thermal coupling), L_j [W/K]:

Building element /Symbol	Aj [m^2]	R'j [m^2K/W]	Lj = Aj/R'j [W/K]	τ_j [-]	τ_j*Lj [W/K]
North Wall (P N)	296.4	0.615	481.95	1	481.95
South Wall (P S)	247.9	0.615	403.08	1	403.08
East Wall (P E)	163.9	0.615	266.50	1	266.50
West Wall (P V)	170.1	0.615	276.58	1	276.58
North Facade (FT N)	34.5	0.5	69	1	69
South Facade (FT S)	66.7	0.5	133.4	1	133.4
East Facade (FT E)	26.0	0.5	52	1	52
West Facade (FT V)	34.5	0.5	69	1	69
Ground Slab (PLS)	664.8	3.18	209.05	0.35	73.17
Ceiling (PLF)	664.8	1.309	507.86	0.9	457.08
TOTAL $t_j \cdot L_j$					**2281.7**

where:
A – element envelope area, [m^2];
R- real thermal resistance of the constructive element, [m^2K/W];
R′- value of the adjusted thermal resistance, [m^2K/W];
τ - dimensionless temperature correction factor, [-].
L_j - coefficients of heat loss through transmission (thermal coupling), [W/K]

For actual building, the global thermal insulation coefficient, G_1 [W/m^3K], was calculated with the relation (1):

$$G_1 = \frac{\sum_j L_j \cdot \tau_j}{V} 0.34 \cdot n \quad (1)$$

where:
V - building volume, [m^3];
n – ventilation rate, [h^{-1}].

After calculating the result: G1 = 0.563 [W/m^3K]
The building is in Category 2, having low / medium thermal inertia (M<400 kg/m2). In conclusion, comparing the values G_1 and G_{1ref} it results: G_1= 0.563 [W/m^3K] > G_{1ref} =0.311 [W/m^3K] and consequently the global level of thermal insulation of the building is inadequate; the correction of the geometrical, thermal, technical and the conformity characteristics of the building covering is required in order to comply with the standard stipulations.

4.2. Reference Building

The thermal resistance of the elements of the reference building covering is presented in Table 4 and the coefficients of heat loss through transmission (thermal coupling), in Table 5 [6].

Table 4: Thermal resistance of the building elements of the reference building covering

Building element /Symbol	R_j [sqmK/W]	τ_j [-]	R'_j [m K/W]
North Wall (P N)	2.997	1	2.997
South Wall (P S)	2.997	1	2.997
East Wall (P E)	2.997	1	2.997
West Wall (P V)	2.997	1	2.997
North Facade (FT N)	0	0	0.5
South Facade (FT S)	0	0	0.5
East Facade (FT E)	0	0	0.5
West Facade (FT V)	0	0	0.5
Ground Slab (PLS)	**3.231**	**1**	5.48
Ceiling (PLF)	**5.249**	**1**	5.249
Average corrected thermal resistance of the covering [m^2K/W]			**2.741**

Table 5: Coefficients of heat loss through transmission (thermal coupling), L_j [W/K]

Building element /Symbol	A_j [m^2]	R'_j [m^2K/W]	$L_j = A_j/R'_j$ [W/K]	τ_j [-]	$\tau_j \cdot L_j$ [W/K]
North Wall (P N)	296.4	2.997	98/899	1	98.899
South Wall (P S)	247.9	2.997	82/716	1	82.716
East Wall (P E)	163.9	2.997	54/688	1	54.688
West Wall (P V)	170.1	2.997	56/757	1	56.757
North Facade (FT N)	34.5	0.5	69	1	69
South Facade (FT S)	66.7	0.5	133/4	1	133.4
East Facade (FT E)	26	0.5	52	1	52
West Facade (FT V)	34.5	0.5	69	1	69
Ground Slab (PLS)	664.8	5.48	121/31	0/35	42.46
Ceiling (PLF)	664.8	5.249	126/65	0/9	113.98
TOTAL tj·Lj					**772.90**

For the reference building, the global thermal insulation coefficient, G_1 [W/m^3K], was calculated with the relation (1) and the resulting value was 0.191 [W/m^3K].
The building is in Category 2, having low / medium thermal inertia (M<400 kg/m^2). In conclusion, comparing the values G_1 and G_{1ref} it results: G_1= 0.191 [W/m^3K] > G_{1ref} =0.311 [W/m^3K] and consequently, the global level of thermal insulation of the building is adequate.

5. Technical solutions recommended for the energy efficiency refurbishment of the building

The energy efficiency refurbishment will be achieved by investment in the building and modification of the building installations [6].

5.1. Modifications of the building

The modifications brought to the building are aiming to reduce the heat needed by the thermal insulation of the structure and by reducing the infiltration through gaps:

- improvement of the thermal insulation - the thermal insulation of the existing building aims to reduce the thermal flow by conduction through the building covering;
- thermal insulation of the horizontal opaque building elements - thermal insulation of the floor below the roof truss shall be solved as follows:
  - the following shall be laid over the last layer:

- the waterproofing layer shall be eliminated, slope concrete, thermal insulation layer;
- an equalizing screed shall be poured;
- 1K Spezial Bituminous emulsion shall be applied at cold (vapors barrier and adhesive layer for stone wool);
- 20 cm-thick stone wool;
- polyethylene sheet; slope concrete; renewal of waterproofing layer.

○ thermal insulation of the boarded floor on soil:

- dismantling of the existent boarded floor;
- base slab;
- 6 cm thick expanded polystyrene over the base slab; protection screed; renewal of boarded floor.

- thermal insulation of vertical opaque building elements - the exterior thermal insulation of the exterior walls is not necessary.

5.2 Improvement of air tightness

Replacing the existing windows and doors having wooden joinery with double-glazing glass R'=0.87 m^2K/W. The fresh air necessary for a quality comfort of the interior air and limitation of humidity and sweat that could have negative impact over the building will be provided by periodically opening of windows.
The exterior doors will be provided with automatic closing systems.

6. Modification of the installations

The proposal for the rehabilitation of the interior installations is the following [6]:

- Fitting of thermoregulator valves on the radiators;
- Replacement of the electrical installations with LED-type source lighting installation;
- Installing a solar panel system for domestic hot water production;
- Installing a thermal agent producing system using a heat pump;
- Installing a low temperature heating system for the thermal agent produced by the heat pump.

In order to carry out the works regarding the rehabilitation solutions, specific technical solutions or packages of solutions containing the above technical solutions may be proposed.

7. The following scenarios are proposed:

***Scenario no. 1*:** It contains the minimum measures package regarding the thermal refurbishment of the building [6].
This package contains rehabilitation solutions for:

- opaque horizontal surfaces, the floor below the roof truss/the floor above the soil, and improvement of air tightness - solutions are presented in chapters 5.1 and 5.2;
- the interior installations – by fitting of thermoregulator valves - solutions are presented in chapter 6;
- replacement of the electrical installations - LED-type source lighting installation - solutions are presented in chapter 6.

***Scenario no. 2*:** It contains the minimum measures package regarding the more efficient thermal refurbishment of the building [6].
This package contains rehabilitation solutions for:

- opaque horizontal surfaces, the floor below the roof truss / the floor above the soil, and improvement of air tightness - solutions are presented in chapters 5.1 and 5.2;
- the interior installations – installing a heat carrier producing system using heat pump, installing a low temperature heating system for the heat carrier produced by the heat pump and installing a solar panel system for domestic hot water production - solutions are presented in chapter 6;

- replacement of the electrical installations - LED-type source lighting installation, solutions are presented in chapter 6.

8. Advantages and Disadvantages of solutions:

- **Advantages of Scenario no. 1:**

Technical thermal rehabilitation solutions are solutions that increase the thermal resistance of vertical and horizontal opaque building elements, correcting most thermal bridges, protecting load-bearing elements and the overall structure against the effects of temperature variation; does not affect plastering, painting, and interior painting, and at the same time allows the facade to be rehabilitated. Fitting thermoregulator elements on the radiator's feeding line increases the use performance of the energy generated by the use of fuel. Replacing the existing electrical installations with LED-type sources increases the safety of building operation, avoiding the eventual problems related to operation safety and fire hazards.

- **Disadvantages of Scenario no. 1:**

Implementing these measures, the building continues to use only non-renewable energy sources.

- **Advantages of Scenario no. 2:**

Technical thermal rehabilitation solutions are solutions that increase the thermal resistance of vertical and horizontal opaque building elements, correcting most thermal bridges, protecting load-bearing elements and the overall structure against the effects of temperature variation; does not affect plastering, painting and interior painting, and at the same time allows the facade to be rehabilitated. Installing the local heat carrier production system using a heat pump, the efficiency of the production system is maximized, this type of energy being renewable. Installing the low temperature heating system is a special requirement for using the heat carrier produced by the heating pump, using the built-in floor heating with serpentine heating tube. Installing the system for hot water production using solar panels is an efficient solution with low operation costs. Replacing the existing electrical installations with LED-type sources increases the safety of building operation, avoiding the eventual problems related to operation safety and fire hazards.

- **Disadvantages of Scenario no. 2:**

The disadvantages of the heat pump are related to the costs of the initial investment, by costs related to the heat pump and also to the primary heat exchanger needing great depth pit which is very expensive especially for this type of soil and also due to the small land plot which is available;
Installing a low temperature heating system involves pretty high implementation costs and needs special operation and setting instructions.

9. Conclusions

Scenario no. 1 is recommended for the work performance. This package proposes rehabilitation solutions that are the best from a technical and economical point of view, depending on the type of activity carried out in the building. In order to perform these works, the building is brought to a high energy efficiency level both from the point of view of the exploitation and operation costs.
The following energy efficiency refurbishment of the building covering and of the interior installations have been taken into consideration:

- Thermal insulation of the floor below the roof truss with stone wool of 20 cm and waterproofing renewal;
- Insulation of floor boarding with 6 cm extruded polystyrene and renewal of floors;
- Replacement of existing windows with double-glazed and wood joinery windows (R'=0.87 m^2K/W);
- Fitting of thermoregulator valves; Installing solar panel systems for domestic hot water production. Installing a solar panel system for domestic hot water production;
- Replacement of the electrical installations, LED-type source lighting installation.

It can be concluded that the application of measures, established following the energy assessment of buildings, contributes to the reduction of energy consumption and CO_2 emissions, which will ensure the adaptation of buildings to effects of climate change.

References

[1] The Intergovernmental Panel on Climate Change (IPCC). "Climate change widespread, rapid, and intensifying – IPCC." *IPCC Working Group I report*, "Climate Change 2021: The Physical Science Basis." Geneva, August 9, 2021.
[2] ***. "How we adapt buildings to the ever-widening effects of climate change." / "Cum adaptăm clădirile la efectele tot mai ample ale schimbărilor climatice." *Efficient Romania / România Eficientă*. Accessed August 3, 2022. https://www.romania-eficienta.ro/cum-adaptam-cladirile-la-efectele-tot-mai-ample-ale-schimbarilor-climatice/.
[3] Oancea, D. "How many buildings need energy rehabilitation? The renovation rate remains low." / "Câte clădiri necesită reabilitare energetică? Rata de renovare rămâne scăzută." *Mediafax.ro*, December 16, 2021. Accessed August 3, 2022. https://www.mediafax.ro/social/cate-cladiri-au-nevoie-de-reabilitare-energetica-rata-de-renovare-ramane-redusa-20406983.
[4] European Commission. "Sustainable Development Goals – Overview." *Eurostat*. Accessed August 4, 2022. https://ec.europa.eu/eurostat/web/sdi.
[5] ***. The surveys made available by the town planning office within the Giera City Hall, 2017.
[6] Kaba, N. E. "The energy audit of the building" - prepared by the Gr. I energy auditor, 2017.
[7] ***. SR 1907-1:2014, Heating installations. Calculation heat requirement, Calculation method. ASRO, December, 2014.
[8] The Parliament of Romania. Law no. 10/1995 regarding quality in construction, republished, with subsequent changes and additions. Official Gazette no. 765, September 30, 2016.
[9] UTCB. Calculation Methodology MC001-2006 of Law 372-2005, Official Journal, Part I no. 1144, 2005.
[10] The Parliament of Romania. Law no. 372/2005 on the energy performance of buildings. Published in the Official Gazette, Part I no. 764, September 2016. Form applicable on March 6, 2020.
[11] MLPAT, NP 048-2000: Norm for thermal and energetic expertise of existing buildings and heating and hot water preparation installations. *Construction Bulletin* 4, 2021.
[12] ***. GT 032-2001: Guide regarding the procedures for carrying out the measurements necessary for the thermo energetic expertise of constructions and related installations, 2001.
[13] ***. C 107/1-2005: Norm regarding the calculation of global coefficients of thermal insulation in residential buildings, 2005.
[14] ***. C 107/3-2005: Norm regarding the thermotechnical calculation of building construction elements, 2005.
[15] ***. C 107/5-2005: Norm regarding the thermotechnical calculation of building elements in contact with the ground, 2005.
[16] ***. SR 4839-1997, Heating systems. Annual number of degree-days, IRS, 1997.
[17] ***. NP 049-2000: Norm for the development and granting of the energy certificate for existing buildings, 2000.
[18] ***. NP 060-2002: Norm regarding the establishment of thermo hydroenergetic performance of the envelope of existing residential buildings for thermal rehabilitation, 2002.

Modelling and Simulation of the Transient Performance of a Direct Operated Pressure Relief Valve

Prof. PhD **Sasko DIMITROV**[1,*], Ass. PhD **Dejan KRSTEV**[1]

[1] Faculty of Mechanical Engineering, University of Shtip, N. Macedonia

* sasko.dimitrov@ugd.edu.mk

Abstract: *The dynamic characteristics determine variations of the inlet pressure in front of the valve in function of the flow through the valve in the time. In any hydraulic system, the valve is connected at least by a pipe at the outlet, and at its inlet there is some volume of compressible oil which influences the quality of the transient process. When switching the directional control valve in the hydraulic system with direct-operated pressure relief valves, a transient process occurs in which it is possible for the pressure to reach values many times higher than the set value. This causes the system to be overloaded with undesirable consequences.*
This paper examines experimentally and theoretically the transients in hydraulic systems with these valves. From the experimental static characteristics, the coefficient of hydrodynamic force acting on the valve poppet is determined.

Keywords: *Static and dynamic characteristics, pressure relief valve, transient response*

1. Introduction

The pressure control valves can perform different functions in the hydraulic systems, such as establish maximum pressure, reduce pressure in some circuit lines, and establish sequence movements, among other functions. The main operation of these valves consists of providing a balance between the pressure difference and the force load on a spring. Most of these valves can be positioned in many different levels, between totally open and totally closed, depending on the flow and the differential pressure. The pressure control valves are usually named according to their primary functions, and their basic function is to limit or to determine the pressure of the hydraulic system for the attainment of a certain function of the equipment in motion. In order to protect a hydraulic circuit against overloads and limit the work pressure, pressure relief valves are used. The main function of these valves is to limit the maximum working pressure in the hydraulic system. They are normally positioned after the hydraulic pump. In this case, the valve does not require an external power source, meaning that the fluid pressure is enough to open or close the valve. This means that the function of this class of valves is done automatically. This makes this class of valves indispensable for the hydraulic circuit function and operation.
There are two types of the pressure relief valves: direct operated and pilot operated. The direct operated pressure relief valves have higher deviation of the adjusted pressure in the static characteristics than pilot operated one, which leads to overloading of the hydraulic system [1]. The reason for this deviation is the hydrodynamic reaction force that acts on the valve poppet and always tends to close the poppet. To reduce the influence of the hydrodynamic reaction force to the slope of the static characteristics, shape modification of the valve poppet has been done.
Many authors have investigated the static and dynamic characteristics of direct operated pressure relief valves. Brodowski [3] has presented experimental and theoretical dynamic characteristics and shown that the magnitude of the pressure peak is far higher than the steady-state magnitude. He also has proved that the pressure peak depends on the size of the damping orifice. Many authors have worked on dependence of the discharge coefficient in the control orifice. During an unsteady process, the flow presumably passes in and out of laminar and turbulent regions. So, it is needed a model which describe both regimes simultaneously. That kind of model is recommended by Borutzky [8]. Another, empirical model for the discharge coefficient has been presented in [7]. For the pressure relief valve it is suitable to determine the discharge coefficient in the control orifice based on the experimental static characteristics [12]. That kind of model is presented and used in this paper to determine the discharge coefficient of the investigated pressure relief valve. High

impact to the static and dynamic characteristics has the hydrodynamic reaction force of the flow [2], [4], [10]. In the dynamic mode, it can even cause unstable work of the valve.
Dasgupta and Karmakar [5] studied the dynamics of a direct operated pressure relief valve with directional damping through bond graph simulation technique. The authors concluded that some significant parameters of the valve response are identified, which can be modified to improve the dynamic characteristics of the valve. Their theoretical research they have compared with the experimental dynamic characteristic presented by Watton [6].
Although this class of valves is indispensable for the function and operation of the hydraulic systems, a review of the available researches shows that their study is not well covered and there is a need for an in depth study of modeling and simulation of their performance. Therefore, a comprehensive study of the modeling and simulation of the performance of this class of valves, in the steady-state and transient modes of operation, is carried out in this paper. A comprehensive nonlinear mathematical model, taking into account most nonlinearities of the valve, is developed. The steady-state and transient performance of the studied valve are investigated theoretically and experimentally. The experimental study is also used to validate the simulation program of the studied valve in the steady-state and transient modes of operation.

2. Valve components description and schematic diagram

The objective of the pressure relief valve is to limit a system pressure downstream the valve. Fig. 1 shows the basic components of the studied valve, while its schematic diagram is shown on fig. 2. This valve basically consists of sleeve 1, adjusting spring 2, poppet with damping piston 3, and adjustment element 5. The system pressure setting can be infinitely varied by means of adjustment element 5. Spring 2 presses poppet 3 onto its seat. Port P is connected to the system. The system pressure acts on the poppet area. When the pressure in the port P rises above the value adjusted on spring 2, the poppet 3 moves against spring 2 and the valve is opening. Hydraulic oil can now flow from port P towards port T. The stroke of poppet 3 is limited by embossment 6.

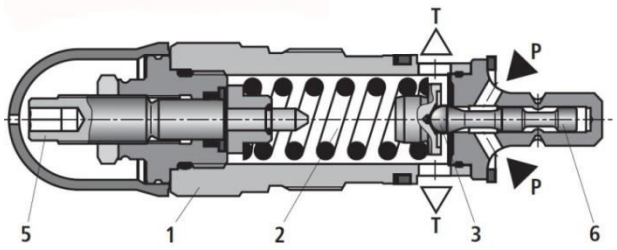

Fig. 1. Schematic diagram of the valve

On fig. 2 schematic diagram of the test rig with the studied pressure relief valve, volume of oil at its inlet V_0 and output pipeline with linear R_p and inertial L_p resistance is shown. To isolate the oil compressibility between the pump and the valve and for reducing pressure pulsation of the pump, it is included a throttle with high inertial resistance.

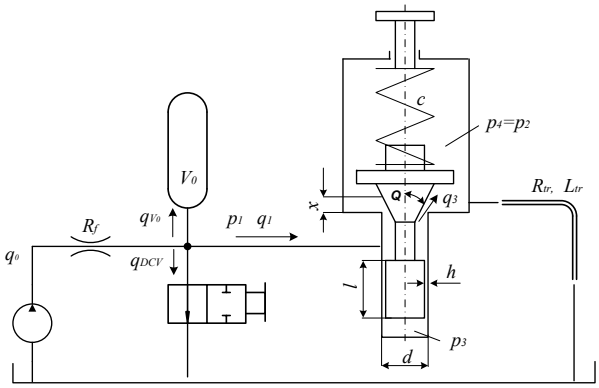

Fig. 2. Functional diagram of the test rig

The valve is normally closed. When the pressure p_1 is lower than the value necessary to move the poppet against the spring, the main valve throttling area remains closed and the valve poppet presses onto its seat. Rapidly activating the control valve V_1, the pressure begins to rises in the volume V_0 and in front of the valve and the transient process starts. When the pressure is high enough, the valve poppet lifts from its seat and the valve opens. Thus, the valve limits additional rising of the pressure downstream the valve.

3. Mathematical modelling of the studied valve

To model the studied valve, some assumptions are made in developing the nonlinear mathematical model. It is assumed that the tank pressure is constant at atmospheric pressure; the geometry and discharge area of the valve restriction usually change nonlinearly; the pressure losses in the short pipe lines are neglected; the oil temperature and viscosity are kept constant. During the transient mode of operation, the flow rate passing through the valve throttling area is of high Reynolds number. The discharge coefficient of this throttling area change with the Reynolds number in a complicated manner. For this reason, the discharge coefficient for the valve throttling is determined by the experimental static characteristics of the valve.

3.1. Coefficient of the hydrodynamic reaction force

The design of the poppet of this type of valve is characterized with turning the streaming flow of the oil with the ring 1, fig.3.
This turning of the streaming flow is leading to decreasing of the component of the hydrodynamic force F_h which, together with the spring force F_s, tends to close the valve. With this design modification, the error in the static characteristic is decreased. The value of the hydrodynamic force depends on the diameter and the shape of the ring 1 of the poppet and it is difficult to define it. Thus, it is necessary to use the experimental static characteristics with the displacement of the poppet of the valve measured, to determine the coefficient of the hydrodynamic reaction force.

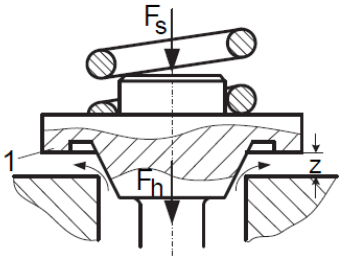

Fig. 3. Hydrodynamic force compensation

Experimental static characteristics of the specified direct operated pressure relief valve are presented on fig.4.

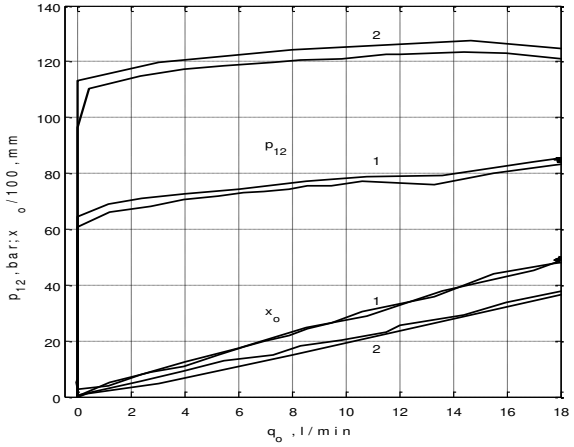

Fig. 4. Experimental static characteristic of the specified valve

For a given flow q_0, a pressure drop $p_{1,2}$, a poppet area A_k and a valve spring constant c and measured pressure – flow constant k_{st} of the static characteristic of the valve and displacement of the poppet x_0 of the valve (fig.3), the coefficient of the hydrodynamic force r_h has been calculated by the expression [12]:

$$r_h = \frac{\frac{k_{st} \cdot q_0 \cdot A_k}{x_0} - c}{p_{1,2}} \tag{1}$$

3.2. Discharge coefficient of the valve throttling area

As it is already mentioned, the discharge coefficient of the main throttling area of the studied pressure relief valve depends on the Reynolds number in a complicated manner. In the transient mode, the flow rate passing through the opening area of the valve restriction is assumed to be turbulent of unknown Reynolds number. Therefore, the flow rate q_3 passing through the main valve throttling area is given by the following equation:

$$q_3 = \mu \cdot \pi \cdot d \cdot x \cdot sin\theta \cdot \sqrt{\frac{2}{\rho} \cdot p_{1,2}} \tag{2}$$

where μ and $\pi \cdot d \cdot x \cdot sin\theta$ are the discharge coefficient and the opening area of the main throttling area of the valve. According to the eq. (2) it is possible to compute the discharge coefficient from the experimental static characteristics. The experimental discharge coefficient of the valve throttling area depending on the Reynolds number is expressed on fig.5.
The Reynolds number of the valve throttling area is given with the equation:

$$Re = \frac{v \cdot d}{\nu} = \frac{2 \cdot q_3}{\pi \cdot d \cdot \nu} \tag{3}$$

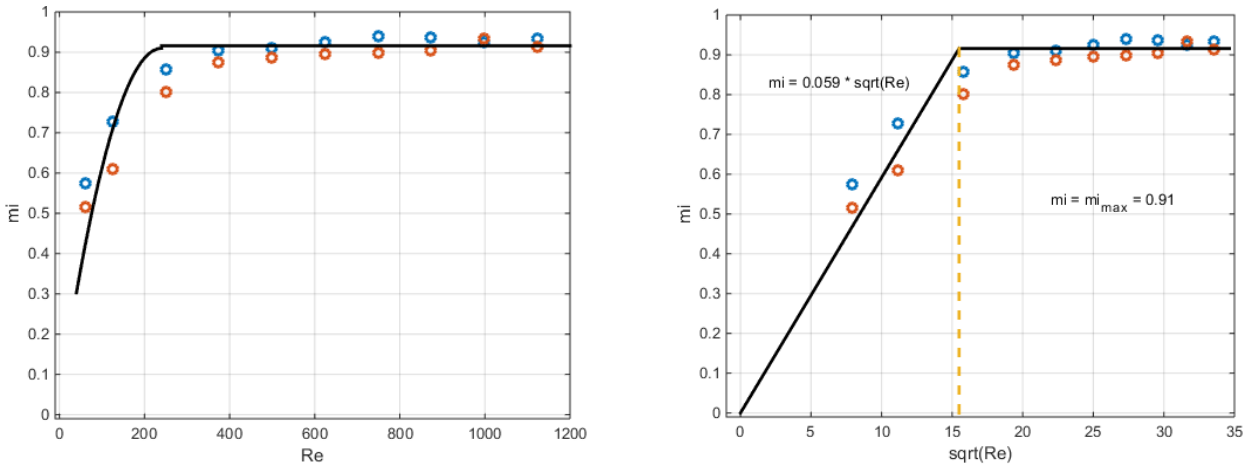

Fig. 5. Discharge flow coefficient for the throttling area of the valve

As it is presented on fig.5 the discharge coefficient is changing linearly with the square root of Re up the limit value of $Re_{lim} = 240$ or $\sqrt{Re_{lim}} = 15.5$. After Re_{lim} the discharge coefficient is constant and it is around 0.91.
According to above statements the discharge coefficient can be expressed by the following equations:

$$\mu = \mu_{max} = 0.91 \quad for\ Re > Re_{lim}$$
$$\mu = 0.059 \cdot \sqrt{Re} \quad for\ Re < Re_{lim} \tag{4}$$

For the simplicity of calculation, in this paper the discharge coefficient is taken to be constant.

Woben [10] and Zehner [4] have presented the experimental discharge coefficient for different geometric parameters of the valve.

3.3. Mathematical model of the valve

Mathematical model of the system is described by the following equations:
According the fig. 2 the equation of continuity in front of the investigated pressure relief valve can be expressed as:

$$q_0 = q_{in} + q_v + q_1 \tag{5}$$

where q_{in}, q_v, and q_1 are the flow rate through restriction area in the directional control valve V1, the flow rate which enters in the volume V_0 and the flow rate entering in the valve, respectively. The transient variation of the restriction area of the directional control valve V1 affects the studied valve transient response. The flow rate q_{in} passing through the directional control valve is given by

$$q_{in} = (1 - \frac{t}{t_1}) \cdot \mu_v \cdot \pi \cdot d_v \cdot x_v \cdot \sqrt{\frac{2}{\rho} \cdot p_1} \tag{6}$$

where t_1 is closing time of the DCV, μ_v, d_v and x_v are the discharge coefficient, the diameter of the valve spool and valve spool displacement, respectively. The flow which enters in the volume V_0 can be expressed by the equation of the compressibility effect in the volume V_0:

$$q_v = \frac{V_0}{K} \cdot \frac{dp_1}{dt} \tag{7}$$

where K is the bulk modulus of the oil.
Equation of continuity in the valve in front of the control orifice and after it is

$$q_1 = q_2 = q_3 + A_k \cdot \frac{dx}{dt} \tag{8}$$

where: A_k – the area of the valve poppet; q_3 – the flow through the control orifice in the valve.
The equation of motion of the valve poppet is

$$m \cdot \frac{d^2x}{dt^2} + c \cdot (h_0 + x) + r_h \cdot x \cdot p_{1,2} = A_k \cdot (p_3 - p_4) - F_T \tag{9}$$

where: $m = m_k + \frac{1}{3}m_f$ – the equivalent mass of the valve poppet m_k and the spring m_f; c – the stiffness of the spring; h_0 – the deformation of the spring when $\mathrm{x} = 0$; r_h– the coefficient of the hydrodynamic force obtained by the expression (1); F_T – friction force between the valve poppet and the body of the valve.
The pressure in the lower chamber of the closing element of the valve p_3 depends on the losses in the orifice h between the piston of the valve poppet and the body of the valve:

$$p_3 = p_1 - R_{a,l} \cdot A_k \cdot \frac{dx}{dt} - R_{a,m} \cdot \left(A_k \cdot \frac{dx}{dt}\right)^2 - L_a \cdot A_k \cdot \frac{d^2x}{dt^2} \tag{10}$$

where: $R_{a,l}$, $R_{a,m}$ and $L_a = \rho \frac{l}{\pi dh}$ are linear, local and inertial resistances in the orifice with length l.
The pressure in the upper chamber above the valve poppet is obtain analogically when for this type of the valve is $p_4 = p_2$.
The pressure drop in the outlet pipeline is

$$p_2 = R_{p,l} \cdot q_2 + R_{p,m} \cdot q_2^2 + L_p \cdot \frac{dq_2}{dt} \tag{11}$$

where: $R_{p,l}, R_{p,m}$ and $L_{p,t}$ respectively linear, local and inertial resistance of the outlet pipeline with length l_p and diameter d_p.
Additional conditions were taken into account when solving the nonlinear system of the differential equations: the flow rate q_1 is zero when the valve is closed; the pressure p_1 cannot be less than the absolute vacuum; the displacement x of the valve poppet cannot be negative; the flow rate q_{in} is zero at $t > t_1$, etc., The mathematical model (2),(5)-(11) can be solved with computer programs for solving nonlinear differential equations. For solution of the system of the nonlinear differential

equations, the adaptive Runge-Kutta method has been used. This method based on the forth order Runge-Kutta method estimate the truncation error at each integration step and automatically adjust the time step size to keep the error within prescribed limits.

4. Experimental and theoretical characteristics of the researched valve

Fig. 6 presents the results of experimental and theoretical studies of a Bosch Rexroth type valve for a pressure of $60\,bar$ and oil volumes $V_0 = 52\,cm^3$ and $480\,cm^3$. The closing time t_1 of the directional control valve is less than $20\,ms$ and the flow rate of the pump is $q_0 = 25\,l/min$. The outlet pipe is $12\,mm$ in diameter and $1\,m$ long. The experiment was performed with pressure and displacement transducers and was recorded on a computer.
With a volume of oil at the inlet of $52\,cm^3$, a relatively large dynamic load is obtained, as the pressure reaches $100\,bar$ and the natural frequency is $742\,rad/s$. This leads to system overload, which in many cases is unacceptable. As the volume increases to $480\,cm^3$, the maximum pressure and the natural frequency of the transient process decrease to $85\,bar$ and $206\,rad/s$, respectively.

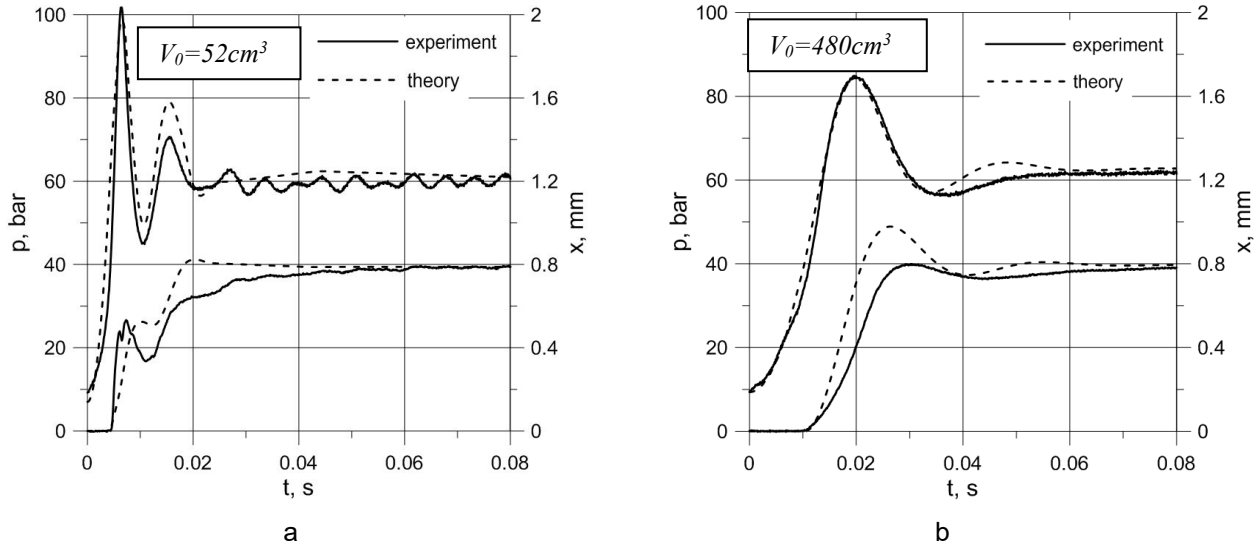

Fig. 6. Experimental and theoretical dynamic characteristics of the specified valve for different pressures and volumes at inlet port

The poppet of the valve opens when the spring-set pressure of $60\,bar$ is reached. The pressure in this phase of the transient process changes at a rate determined by the flow rate of the pump, the volume of oil at the inlet and the closing time of the directional control valve t_1. The difference between the experiment and the theoretical solution is due to the change in the hydrodynamic force and the slope of the static characteristic during the transient process, which are not taken into account in the mathematical model.

5. Conclusion

The steady-state and transient characteristics of a direct operated pressure relief valve are researched theoretically and experimentally. A comprehensive nonlinear mathematical model of the studied valve is deduced to predict the performance of the studied valve in the steady-state and transient modes of operation. The developed model, which takes into consideration most nonlinearities of the studied valve, is used to develop a computer simulation program. The steady-state and transient characteristics of the studied valve are simulated using this program. The experimental work aimed at validating the studied valve proposed model and the simulation program. The results showed good agreement between simulation and experimental results in the steady-state and transient modes of operation. The analysis of the simulation results showed that, when studying the performance of the hydraulic control valves, nonlinearity occurs due to the

transient fluctuation in the valve operating pressures and the fluctuation in the throttling areas of the valve restrictions and their discharge coefficients. The transient fluctuation in the valve operating pressures causes nonlinear velocity changes of the fluid flow due to the high bulk modulus, which decreases during the valve operation. The throttling areas of the valve restrictions usually have nonlinear mathematical formulas. The discharge coefficients of these areas are assumed constant independent of flow rates and opening areas. They change in a complicated manner with the flow rates, Reynolds numbers, and the dimensions of the throttling areas. It was also found that the geometry of the throttling orifice, which connects the valve inlet port to the downstream port, plays an important role in the steady-state and transient performance of the studied valve. This result implies the need for further investigation the effect of the geometric parameters of the valve poppet on the steady-state and transient performance of hydraulic control valves.

References

[1] Backé, W., and H. Murrenhoff. *Basics of Oil Hydraulics* / *Grundlagen der Ölhydraulik*. Institut für fluidtechnische Antriebe und Steuer-ungen RWTH Aachen, 1994.
[2] Will, D., H. Ströhl, and N. Gebhardt. *Hydraulics* / *Hydraulik*. Berlin, Springer-Verlag, 1999.
[3] Brodowski, W. "Contribution to clarifying the steady-state and dynamic behavior of direct-acting pressure relief valves" / "Beitrag zur Klärung des stationären und dynamischen Verhaltens direktwirkender Druckbegrenzungsventile." Dissertation, RWTH Aachen, 1974.
[4] Zehner, F. "Pilot operated pressure valves with direct hydraulic-mechanical and electrical pressure measurement " / "Vorgesteuerter Druckventile mit derekter hydraulisch-mechanischer und elektrischer Druckmessung." Dissertation, RWTH Aachen, 1987.
[5] Dasgupta, K., and R. Karmakar. "Modelling and Dynamics of Single Stage Pressure Relief Valve With Directional Damping." *Simulation Modelling Practice and Theory* 10, no. 1-2 (October 2002): 51-67.
[6] Watton, J. "The Design of a Single-Stage Relief Valve With Directional Damping." *The Journal of Fluid Control Including Fluidics Quarterly* 18, no. 2 (March 1988): 22-35.
[7] Wu, D., R. Burton, and G. Schoenau. "An Empirical Discharge Coefficient Model for Orifice Flow." *International Journal of Fluid Power* 3, no. 3 (2002): 17-24.
[8] Borutzky, W., B. Barnard, and J. U. Thoma. "An orifice flow model for laminar and turbulent conditions." *Simulation Modelling Practice and Theory* 10, no. 3 (2002): 141-152.
[9] Lichtarowicz, A., R. Duggins, and E. Markland. "Discharge Coefficients for Incompressible Non-Cavitating Flow Through Long Orifices." *J. Mech. Eng. Sc.*, no. 2 (1965): 210 – 219.
[10] Wobben, G.D. "Static and dynamic behavior of pilot operated pressure relief valves with particular consideration of the flow forces" / "Statisches und dynamisches Verhalten vorgesteuerter Druckbegrenzungsventile unter besonderer Berücksichtigung der Strömungskräfte." Dissertation, RWTH Aachen, 1978.
[11] Robson, P., and B. Zähe. "A new type of relief Valve." *O+P*, no. 11-12 (2006).
[12] Dimitrov, S. "Synthesis of pressure relief valves." Dissertation, Technical University of Sofia, Sofia, 2013.
[13] Stone, J. A. "Discharge Coefficients and Steady-State Flow Forces for Hydraulic Poppet Valves." *Transactions of the ASME* 82 (March 1960): 144–154.
[14] Wobben, D. "Flow forces on 2-way cartridge valves." / "Strömungskräfte an 2-Wege-Einbauventilen." *Industrie-Anzeiger*, no. 22, v.17.3., 1978.
[15] Altare, G., M. Rundo, and M. Olivetti. "3D Dynamic Simulation of a Flow Force compensated Pressure Relief Valve." Paper presented at ASME 2016 International Mechanical Engineering Congress and Exposition, Phoenix, Arizona, USA, November 11-17, 2016.

Main Constructive Solutions for Actual Wind Turbines Used for Green Power Generation

Associate Professor **Fănel Dorel ȘCHEAUA**[1,*]

[1] "Dunărea de Jos" University of Galați, MECMET Research Center, * fanel.scheaua@ugal.ro

Abstract: *It can be said that at the present time there is more than ever a need for energy at the global level to support the activities undertaken by the industrial branches as well as by the human communities. The possibilities of obtaining energy are limited and if we refer to the burning of fossil fuels, they have a direct effect on the environment, contributing decisively to the increase in global temperature values. Therefore, special attention must be paid to alternative methods that can be used to obtain energy; here we are talking about the action of the wind, the sun, or the force of sea waves. This paper presents the possibilities of obtaining energy from the wind action, on different models of wind turbines, with specific efficiency values for each of them, the main projects that have been carried out for capture both on land and offshore facilities, some of the most important onshore and offshore wind turbine parks established worldwide and for the Romanian area, but also the main results obtained at the present time in terms of energy amounts of these wind facilities.*

Keywords: *Wind action, turbine, constructive solutions, wind farm, power generation*

1. Introduction

The wind action can be used for power generation at the level of a turbine rotor that is able to convert wind mechanical energy into electric energy by means of an electric generator.
The turbine constructive solution result as an entire assembly that based on the wind force can generate energy in a constant manner.
The wind interaction with the turbine rotor takes place at the blades level, which are specially designed and constructed to be oriented directly towards the wind action direction to achieve a lift displacement and then rotation movement necessary for a continuous operation that coincides with the duration of the wind action.
Hence, the areas differentiation where the wind turbines facilities installation is indicated where the wind velocity values are constant and over a long period of time throughout the year.
The main types of wind turbines used mainly for wind farms with high production capacity (installed power) are three bladed horizontal axes (HAWT), while the vertical axis wind turbines (VAWT) are mainly used for smaller applications and where the wind speed is not very high, as they have the possibility to start and operate at low wind speeds.

2. The atmospheric masses movement and the winds action formation

Due to the atmospheric pressure values, in conjunction with the uneven heating of the atmospheric masses and the Earth rotational movement, a continuous movement of the air masses at the planetary level is created.
It should be emphasized that the Earth rotation movement involves concerted actions between the Coriolis forces, the centrifugal force, the frictional force between the air particles that act differently depending on the non-uniform character of the Earth's surface, the pressure gradient, the effects of turbulence, as well as the possibility of atmospheric air masses to transport water vapor (advection).

Table 1: Specific involved efforts in air masses displacement

Current number	Effort type	Specific relation
1.	Coriolis	$F_{Cor} = 2\omega v \sin\phi$
2.	Centrifugal	$F_{Cen} = m\omega^2 r$

3.	Turbulence	$F_D = \frac{1}{2}\rho u^2 c_D A$
4.	Pressure gradient	$F_{PG} = \rho a dA dz$

In figure 1 are presented the Coriolis and centrifugal effects created at Earth level due to continuous rotation that have a direct influence in directing the air masses movement.

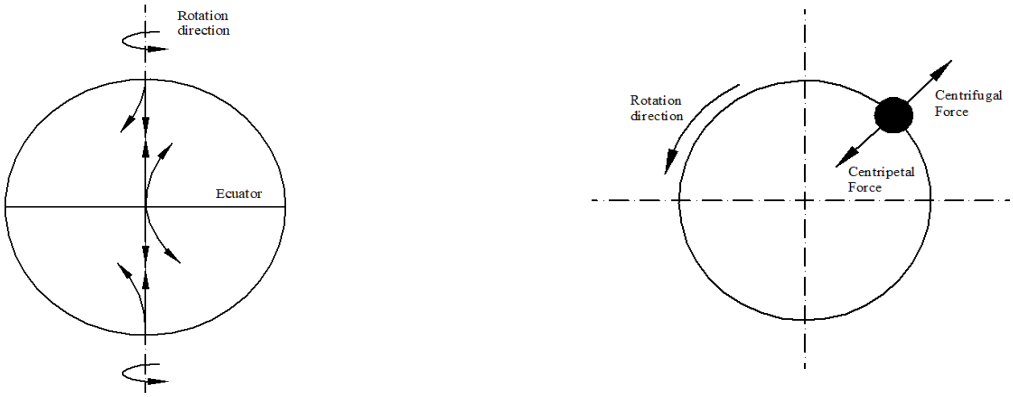

Coriolis effect Centrifugal force effect

Fig. 1. Coriolis and centrifugal Earth effects schematically representation

A continuous exchange in heat and humidity amounts is thus achieved through the transport of water vapor produced by evaporation between different areas, there being a general tendency to balance the values between the different terrestrial areas of the globe.
It is established that atmospheric air particles move along 3 components, horizontal with meridian orientation, vertical and zonal.
The meridian component of the movement of atmospheric masses defines their movement along terrestrial meridians in the direction from the poles to the equator and vice versa, the zonal one is described as the atmospheric exchange that takes place between the different areas, and the vertical component is limited to low values compared to the other two components being represented by raising or lowering to ground level at a certain covered area.

3. Brief history of wind action harvesting solutions

The use of the wind energy resource has been used since ancient times by humans to pump water, irrigate farmland, or for navigation.
In ancient Egypt sail boats were also propelled by wind (5000 IH), also in China and Persia windmills were used to grind grain and pump water (200 IH).

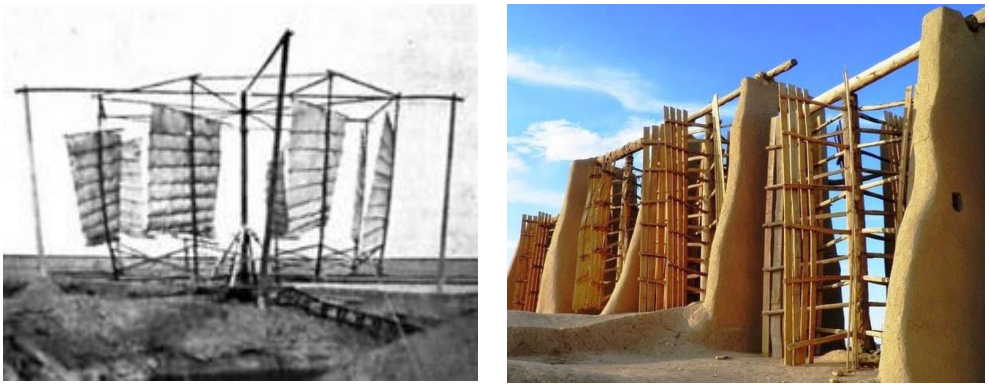

Chinese windmill Persian windmill

Fig. 2. Ancient wind utility applications

It can be observed that for the presented wind application models used in antiquity, the principle of operation with a vertical axis was adopted.
Later in Europe, windmills were developed adopting the rotor horizontal axis principle in operation, which means the transition from drag to lift force at the level of the wind blades.
Such applications using the wind force have been developed in the Netherlands to pump water from dammed plots and taken from the coastal area of the sea. They feature significant wind direction improvements to streamline operation and ensure optimal performance even when the wind changes direction.
Later, in the United States, wind turbines have been used to pump water from the depths and to irrigate agricultural land with a steel multiblade rotor representing a practical solution based on the wind action.

Traditional Dutch wind applications

American multiblade

Fig. 3. Dutch and American Wind turbines

An improved wind turbine was built in 1888 by the American scientist Charles Bush, which featured a large rotor constructive solution, being one of the first applications meant for wind power production (figure 4).

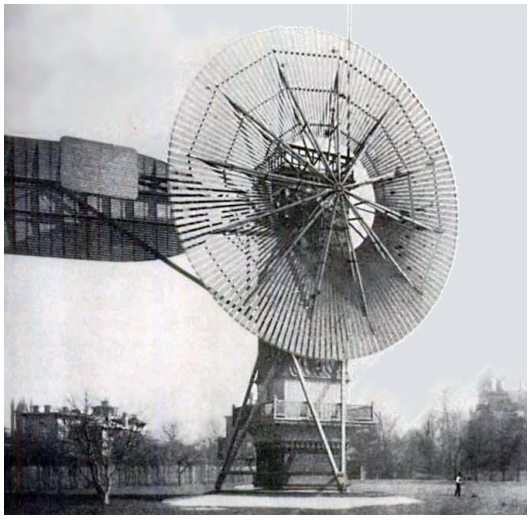

Fig. 4. Wind turbine constructed by Charles Bush in 1888

In the 20th century, while the airplane was invented by the Wright brothers (1903), and the principle was further used to develop a wind turbine that would work for power generation, using the airplane wing model to develop the turbine blades.
For the generation of electricity, there were attempts at the end of the 19th century, and then in the following century, with applications of wind turbines with a horizontal axis (HAWT), and for the variants with a vertical axis (VAWT), the Savonius (1922) and Darrieus (1931) turbines were developed (figure 5).

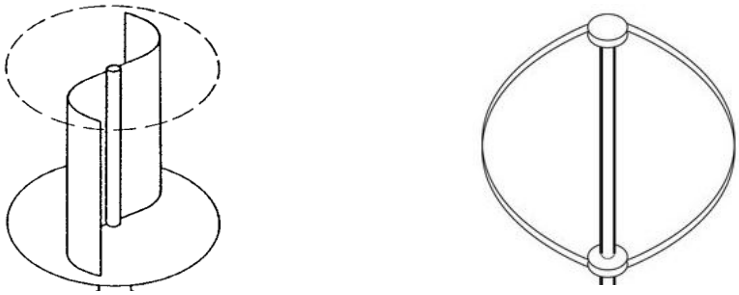

Savonius turbine rotor Darrieus turbine rotor

Fig. 5. Vertical axes wind turbine rotors constructive variants

The current trend of producing and harnessing energy based on wind turbines has existed since the 90s. This trend has continued since then until the present time, during which remarkable results have been achieved in terms of the development of constructive models of wind turbine rotors, an increase regarding the possibility of energy production through the continuous optimization of the turbine rotor designed blades and based on these facts today it is possible to obtain significant amounts of energy per turbine unit.

4. Wind turbine main types and their efficiency criteria

The modern wind turbines currently used to harvest energy from the wind action are based on two main typologies that challenge their operation, namely the positioning of the turbine rotor axis in horizontal and vertical direction.
In principle, horizontal axis turbines (HAWT) benefit from advantages in terms of efficiency obtained in operation that clearly exceeds the energy efficiency values recorded at the level of vertical axis wind turbines (VAWT).
On the other hand, the advantages of using vertical axis turbines are also highlighted in the sense that they can be used for lower values of wind speed, as well as advantages related to the direction of wind action, as they can work independently of the wind action direction and for this reason they can remain in action even when the wind direction changes.

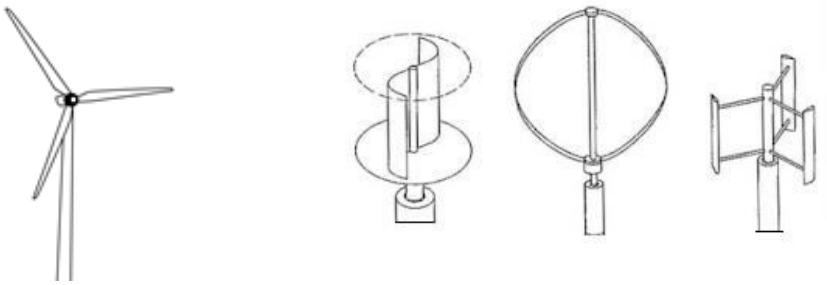

Horizontal axis three bladed wind turbine (HAWV)

Vertical axis wind turbines (VAWV) of SAVONIUS, DARRIEUS and H-rotor types

Fig. 6. Main constructive solutions for wind turbine applications

The main wind turbine constructive types are shown in the figure 6, being emphasized that the operation is based on lift force type for the constructive version with a horizontal axis and of the drag force type for those with a vertical axis.
A graphical situation representing the obtained power values for the main constructive solutions of wind turbines is presented in figure 7, being emphasized the proper values produced by different rotor types.

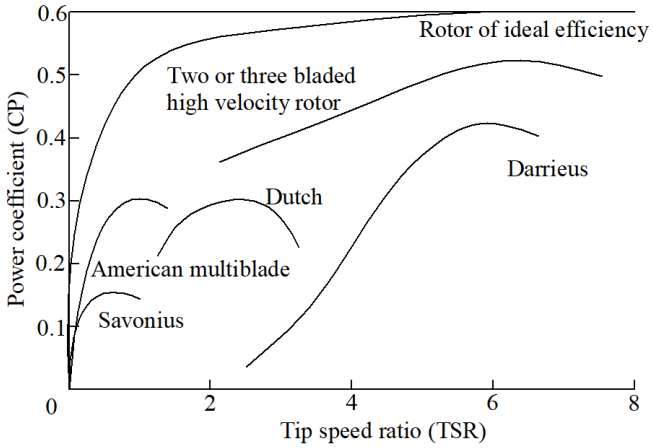

Fig. 7. Specific efficiency values as a function of TSR for the main constructive rotor typologies of wind turbines

5. Prospects for the actual and future efficiency results in the field of wind energy

Constructive solutions for wind turbines are currently being developed and designed so that they can be implemented in the coastal and marine area by continuously increasing the constructive dimensions and the installed power.
Such prototype models are offered by established world manufacturers such as Siemens, Vestas or General Electric which who have developed models that represent the top of the range in terms of wind power generation.

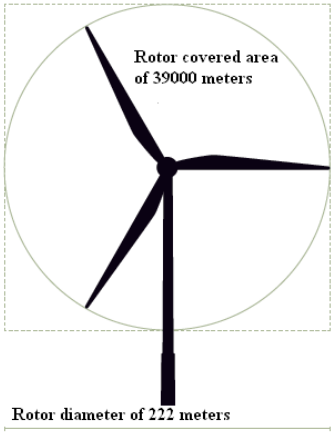

Siemens Gamesa 14-222 DD wind turbine rotor

General Electric Haliade X constructive solution

Vestas V236 prototype for offshore wind applications

Fig. 8. Ultimate constructive models for wind turbine rotors

For the presented models, high values are expected to be obtained in terms of energy produced on a single turbine unit, considering the impressive overall dimensions at which these wind turbines are designed and produced.
Table 2 shows the specific dimensions and energy values for each constructive type presented.

Table 2: Main dimensions and power values of novel wind turbine for on and offshore wind energy applications

New generations of wind turbine rotors						
Current number	Provider/Model	Power in nominal value (MW)	Rotor covered area (m2)	Rotor blade lenght (m)	Diameter of the rotor (m)	Functional options
1.	Siemens Gamesa/14-222 DD	14	39000	108	222	Variable rotational velocity, pitch control
2.	General Electric/Haliade X	12/13/14	38000	107	220	Digital velocity and pitch control
3.	Vestas/V 236	15	43742	155.5	236	Variable velocity, pitch control

Some of the main offshore wind farms currently operating in northern Europe had an installed capacity of around 23.2 GW for 2018, while the total is expected to increase to around 140 GW by 2030.
Table 3 shows some wind farms currently operating offshore in the northern area of Europe.

Table 3: Offshore wind farms in operation in northern Europe (UK)

Current number	Offshore wind farm	Installed power capacity (MW)	Number of turbines	Turbine type	Turbine power (MW)
1.	Walney Extension	659	87	Vestas	7-8
2.	London Array	612.5	175	Siemens Gamesa	3.5
3.	Hornsea 1	1218	174	Siemens Gamesa	7
4.	Gemini Wind	600	150	Siemens Gamesa	4
5.	Beatrice	588	84	Siemens Gamesa	7

Various other offshore wind farms are in progress for the near future, such as the one at Dogger Bank in the north-east of the UK which will have a capacity of 3.6 GW using HALIADE X turbine types from General Electric (GE) of 12 MW power each.
For the onshore area, the Gansu wind farm located in central western China, which has an estimated installed power of 20 GW benefits from a desert area with wind potential. At the end of 2015, this wind farm was operating at less than half of its potential (40%) since there is a low demand for energy in the production area and the transmission and distribution network to the large cities in the east is not being developed.
In addition, for the onshore area, the Mojave wind farm is the largest wind farm in America in terms of installed power capacity, with 1550 MW, with 600 Vestas turbines of 1.55 MW each.
For the near future there it is predicted that over 355 GW of new capacity will be added until 2024, representing over 71 GW for new applications each year until 2024.
At the offshore locations, the predictions are to rise from 6 GW for 2019 to nearly 80 GW for 2024.
For the 2019 compared to the 2018 global development of new wind power installations was achieved a 19% growth exceeding 60 GW, reaching the total installed capacity to 650 GW. In the onshore locations, wind applications raised at 54.2 GW, while also developing the offshore wind farms that were achieved 6 GW installed power.

At the world level, there are the first places for 2019 new installations attributed to China, the US, the UK, India and Spain.
In Romania, there are wind turbine parks in operation located mainly in the Dobrogea area with the largest installed power capacities. Investors' interest in developing these parks is high due to the existing possibilities to take over the produced energy by the national energy system. The total capacity of energy produced and delivered in the national grid of Romania is approximately 1529 MW.

6. Conclusions

There is obvious interest in developing wind power generation capabilities in locations where there is a high wind action potential. In addition, the share of wind energy is increasing, being possible through the continuous modernization of the production units made either through innovative design solutions of the turbine blades, or by increasing the dimensions of the rotor made in the last period, especially for the units that are located on offshore areas. The main turbines typologies that were and are currently used for wind production facilities were presented in the paper, with an emphasis, on horizontal axis turbines that show increased efficiency at certain values of the wind speed. However, the vertical axis variants of turbines can be used to produce energy from the wind action, especially where the wind speed is lower, while also having the possibility to start and operate regardless of the wind direction.
The turbines constructive models from the world's leading manufacturers that offer impressive production capacities per unit are highlighted, which are currently available and are being installed for wind farms, especially in marine areas where there is high wind potential with constant values over time. A review of some of the largest wind farms in terms of installed power that exist or are currently being built worldwide is also carried out.
The example of Romania is also presented, which has the largest wind farm in the Dobrogea area where there is an area suitable for wind energy applications, currently in operation delivering a significant percentage of energy obtained from renewable sources to the national grid.
All these activities undertaken in the past as well as the current ones in terms of setting up wind energy production units represent a good start and a continuous path to follow in the direction of development aiming to achieve the goal of replacing the fossil fuels in energy production and implicitly to avoid releasing gases into the atmosphere and affecting the environment.

References

[1] Vasilescu, Al. A. *Fluid Mechanics* / *Mecanica Fluidelor*. Galați, University of Galati, 1979.
[2] Florea, J., and V. Panaitescu. *Fluid Mechanics* / *Mecanica Fluidelor*. Bucharest, Didactic and Pedagogical Publishing House, 1979.
[3] Florescu, Adriana, Sorin Barabas, and Tiberiu Dobrescu. "Research on increasing the performance of wind power plants for sustainable development." *Sustainability* 11, no. 5 (2019): 1266.
[4] Chiulan, Elena-Alexandra, and Anton Anton. "The (r)evolution of wind energy systems in Romania: state-of-the-art, new trends and challenges." *IOP Conference Series: Earth and Environmental Science* 664, no. 1 (2021): 012016.
[5] Kaldellis, John K., and Dimitris Zafirakis. "The wind energy (r) evolution: A short review of a long history." *Renewable Energy* 36, no. 7 (2011): 1887-1901.
[6] Papadis, Elisa, and George Tsatsaronis. "Challenges in the decarbonization of the energy sector." *Energy* 205 (2020): 118025.
[7] Ellabban, Omar, Haitham Abu-Rub, and Frede Blaabjerg. "Renewable energy resources: Current status, future prospects and their enabling technology." *Renewable and Sustainable Energy Reviews* 39 (2014): 748-764.
[8] Ruan, Xiang, Rong Sheng, and Tuo Lin. "Environmental policy integration in the energy sector of China: The roles of the institutional context." *International Journal of Environmental Research and Public Health* 17, no. 24 (2020): 9388.
[9] GWEC. "Global Wind Energy Council 2019." Accessed September 1, 2022. https://gwec.net/global-wind-report-2019/.
[10] Sauer Energy International. "Five of the World's Largest Offshore Wind Energy Farms." Accessed September 10, 2022. https://www.saurenergy.com/solar-energy-blog/worlds-largest-offshore-wind-energy-farms.

Using Hydrological Concepts and an Artificial Neural Network to Model the Rate for COVID-19 Infections versus Deaths

Maritza Liliana ARGANIS JUÁREZ[1,2,*], Margarita PRECIADO JIMÉNEZ[3], Sandra Lizbeth ROSALES SILVESTRE[1]

[1] National Autonomous University of Mexico, Institute of Engineering

[2] National Autonomous University of Mexico, Faculty of Engineering

[3] Mexican Institute of Water Technology, Hydrology Coordination

* Corresponding Author: MArganisJ@iingen.unam.mx

preciado@tlaloc.imta.mx

SRosalesS@iingen.unam.mx

Abstract: *Models were run to reproduce COVID-19 infections versus deaths in Mexico City. The first model was made using rain runoff concept, emulating rain as number of infections reproducing runoff as number of deaths given as of March 2020. The second consisted of using an artificial neural network (ANN) proposed as an initial condition function to be implemented in the model with delay. These models were applied to fit accumulated confirmed case data, obtaining fit corroborated by coefficient of determination, R^2. The R^2 value produced by model was 0.0528 in case of infections comparison vs. official deaths reported by the Ministry of Health, 0.0571 for t case of infections vs. modelling using the HEC-HMS tool, and 0.0937 for case of contagion vs. modelling using ANN.*

Keywords: *Rain-Runoff, Artificial intelligence, infections, deaths, SARS-CoV-2, analogy*

1. Introduction

The COVID-19 pandemic due to the SARSCov-2 virus has persisted for just over two years worldwide. Numerous efforts have been made to obtain models that reproduce contagion behaviour events against deaths in different parts of the world. Basu and Campbell [1] proposed a Long Short-Term Memory (LSTM) based model, used accumulated data on infections and deaths, as a decision support tool for reopening or staggering of activities in a country, utilize data from the Johns Hopkins University repository and made cumulative case predictions for the United States. Dal Molin Ribeiro et al. [2], used regression models to obtain short-term predictions of cumulative covid-19 infections for Brazil.

Understanding population growth phenomena has been a task that over time has provided various challenges to mathematicians, physicists, biologists, medics, economists and many others. From economic areas, where applying growth models to poultry allows making imperative predictions for the profitability of operations, to biological and medical areas, where growth models have been applied to the growth of animals, plants, yeast cells, tumours, and recently to adjust and model COVID-19 pandemic data in order to model phenomena with greater precision, fractional calculus has been implemented in growth models and they were applied to describe cumulative confirmed cases for COVID-19 in Mexico, US and Russia, obtaining an excellent adjustment corroborated by a coefficient determination R^2>0.999 [3].

Since the beginning of pandemic, the effect of COVID-19 has been different throughout the world; however, even with the various measures that each country has taken, the accumulated confirmed cases continue to have a sigmoidal behaviour.

For approximation to description for flow models characteristics, the most conventional hydrological models, it has been divided into three sections that cover (1) the technical and modelling aspects, (2) the enumeration of examples with work done with hydrological models and (3) the description of some widely disseminated models. The models to which reference will be made are those of a semi-distributed and distributed nature, those with the greatest potential and current development [4]. The characteristics of the models are analysed, firstly, taking into account

the architecture or way of structuring the modelling process, usually by components of the hydrological cycle, and, secondly, by the modelling approaches. The structure that a model acquires is independent of the representation detail, the number of parameters and the temporal definition used by the hydrological model in question. Currently those of a distributed and/or semi-distributed nature have approached the modelling process by building a modular structure. The conceptualization in components practically forces the models to be built using this modular architecture; that is, dividing the model into different interconnected sub models.
Hydrological simulation models can be of two types: An event model simulates a specific hydrological event: "This downpour would produce this hydrograph." It calculates what part of the precipitation will be net precipitation, and with it calculates the direct runoff that is generated and the rest of the precipitation (abstractions or losses) forgets it. A continuous model attempts to simulate the evolution of the entire hydrological process. It calculates what part of the rainfall is retained on the surface (interception in the vegetation and 'puddles'), what part infiltrates into the ground and what part generates surface runoff. Once the precipitation has passed, it should be considered if the precipitation that was stored in soil evapotranspires or infiltrates into aquifers. Finally, from these they can be lost to a deep circulation (outside the scope of the model) or feed the channels. An event model usually works from a few minutes to several days, while in continuous models' periods from months to several years are common. HEC-HMS was initially a model to simulate specific events, although now it has methods that allow it to be used continuously, as is the case of the application presented in this document.
In this paper, two models will be applied to simulate the process of infections against deaths by COVID-19. The first with a rain runoff model, in the free use program HEC-HMS, calibrating the time of occurrence between infections and deaths (delay time), emulating the rain as infections number to reproducing runoff as deaths number that occurred from March 2020 when the pandemic officially began in Mexico. The second model consisted of using an artificial neural network (ANN) that takes as input data the daily infections number as outputs functions number, preserving the cyclical nature of the phenomenon. The procedure was applied to adjust the data on cases of COVID-19 in Mexico City, obtaining the adjustment.

2. Material and methods

2.1 HEC-HMS

Adjustment parameter used in modelling used by HEC-HMS was implementation of lag effect; global phenomenon was decomposed into its local parts, allowing each outbreak and its different characteristics to be directly compared. The Soil Conservation Service (SCS) dimensionless unit hydrograph procedure is one of best-known methods for deriving synthetic unit hydrographs in use today. References for this method can be found in most hydrology textbooks or manuals. The main reference for this method can be considered as the Soil Conservation Service - National Engineering Manual, Section 4, Hydrology [5].
Dimensionless unit hydrograph used by the SCS was developed by Victor Mockus and was derived based on a large number of unit hydrographs from basins that varied in characteristics such as size and geographic location. Unit hydrographs were averaged and final product was made dimensionless considering the ratios of q/qp (flow rate/peak flow rate) on the ordinate axis and t/tp (time/time to peak) on the abscissa axis, where the units of q and qp are volume/time. This final dimensionless unit hydrograph, which is the result of averaging a large number of individual dimensionless unit hydrographs, has a time to peak located at approximately 20% of its time base and an inflection point at 1.7 times the time to peak final top. The dimensionless unit hydrograph and the cumulative mass curve for dimensionless unit hydrograph are illustrated in Fig. 1.
Curvilinear unit hydrograph can also be represented by an equivalent triangular unit hydrograph. However, time parameter is somewhat difficult to estimate and quite subjective; this parameter has a considerable influence on unit hydrograph values. Underestimating the unit hydrographs "time" will cause peak to occur earlier and higher, while overestimating will result in a later and lower peak. There are several methods to estimate time parameter in UHG. The SCS lag equation is an empirical approach developed by SCS, which estimates lag time directly.

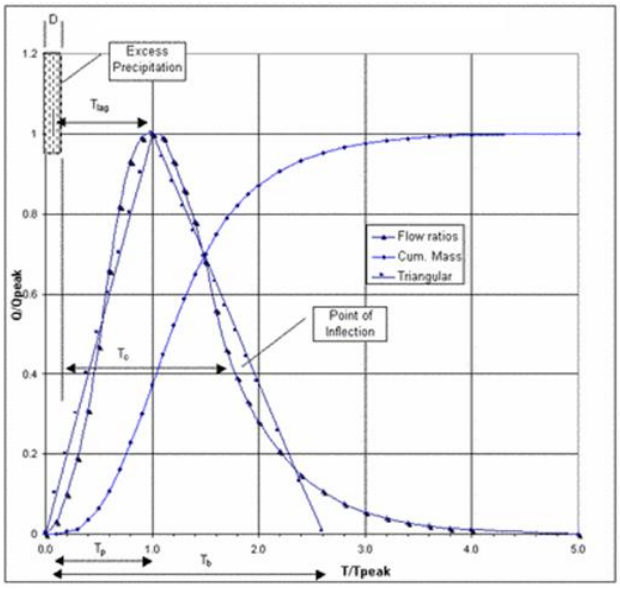

Fig. 1. Dimensionless unit hydrograph of the Soil Conservation Service (SCS)

2.2 ANN

A typical artificial neural network consists of an input (or inputs), a hidden layer of neurons defined by a typically sigmoid function, and a layer with output neurons, traditionally given by a linear function; each layer has weight factors (w) and thresholds or bias (bias, b) and one or more outputs. The neural network goes through the stages of training, validation and testing. The most commonly used algorithm in training is back propagation. In this study, an ANN was used with the configuration given in Fig. 2, from the MATLAB applications [6].

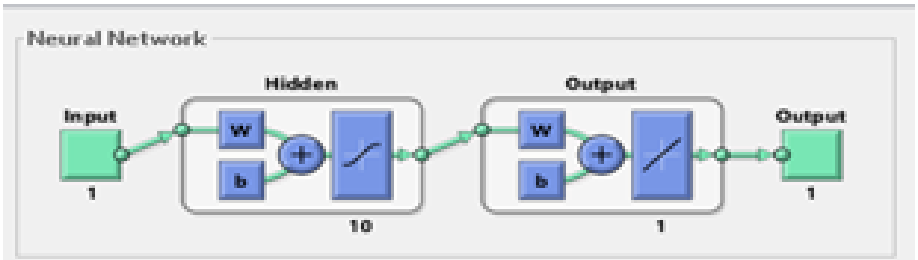

Fig. 2. Configuration of the artificial neural network considered (The MathWorks, 2022)

In this analysis, we propose 10 neurons in hidden layer; a Levenberg-Marquardt backward propagation algorithm for network training, of 646 input data, was considered, too; 646 random samples were considered, occupying 65% for training (Samples that network uses for its training and error is evaluated with these data), 20% for validation (used to measure t network generalization and to stop training when it stops improving said generalization) and 15 % for the test (they do not influence training and give an independent measure of performance for network during and after the training). In this test, the process finished in 12 iterations and in a few seconds.
Additionally, the code of the function created by the neural network can be saved to obtain new deaths from giving the number of cases.

2.3 Delay or lag time

The first case for COVID-19 in Mexico was confirmed by federal government on February 28, 2020, although in its current version, the official database includes a positive case a month before that according to Ministry of Health (SS). One year later, as of mid-February 2021, more than two million infections have been reported, 94.6% of which were confirmed by RT-PCR or antigen

testing. The remaining 5.4% of patients were diagnosed with COVID-19 based on clinical presentation and epidemiological association, in the absence of a valid test result.
In this paper, lag time parameter was proposed where initial function was generalized to model phenomena with recurrent outbreaks. This model was implemented to describe data on confirmed cumulative cases for COVID-19 in Mexico, in the beginning for pandemic until February 2020 to December 25, 2021. Finally, as a result of lag effect, implementation it was possible to break down global phenomenon into its local parts, allowing each outbreak and its respective characteristics to be directly compared.
It is important to note that there is a lag time between date on which a person presents suspected symptoms for COVID-19 and date on which they enter a medical unit to receive care, and therefore be registered into open database. This lag is mainly due to natural development for respiratory disease, which determines t time a person waits to seek medical attention, from time symptoms began. Characterizing lag time is very important to estimate trending the COVID-19 syndrome, since it represents a delay in availability of information that causes an apparent decrease in cases number in the most recent days, which does not correspond with a real decrease in infections. A very important factor in simulating the disease evolution is the time that elapses between infection by virus and symptoms appearance for the disease. Most researches estimated incubation period for COVID-19 range from 1 to 14 days, generally around five days.
Every week a report is issued to the public from the Ministry of Health (SS), in order to provide information on the most up-to-date trend for COVID-19 pandemic by federal entity and by each metropolitan area. These indicators are currently three for ten risk indicators that define the Epidemiological Risk Traffic Light 1 to move towards a new normality, which is a monitoring system for the regulation of public space use of in accordance with the risk for COVID-19 contagion regulated by the SS [7].
Based on lag time analysis, it is possible to determine parameter value such that it corresponds to days that must be discarded at the end of the time series of daily new cases trend for COVID-19 syndrome. Only the delay between the date of symptoms and the date of admission is relevant, which represents the time it takes for a person to seek medical care. In the document entitled Methodology for the analysis of trends in epidemic curves of new cases for COVID-19 syndrome and bed occupancy and deaths registered in the IRAG Network [8], calculation for lag time for Mexico City was 8.85 days, Fig. 3.

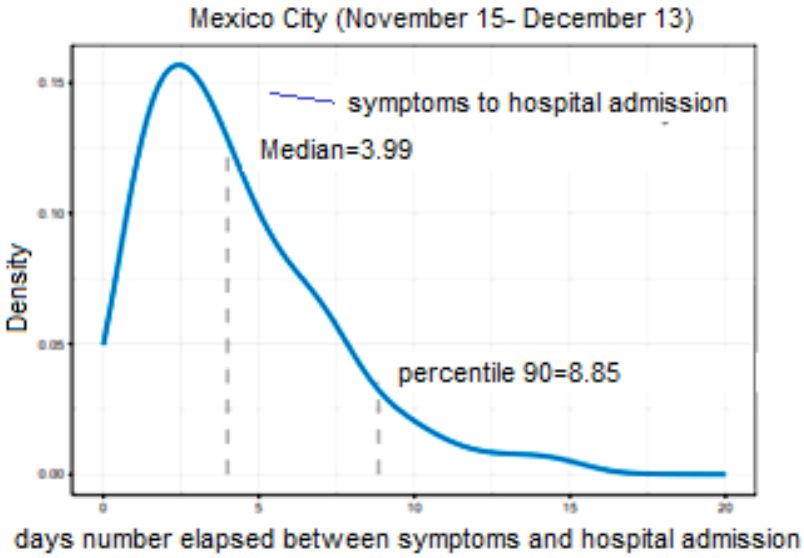

Fig. 3. Estimation between the delay time between infections and deaths in CDMX Source: Methodology for the analysis of trends in epidemic curves of new cases for COVID-19 syndrome and bed occupancy and deaths registered in the IRAG Network

3. Results

To calibrate our model in HEC HMS, calibration of the t_{lag} parameter or lag time was carried out in order to adjust official descent curve with those modeled in HEC-HMS. Delay time used in final modeling was 23,000 minutes. Therefore, lag time used at modeling is 6.38 days.
ANN considered number of infections reported between March 26, 2020 and December 31, 2021 as input variable and deaths data officially reported on those dates in Mexico City as output variable.
The model was applied to adjust accumulated data of confirmed cases in Mexico City, obtaining corroborated adjustment by determination coefficient, R^2, said value gave 0.0528 in case of infections comparison vs. official deaths reported by the Secretary of Health, 0.0571 for case of contagion vs. modeling using HEC-HMS tool and 0.0937 for contagion case vs. modeling using ANN, as shown in figures 4, 5 and 6.

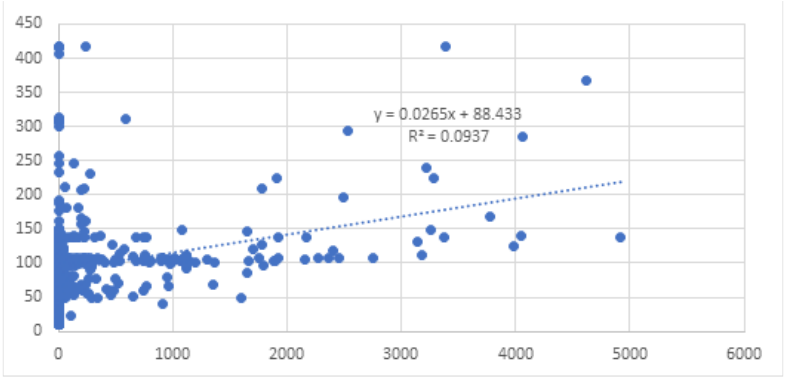

Fig. 4. Infections rate trends (horizontal axis) vs. deaths simulated with ANN (vertical axis)

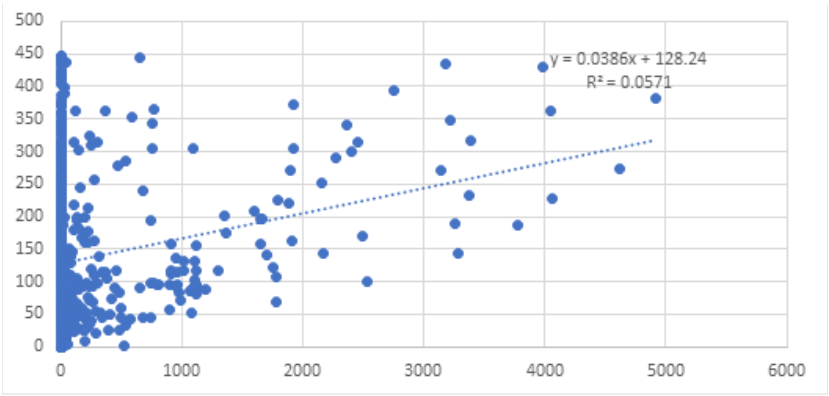

Fig. 5. Infections rate trends (horizontal axis) vs. deaths simulated with HEC-HMS (vertical axis)

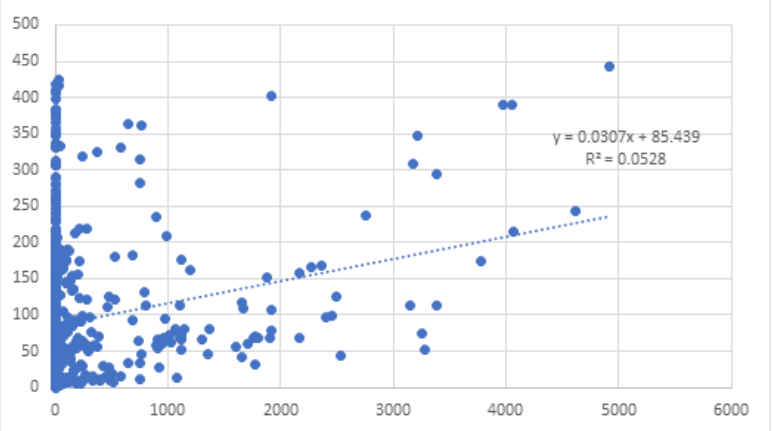

Fig. 6. Infections rate trends (horizontal axis) vs. official deaths (vertical axis)

The vaccination advance for international and national levels was positive altered demographic profile and contagion-hospitalization-death dynamics for pandemic, as one can see in Figure 7. A change in trend is particularly observed at the end of 2021 year. Worth emphasizing, unlike the first two epidemic waves, which are clearly observed in said figure, the growth ratio of the curves of cases, hospitalizations and deaths changed radically in last iteration, which is why the period of time to model it was from the month of February 2020 to December 2021.

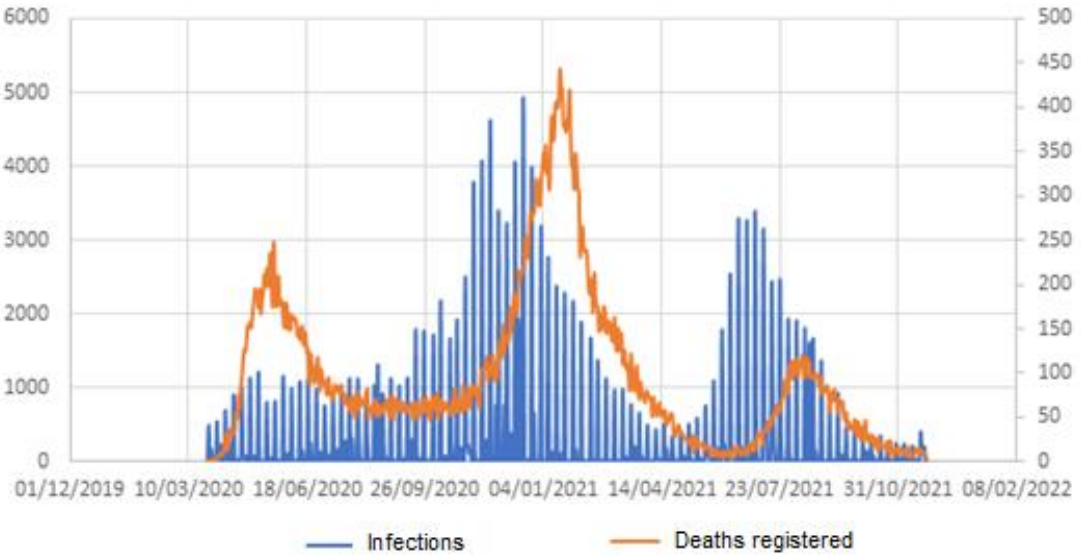

Fig. 7. Infections comparison vs. official registered deaths

Fig. 8 shows the behavior of deaths by considering contagion as an input variable and applying an artificial neural network ANN.

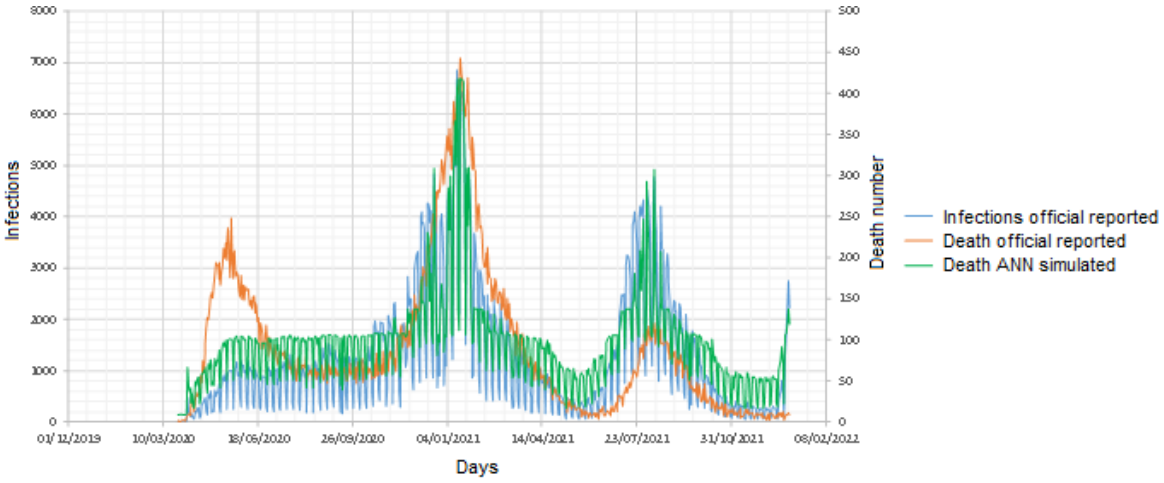

Fig. 8. Infections comparison vs. official and simulated deaths from an ANN

Fig. 9 shows the modeling of the contagion-death process using the HEC-HMS model, which reproduces the behavior of the official contagions reported by the SS, clearly observing the effect of the lag time between the two curves corresponding to the modeled t_{lag} of 6.38 days.

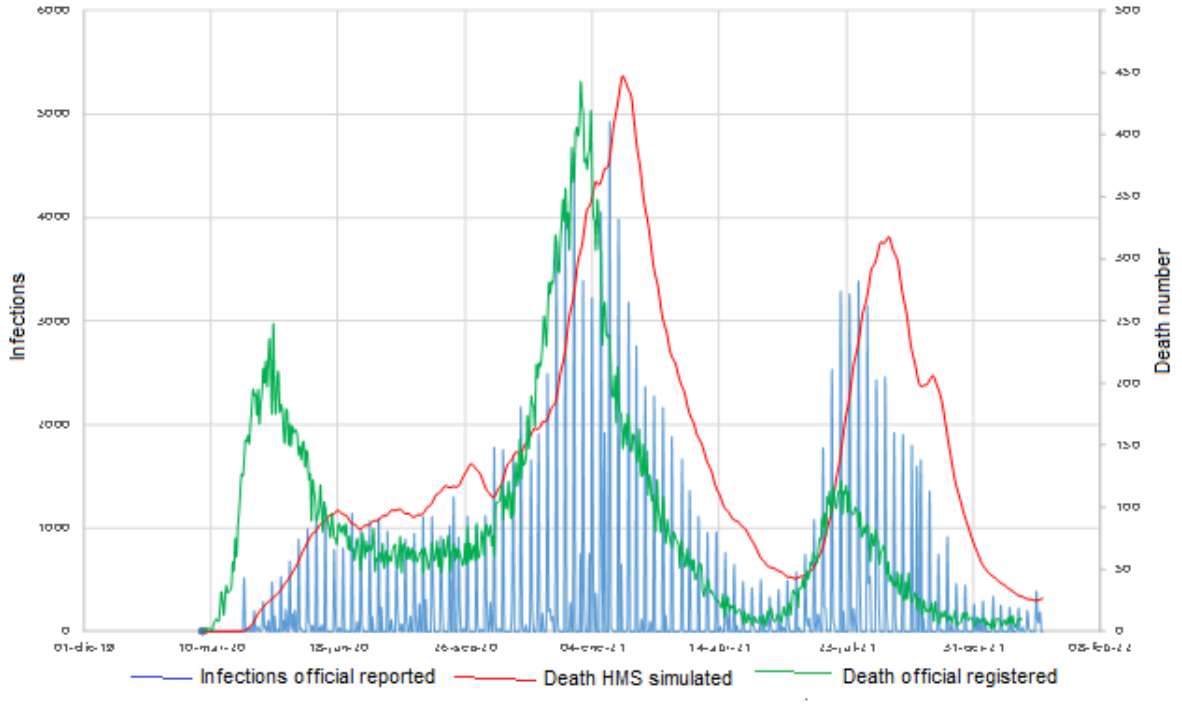

Fig. 9. Infections comparison vs deaths simulated from the HEC-HMS model

Figure 10 shows comparison between official deaths against data modeled from an ANN and what is obtained with the HEC-HMS modeling, observing that in the second wave or peak to HEC-HMS model manages to reproduce the trend and the peak of the officially reported, with an approximate delay of 6 days. On the other hand, the ANN follows the peak times of deaths but, in the third peak, neither of the two models reproduces the number of deaths, but rather the form, which suggests that it is due to the effect of vaccination, which managed to break the upward trend in the number of deaths from COVID-19.

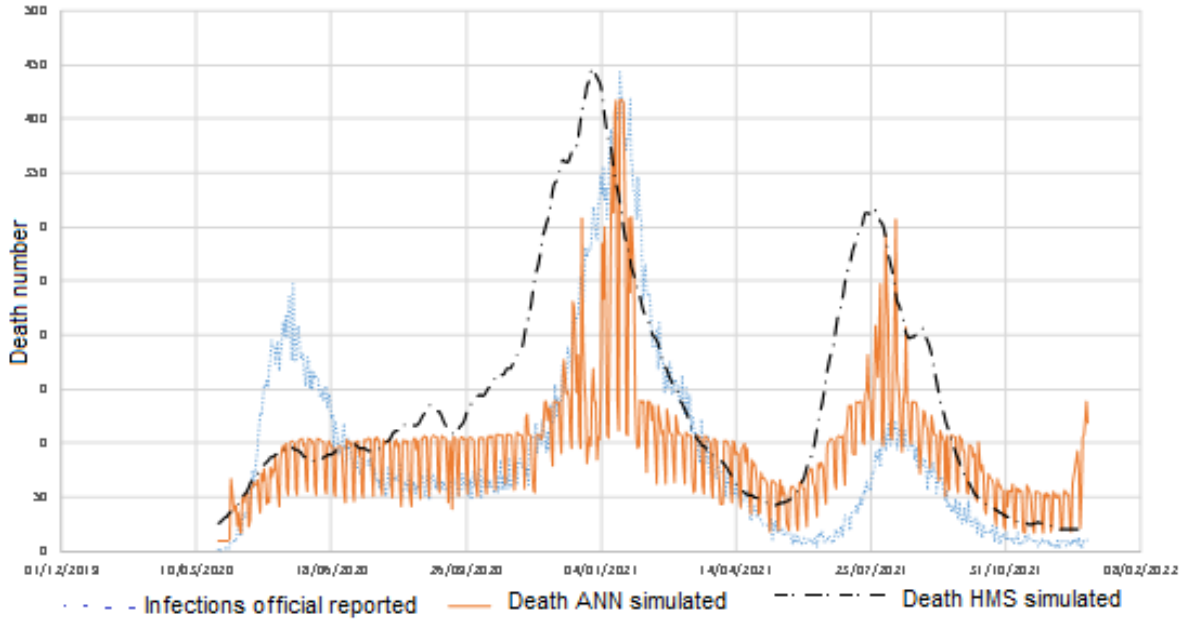

Fig. 10. Comparison of official deaths vs. those modeled by HEC-HMS and ANN

4. Conclusions

Rain runoff models' theory used in hydrology problems was applied to reproduce behavior in deaths by COVID 19 using official information rate infections, taking data in Mexico City. Additionally, an artificial neural network was used to reproduce contagion-death process, which helped to estimate time in which, on average, the COVID 19 disease can lead to an adverse case fatality situation; tested models adequately reproduced shape of death curve from infection function over time, especially in wave that corresponded to the alpha and beta variant; also, with the HEC-HMS it was estimated that approximate time between contagion and possible death was 6.38 days. In the wave for delta variant, an overestimation was observed given by the HEC HMS models and also by the ANN, attributed to a reduction effect in the lethality of the virus due to the intensification of vaccination campaigns. It should be noted that on the part of the ANN the input and output data are daily data of the reports of contagions and officially occurred deaths, that is to say that the data of the death that occurred on the day it is reported, is attributed to a contagion that occurred days ago, so the model implicitly has an autoregressive component. With the HEC HMS, when the curve of infections calculated against the official infections is drawn, an occurrence of the peak of deaths is observed approximately 6 days later compared to what was officially reported.

Acknowledgments

We thank the Government of Mexico for public databases available on the internet for the data used in this study.
This research did not receive any specific grant from funding agencies in the public, commercial, or not-for-profit sectors.

References

[1] Basu, S., and R.H. Campbell. "Going by the numbers: Learning and modeling COVID-19 disease dynamics." *Chaos, Solitons & Fractals* 138 (September 2020): 110140.
[2] Dal Molin Ribeiro, M.H., R. Gomes da Silva, V. Cocco Mariani, and L. Dos Santos Coelho. "Short-term forecasting COVID-19 cumulative confirmed cases: Perspectives for Brazil." *Chaos, Solitons & Fractals* 135 (June 2020): 109853.
[3] Alcántara-López, F., C. Fuentes, C. Chávez, J. López-Estrada, and F. Brambila-Paz. "Fractional Growth Model with Delay for Recurrent Outbreaks Applied to COVID-19 Data." *Mathematics* 10, no. 5 (March 2022): 825.
[4] Jaiswal, RK, S. Ali, and B. Bharti. "Comparative evaluation of conceptual and physical models of rainfall-runoff." *Applied Water Science* 10 (January 2020): 48.
[5] SCS. *Soil Conservation Service. Engineers Corp Army Hec-HMS elementary manual*. Spain, Department of Geology - Univ. Salamanca, 1972.
[6] The MathWorks, Inc., 2022. MATLAB. Version R2014a [Software]. https://la.mathworks.com/.
[7] Health Secretary / Secretaría de Salud. "Guideline for the calculation methodology for COVID-19 epidemic risk traffic light" / "Lineamiento para la metodología de cálculo del semáforo de riesgo epidémico COVID-19". *gob.mx (Gobierno de México)*. Accessed May 20, 2022. https://coronavirus.gob.mx/semaforo/.
[8] Esquivel Vázquez, J., J. Peña Acevedo, D.I. Rodríguez González, I. Sánchez Bravo, and J. L. Salazar Villanueva. *Methodology for the analysis of trends in epidemic curves of new cases for COVID-19 syndrome and bed occupancy and deaths registered in the IRAG Network / Metodología para el análisis de tendencias de curvas epidémicas de casos nuevos de síndrome COVID-19 y de ocupación de camas y defunciones registrados en la Red IRAG*. Mexico, Coordination of Technological Services of CIMAT / Coordinación de Servicios Tecnológicos del CIMAT, 2021.

FLUIDAS

NATIONAL PROFESSIONAL ASSOCIATION OF HYDRAULICS AND PNEUMATICS IN ROMANIA

fluidas@fluidas.ro